Post-synthetic modification of mixed-linker metal-organic frameworks for the design of heterogeneous single-site catalyst materials and their application in liquid phase oxidation reactions

Zur Erlangung des akademischen Grades einer

DOKTORIN DER NATURWISSENSCHAFTEN

(Dr. rer. nat.)

von der KIT-Fakultät für Chemie und Biowissenschaften

des Karlsruher Instituts für Technologie (KIT)

genehmigte

DISSERTATION

von

M. Sc. Ceylan Yildiz

aus

Lampertheim

1. Referent:	Prof. Dr. Wolfgang Kleist
2. Referent:	Prof. Dr. Jan-Dierk Grunwaldt
Tag der mündlichen Prüfung:	18.10.2019

Die Arbeiten zu dieser Dissertation wurden in der Zeit vom 15. November 2015 bis zum 31. August 2019 am Karlsruher Institut für Technologie (KIT), Institut für Technische Chemie und Polymerchemie und an der Ruhr-Universität Bochum (RUB), Fakultät für Chemie und Biochemie − Nanostrukturierte Katalysatormaterialien unter der Leitung von Prof. Dr. Wolfgang Kleist durchgeführt.

Abstract

In recent years, metal-organic frameworks (MOFs) have emerged as interesting materials for heterogeneous catalysis due to their unique and versatile properties. They exhibit well-defined, monoatomic active sites, which can be generated *via* the immobilization of transition metal ions using post-synthetic modification (PSM) approaches. By the combination of the PSM approach and the mixed-linker concept, tailor-made single-site catalyst materials can be achieved featuring high framework porosity and a good distribution of the catalytically active sites. Thus, the beneficial properties of heterogeneous and homogeneous catalysis can be united within one material. The aim of the present thesis included the design of novel single-site catalyst materials based on metal-organic frameworks and their application in oxidation reactions in the liquid phase.

In the first part of this work, mixed-linker MOFs with defined amounts of functionalized linker molecules were prepared. Therefore, mixed-linker metal-organic frameworks with DUT-5 and MIL-53(Al) structure were synthesized with additional 2,2'-bipyridine-, amine- and alkyne-functionalized linker molecules. The 2,2'-bipyridine-5,5'-dicarboxylate linkers were subsequently used for the direct immobilization of metal ions, such as palladium, nickel, copper, cobalt and manganese. The amine-functionalized linkers were post-synthetically modified with maleic anhydride and various aldehydes, like salicylaldehyde, 2-pyridinecarboxaldehyde and 2-imidazolcarboxaldehyde. The resulting chelating side groups were subsequently metalated using cobalt and manganese ions. Furthermore, the alkyne groups were modified with a gold(I)-azide *via* inorganic click reactions (iClick).

The resulting catalyst materials were characterized using powder X-ray diffraction, ATR-IR spectroscopy, N_2 physisorption, NMR spectroscopy and ICP-OES analysis. In addition, X-ray absorption spectroscopy measurements were performed to determine the oxidation states as well as the chemical environment of the metals. It could be confirmed that the metals were incorporated in the desired form and undesired phases, like clusters or nanoparticles, in the pores could be excluded.

In the second part, the synthesized cobalt- and manganese-containing catalysts were applied in aerobic oxidation reactions. The influence of various reaction parameters on the conversion, yield and selectivity was investigated using molecular oxygen as oxidizing agent. Additionally, the activities and selectivities of the catalysts were compared with regard to the location of the

metal ions within the framework materials. For all catalytic reactions, heterogeneity tests were performed, which confirmed major contributions of a truly heterogeneous pathway.

MIL-53(Al)-NH_2(50)-Mal-Mn was applied in the epoxidation of α-pinene, which represents a promising reaction in the development of sustainable catalytic processes. First, relevant reaction parameters were optimized using Mn(III) acetate as a homogeneous catalyst. In the context of green chemistry, oxygen from air and sustainable solvents like diethyl carbonate were preferably used in the catalytic reactions. The optimized conditions were then applied to the manganese-containing MOF, which showed a high activity that was comparable to the manganese salt. The MOF-based catalyst was easily removed from the reaction mixture and could be reused for five catalytic cycles without a significant loss of activity.

Cobalt-, manganese(II)- and manganese(III)-containing MOF materials, in which the metals were immobilized into the DUT-5-BPyDC(10) and DUT-5-NH_2(10)-Sal structures, were tested in the aerobic epoxidation of *trans*-stilbene. For the cobalt-containing catalysts, high conversions up to 90% were obtained and, thus, they were more active than their manganese-based counterparts (up to 54%). Very low catalyst amounts (0.02 mol%) were sufficient for the activation of molecular oxygen. The reaction rate increased with higher temperatures, air flow rates and catalyst concentrations. The variation of the substrate concentration showed a minor influence on the reaction rate, which could be linked to the promoting effect of benzaldehyde for the cobalt-containing catalysts. Turnover numbers up to 3000 for the metal-containing DUT-5 materials were observed. Only manganese(II)-containing materials showed an effect relating to the different positioning of the metal ions. For the manganese-containing catalysts, no clear influence of the oxidation state could be found.

Furthermore, cobalt-containing DUT-5 catalysts were used in the aerobic oxidation of benzyl alcohol. Under optimized conditions, DUT-5-BPyDC(10)-Co resulted in a conversion up to 85% with a benzaldehyde yield of 47%. The amine-functionalized cobalt catalysts, in which the cobalt was located close to the center of the pores, showed higher activities and selectivities than the bipyridine-functionalized catalyst, in which cobalt was located close to the framework walls. Even though the differences of the conversions were not that pronounced, the higher selectivities for the amine-functionalized catalyst materials were already observed after one hour reaction time. Thus, the amine-functionalized DUT-5 materials might enable a better accessibility of the catalytically active sites for substrate molecules resulting in improved reaction rates.

In summary, within this thesis, highly active heterogeneous single-site catalysts based on metal-organic frameworks were synthesized *via* post-synthetic modification, which represent promising materials for future applications.

Kurzfassung

Metall-organische Gerüstverbindungen (*metal-organic frameworks,* MOFs) haben sich in den letzten Jahren aufgrund ihrer einzigartigen und zugleich vielfältigen Eigenschaften zu vielversprechenden Materialien für heterogene Katalysatorreaktionen entwickelt. Sie weisen klar definierte, monoatomare Metallzentren auf, welche durch die Immobilisierung von Metallkomplexen mittels post-synthetischer Modifizierungen (PSM) erhalten werden können. Durch die Kombination von post-synthetischer Modifizierung mit der Verwendung von Metall-organischen Gerüstverbindungen mit gemischten Linkermolekülen (*mixed-linker* MOFs) können maßgeschneiderte Single-Site-Katalysatoren entstehen, die eine hohe Porosität und eine gute Verteilung der katalytisch aktiven Metallzentren aufweisen. Dadurch können die positiven Eigenschaften von heterogener und homogener Katalyse vereint werden. Das Ziel der vorliegenden Doktorarbeit bestand darin, neuartige Single-Site-Katalysatoren, basierend auf Metall-organischen Gerüstverbindungen, herzustellen und diese in Oxidationsreaktionen in flüssiger Phase zu testen.

Im ersten Teil dieser Arbeit wurden zunächst Mixed-Linker-MOFs mit definierten Anteilen an funktionalisierten Linkermolekülen hergestellt. Dabei wurden Gerüstverbindungen mit DUT-5 und MIL-53(Al)-Struktur mit funktionellen Bipyridin-, Amin- und Alkingruppen synthetisiert. An den 2,2‘-Bipyridin-5,5‘-dicarboxylat-Linkern wurden anschließend direkt verschiedene Metallionen wie Palladium, Nickel, Kupfer, Cobalt und Mangan immobilisiert. Die aminfunktionalisierten Linker wurden mit Maleinsäureanhydrid und mit Aldehyden wie Salicylaldehyd, 2-Pyridincarboxaldehyd und 2-Imidazolcarboxaldehyd post-synthetisch modifiziert. An den daraus resultierenden chelatisierenden Seitengruppen wurden im nächsten Schritt Cobalt- und Manganzentren eingebaut. Weiterhin wurden die Alkingruppen mittels anorganischer Click-Reaktion (iClick) mit einem Goldazid-Komplex umgesetzt.

Die hergestellten Katalysatormaterialien wurden mittels Pulverröntgendiffraktometrie, ATR-IR Spektroskopie, Stickstoffphysisorption, NMR Spektroskopie und ICP-OES Analyse charakterisiert. Außerdem wurden mit Hilfe von Röntgenabsorptionsspektroskopie die Oxidationsstufen der Metallzentren sowie deren chemische Umgebung analysiert. So konnte bestätigt werden, dass die Metalle in der gewünschten Form komplexiert waren und keine unerwünschten Phasen, wie Cluster oder Nanopartikel, in den Poren vorlagen.

Im zweiten Teil der Arbeit wurden die synthetisierten Cobalt- und Mangan-Katalysatoren in aeroben Oxidationsreaktionen eingesetzt. Dabei wurde der Einfluss verschiedener Reaktionsparameter auf Umsatz, Ausbeute und Selektivität untersucht. Als Oxidationsmittel diente hierbei molekularer Sauerstoff. Die Aktivitäten und Selektivitäten der Katalysatoren wurden miteinander verglichen, wobei auch der Einfluss der Positionierung der Metallzentren innerhalb der Gerüstverbindung untersucht wurde. Für alle Reaktionen wurden Heterogenitätstests durchgeführt, welche eine wesentliche Beteiligung eines heterogenen Reaktionspfads bestätigten.

MIL-53(Al)-NH_2(10)-Mal-Mn wurde in der aeroben Epoxidierung von α-Pinen, die eine vielversprechende Reaktion für die Entwicklung von nachhaltigen Katalyseprozessen darstellt, eingesetzt. Dabei wurden relevante Reaktionsparameter mit Mn(III)-acetat als homogenen Katalysator optimiert. Dem Konzept der nachhaltigen Chemie entsprechend wurden bevorzugt Luft als Oxidationsmittel und Diethylcarbonat als Lösungsmittel in den katalytischen Testreaktionen eingesetzt. Die optimierten Bedingungen wurden für den Mangan-basierten MOF-Katalysator angewendet, der im Vergleich zum Mangansalz eine ähnlich hohe Aktivität zeigte. Der MOF-basierte Katalysator konnte von der Reaktionsmischung leicht abgetrennt und in fünf weiteren Katalysezyklen ohne einen deutlichen Aktivitätsverlust wiederverwendet werden.

Weiterhin wurden Materialien, die durch Immobilisierung von Cobalt-, Mangan(II)- und Mangan(III) in DUT-5-BPyDC(10) und DUT-5-NH_2(10)-Sal Strukturen hergestellt wurden, in der aeroben Epoxidierung von *trans*-Stilben getestet. Hohe Umsätze von bis zu 90% wurden mit den Cobalt-Katalysatoren erhalten, welche höher als die mit den Mangan-Katalysatoren erhaltenen Umsätze (bis zu 54%) waren. Für die Aktivierung des Oxidationsmittel waren sehr geringe Katalysatormengen (0,02 mol%) ausreichend. Die Reaktionsgeschwindigkeit nahm mit höheren Temperaturen, Flussraten und Katalysatorkonzentrationen zu. Die Variation der Substratkonzentration zeigte nur einen geringen Einfluss auf die Reaktionsgeschwindigkeit, was auf den Promotoreffekt des als Nebenprodukt gebildeten Benzaldehyds auf die Cobalt-Katalysatoren zurückzuführen werden könnte. Eine katalytische Produktivität (*turnover number*, TON) bis zu 3000 wurde für die DUT-5-basierten Katalysatoren beobachtet. In Bezug auf die verschiedenen Positionierungen der Metallzentren zeigten nur die Mangan(II)-Katalysatoren eine Auswirkung auf den Umsatz und die Ausbeute. Ebenso konnte kein signifikanter Einfluss der Oxidationsstufe bei den Mangan-Katalysatoren beobachtet werden.

Des Weiteren wurden DUT-5-Katalysatoren mit Cobaltzentren in der aeroben Oxidation von Benzylalkohol eingesetzt. Unter optimierten Bedingungen lieferte DUT-5-BPyDC(10)-Co einen Umsatz von 85% bei einer Ausbeute von 47% Benzaldehyd. Die aminfunktionalisierten Cobalt-Katalysatoren, in denen sich die Cobaltzentren nahe dem Zentrum der Pore befinden, zeigten höhere Aktivitäten und Selektivitäten als der bipyridinfunktionalisierte Cobalt-Katalysator, dessen Cobaltzentren sich näher an der Gerüstwand befinden. Auch wenn die erhaltenen Umsätze sich nicht stark voneinander unterschieden, konnten die höheren Selektivitäten für die aminfunktionalisierten Katalysatoren schon nach einer Stunde beobachtet werden. Dementsprechend scheinen diese Katalysatoren eine bessere Zugänglichkeit der Substratmoleküle zu den katalytisch aktiven Zentren zu ermöglichen, was zu einer erhöhten Reaktionsgeschwindigkeit führen könnte.

Zusammenfassend lässt sich sagen, dass im Rahmen dieser Arbeit hochaktive Single-Site Heterogenkatalysatoren basierend auf Metall-organische Gerüstverbindungen mittels post-synthetischer Modifizierung synthetisiert wurde, welche vielversprechende Materialien für zukünftige Anwendungen darstellen.

Table of contents

1 Literature overview

1.1 General introduction

In the last decades, metal-organic frameworks (MOFs) or porous coordination polymers (PCPs) have received much attention as a new class of porous materials due to their potential applications in gas storage and separations or heterogeneous catalysis.[1-4] The establishment of metal-organic frameworks started in the early 1990s and, thus, achieved a breakthrough in the porous materials research area, which was pioneered by the groups of Kitagawa[5-8], Yaghi[9-12] and Férey[13-16].

The structure of metal-organic frameworks consists of two types of building units including an inorganic and an organic part that are linked together to form infinite one-, two- or three-dimensional networks. The concept of secondary building units (SBU) describes the inorganic clusters or coordination spheres, which are linked to the organic units, resulting in simple geometric figures. The organic units are defined as linkers that possess at least two functional groups. The majority of used linker molecules exhibits nitrogen donors, *e.g.* 4,4'-bipyridine[10], or oxygen donors like carboxylates.[17] The first carboxylate-based MOF syntheses were reported using benzene-1,3,5-tricarboxylic acid (H_3BTC)[9] or benzene-1,4-dicarboxylic acid (H_2BDC)[11]. The choice of a certain combination as well as the variation of these building units leads to an almost infinite variety of well-defined MOF structures. In the meantime, approximately 70,000 MOF structures have been reported in the Cambridge Structural Database (CSD).[18]

Metal-organic frameworks are crystalline materials that possess highly porous structures with specific surface areas usually in the range of S_{BET} = 1000 – 2000 m^2/g. Frameworks with ultrahigh specific surface areas (S_{BET} > 4000 m^2/g) have also been reported.[19] Furthermore, MOF materials exhibit relatively high chemical and thermal stability compared to, *e.g.*, organic polymers. There are also some examples of MOFs, whose structures feature the so-called breathing effect, which describes changes in the pore geometries of the framework upon external stimuli (*e.g.* adsorption/desorption of guest molecules).[7,20,21]

1.2 Isoreticular framework synthesis

The interest to tailor metal-organic frameworks materials through the manipulation of processing parameters has become much larger in recent years. One major challenge concerns

the systematic alteration of the chemical composition, functionality or molecular dimensions without changing the underlying topology. The strategy of isoreticular synthesis describes the design of porous structures in which pore size and functionality could be varied, while the framework topology remains the same. Isoreticular metal-organic frameworks (IRMOFs) have been synthesized with the formula $Zn_4O(L)_3$, in which L is a rigid linear dicarboxylate, resulting in 16 different materials that have the same topology like MOF-5, which is also named IRMOF-1 (Figure 1). In IRMOF-2 to IRMOF-7, benzene-1,4-dicarboxylate linkers bearing bromo, amino, *n*-propoxy, *n*-pentoxy, cyclobutyl or fused benzene functional groups have been used. The use of functionalized linkers for isoreticular MOF synthesis was termed as 'isoreticular functionalization'. Furthermore, the pore size of the material could be expanded using elongated linker molecules like biphenyl, tetrahydropyrene, pyrene and terphenyl compounds (IRMOF-8 to IRMOF-16). The increase of the pore size while retaining the same topology was named as 'isoreticular expansion'.[22-24]

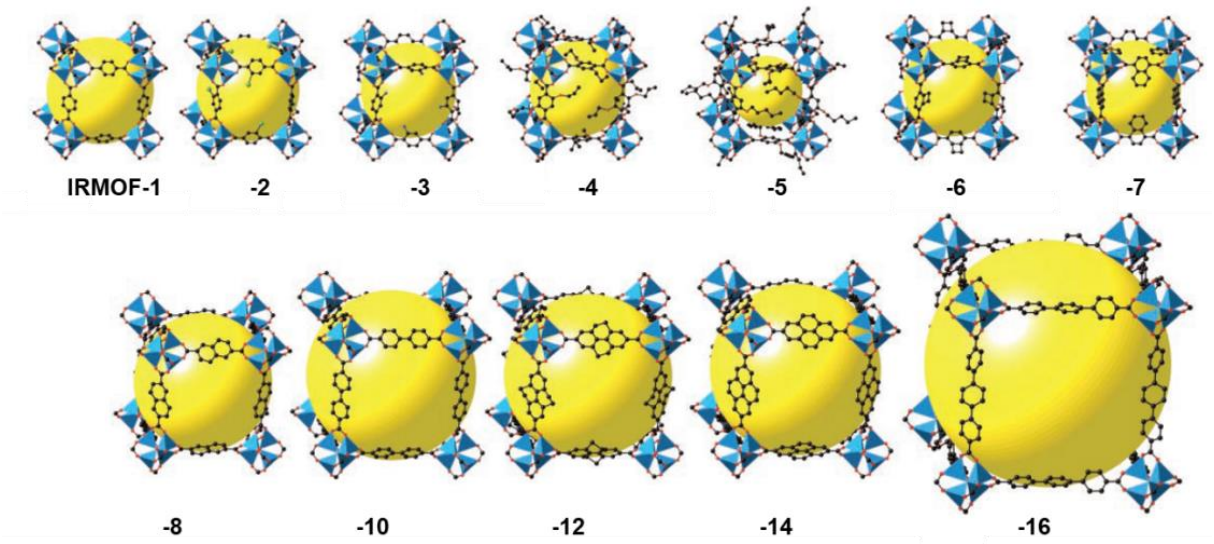

*Figure 1. Series of isoreticular metal-organic frameworks (IRMOFs) based on MOF-5 (IRMOF-1); blue polyhedral: Zn, red spheres: O, black spheres: C, green spheres in **-2**: Br, blue spheres in **-3**: amine-groups. The large yellow spheres represent the largest van der Waals spheres that would fit in the cavities without touching the frameworks. From [22]. Reprinted with permission of AAAS.*

The synthesis of isoreticular frameworks included not only the use of related linkers, but also the exchange of the metal nodes can lead to isoreticular framework structures. The MIL-53 structure is among the most widely studied material of all metal-organic frameworks due to its easy preparation and its thermal stability up to 500 °C. The synthesis of chromium-containing MIL-53, in which Cr-OH chains are linked by benzene-1,2-dicarboxylate (BDC), was first described by the group of Férey in 2002.[25] At the same time, the synthesis of MIL-47, a

vanadium analogue of MIL-53, was published by the same group.[26] Millange and Walton made a detailed analysis of the frameworks based on the MIL-53 type structure.[27] In the meantime, MIL-53 materials containing trivalent metals, such as Al[28], Fe[29], Sc[30], Ga[31] and In[32], and bivalent metals[33], such as Mn^{2+}, Co^{2+} and Ni^{2+}, have been reported. Different types of linker, which were used to synthesize MIL-53 analogues, are summarized in Figure 2. [34,35] Due to its great chemical stability, MIL-53 analogue framework materials with elongated linker represent promising materials, since their larger pores might be beneficial for applications in gas storage, separation or for post-synthetic modification approaches.[36-42]

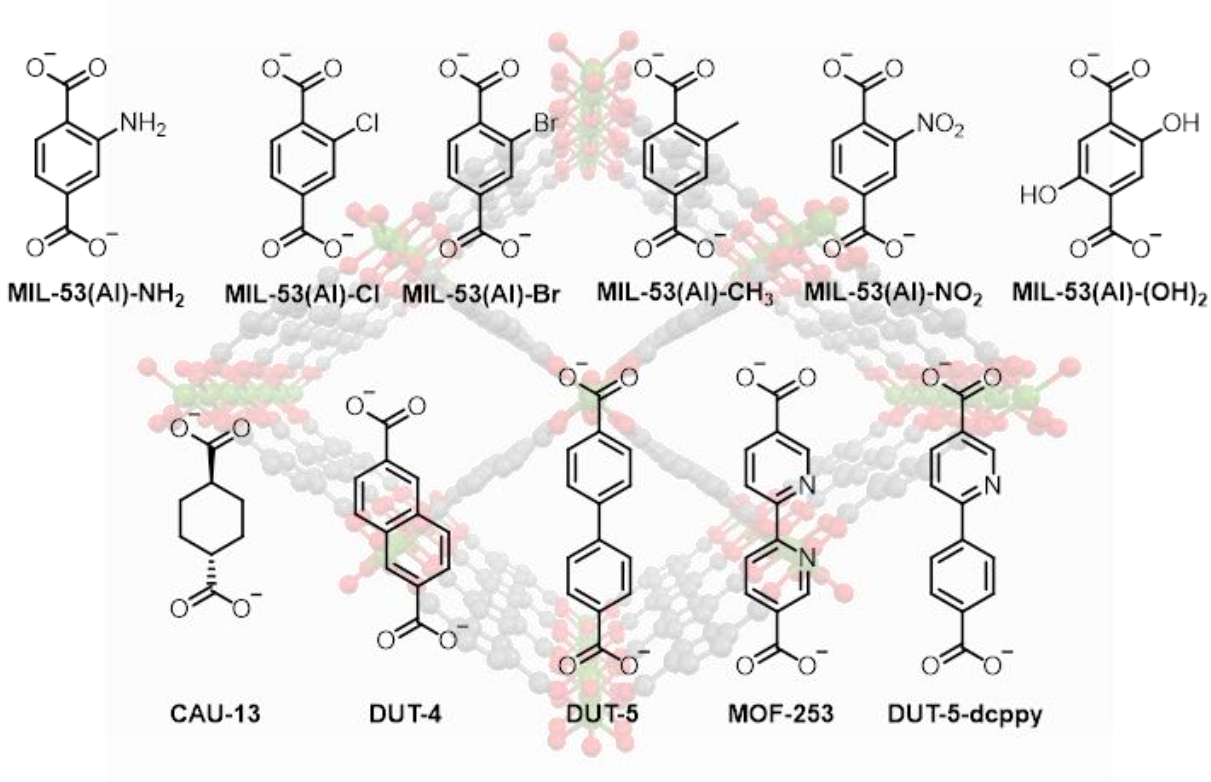

Figure 2. Various functionalized and elongated linkers used for the synthesis of isoreticular MIL-53(M) analogues. Adapted from [27]. Copyright © 2018 Wiley-VCH Verlag GmbH & Co. KGaA Weinheim.

Metal-organic frameworks with large pore dimensions exhibit higher surface areas, which afford a couple of advantages for, *e.g.*, post-synthetic modification or catalytic approaches. The introduction of larger substrates can be facilitated and, thus, the pores will be still free for substrate molecules during the catalytic reactions. In the following chapter, different framework structures containing 4,4'-biphenyldicarboxylate linkers are presented to emphasize these aspects.

1.3 Metal-organic frameworks with 4,4'-biphenyldicarboxylate based linkers

1.3.1 DUT-5

The metal-organic framework DUT-5, which is named after the Dresden University of Technology, was introduced by the group of Kaskel in 2009.[40] The typical reaction between $Al(NO_3)_3 \cdot 9\,H_2O$ and 4,4'-biphenyldicarboxylic acid (H_2BPDC) under hydrothermal conditions results in a rigid 3D framework structure with large one-dimensional pores (about 22.7 Å × 19.2 Å) and, thus, proved to be the elongated isoreticular form of MIL-53(Al) (Figure 3). The aluminum is surrounded by six oxygen atoms in a distorted octahedral geometry. Infinite $[Al(OH)]_n$ chains are formed by the occupation of hydroxyl groups in the axial position of the octahedron. DUT-5 showed high chemical and thermal stability up to 430 °C. Nitrogen physisorption measurements revealed a type I isotherm, which is characteristic for microporous materials, with a total pore volume of 0.81 cm^3/g and a specific surface area of S_{BET} = 1600 m^2/g ($S_{Langmuir}$ = 2335 m^2/g).

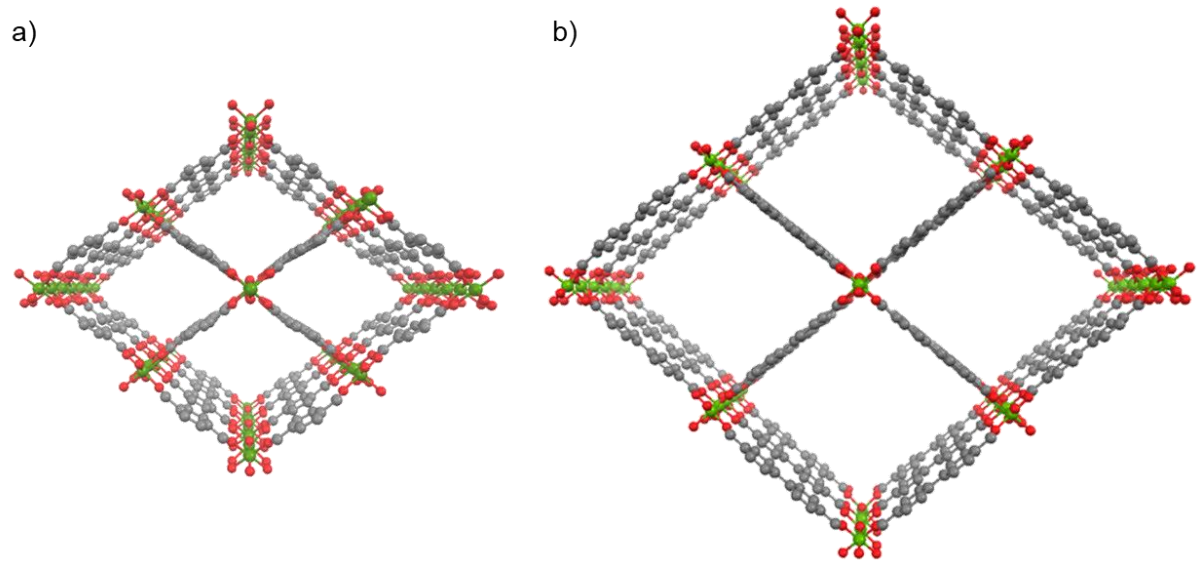

Figure 3. Schematic representation of the structure of MIL-53(Al)[28] (a) and DUT-5[40] (b); green: Al, grey: C, red: O.

The high crystallinity and porosity of DUT-5 make it a promising material for many applications. In 2015, Couck *et al.* synthesized a sulfone-functionalized DUT-5 material using 2,2'-sulfone-4,4'-biphenyldicarboxylic acid.[43] These incorporated sulfone groups were able to enhance the adsorption properties compared to the unmodified DUT-5 and have been used in

the gas separation of alkanes, alkenes and aromatics. The group of Stock published the synthesis of DUT-5 containing amine- and nitro-groups, which were used for CO_2, H_2 and CH_4 gas uptake applications.[44] Krajnc *et al*. used the synthesis of DUT-5 consisting of biphenyl- and bipyridinedicarboxylic linkers for demonstrating a NMR-based method for studying the spatial distribution of linker molecules.[45] Gotthardt *et al*. presented the synthesis of single- and mixed-linker amine-, nitro-, alkyne- and azide-functionalized DUT-5 materials.[46] Thermogravimetric or physisorption measurements showed that the properties of the frameworks could be tuned by varying the number of functional groups. Furthermore, the amine-functionalized DUT-5 materials were modified using anhydrides and aldehydes *via* post-synthetic modification resulting in bidentate chelating side groups. In 2017, a bimetallic Al/V metal-organic framework was synthesized, which was based on the monometallic isoreticular frameworks COMOC-2(V) [V(O)BPDC][47] and DUT-5(Al) [Al(OH)BPDC] (Figure 4).[48] CO_2 sorption measurements showed that the incorporation of vanadium into the DUT-5 structure affected the breathing behavior of the framework. Xiao *et al*. used DUT-5 for the immobilization of enzymes, such as glucose oxidase (GOx) and uricase, and utilized the materials as efficient sensors in the colorimetric detection of glucose.[49] Only recently, DUT-5 was used as catalyst in the Meerwein-Ponndorf-Verley reduction of ketones and aldehydes.[50]

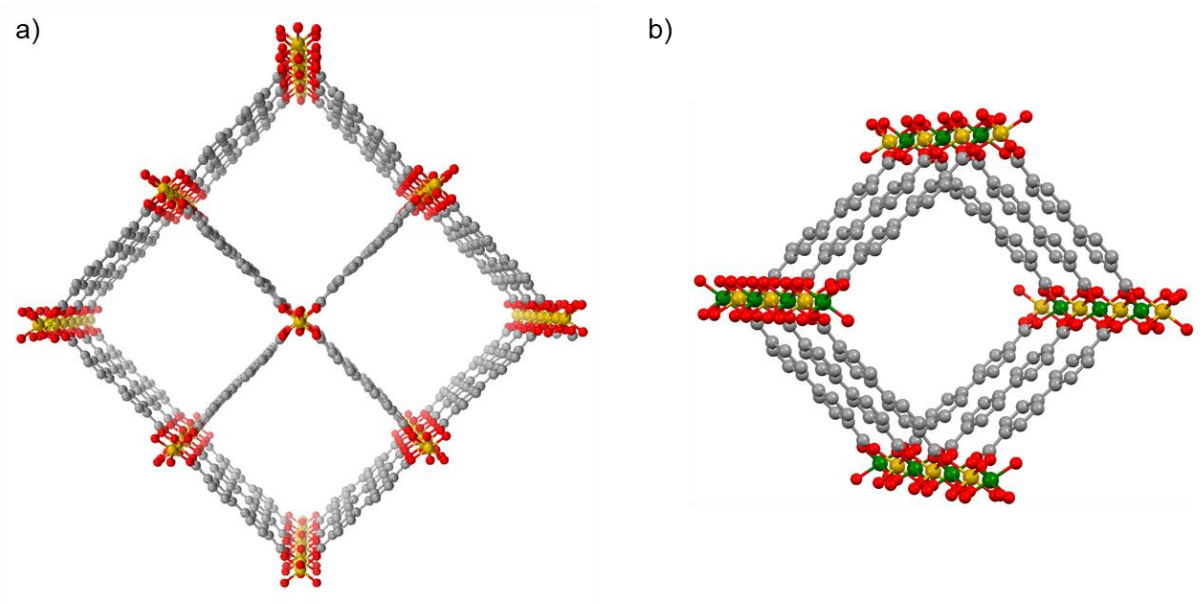

Figure 4. Schematic representation of COMOC-2[47] (a) and the bimetallic Al/V metal-organic framework V(O)BPDC$_x$Al(OH)BPDC$_{1-x}$[48] (b); yellow: V, green: Al, grey: C, red: O.

1.3.2 MOF-253

The synthesis of the metal-organic framework MOF-253 was first performed by Bloch *et al*.[41] In analogy to the synthesis of DUT-5, the reaction of $AlCl_3 \cdot 6\ H_2O$ and 2,2'-bipyridine-5,5-

dicarboxylic acid (H_2BPyDC) as linker in *N*,*N*-dimethylformamide (DMF) at 120 °C for 24 h afforded MOF-253 as a white microcrystalline solid. The structure is isoreticular to DUT-5 with a thermal stability of 400 °C. N_2 physisorption measurements revealed a type I isotherm with a pore volume of 0.89 cm^3/g and a specific surface area of S_{BET} = 2160 m^2/g ($S_{Langmuir}$ = 2490 m^2/g). The material contains open bipyridine sites, which can act as donor ligands for the immobilization of metals. Bloch *et al.* used the MOF-253 material for a subsequent complexation of Pd^{2+} and Cu^{2+}, which resulted in an enhanced selectivity for the adsorption of CO_2 in the presence of N_2. Apart from that, MOF-253 was used for the immobilization of ruthenium, palladium or copper ions, which were applied as heterogeneous catalysts in various reactions (see chapter 1.5.3).[51-54]

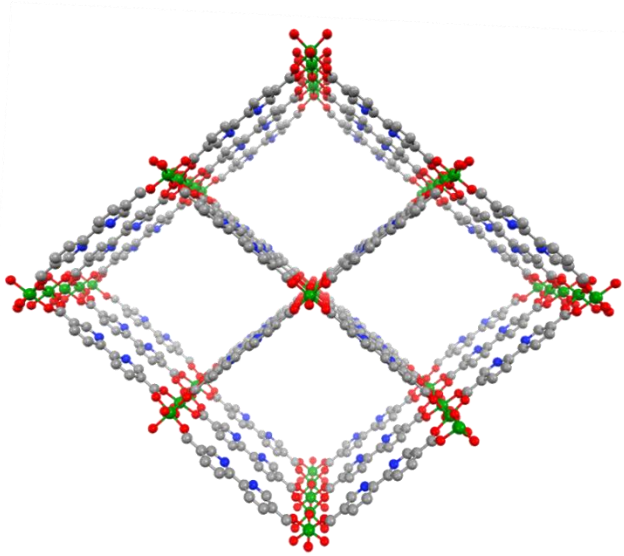

Figure 5. Schematic representation of MOF-253; green: Al, grey: C, blue: N, red: O.[41]

1.3.3 UiO-67

The zirconium-based metal-organic framework UiO-67 (University of Oslo) was first synthesized by the group of Lillerud by using ZrO_4 and 4,4'-biphenyldicarboxylic acid (H_2BPDC).[55] The structure exhibits two types of pores; an octahedral one (with a pore diameter of 12 Å) and a tetrahedral one (with a pore diameter of 16 Å). Thereby, the octahedral pore is face-sharing with 8 tetrahedral pores and edge-sharing with 8 additional octahedral pores (Figure 6). However, the access to the internal surface of UiO-67 is limited by a window with approx. 8 Å diameter. In addition to UiO-67 with BPDC linkers, isoreticular framework structures were synthesized using benzene-1,4-dicarboxylate (UiO-66) or *p*-terphenyl-4,4''-dicarboxylate (UiO-68) linkers.

The materials revealed a thermal stability up to 540 °C and, thus, the different linkers have no significant influence on the stability of the MOF. The Langmuir surface area of UiO-66 was $S_{Langmuir}$ = 1187 m^2/g and increased with longer linkers to 3000 (UiO-67) and 4170 m^2/g (UiO-68). Various functionalized UiO-66/67 materials using amine and nitro[56-60], bromo[61] or hydroxyl[62] groups have also been synthesized. Further isoreticular synthesis of UiO-67 was performed using 2,6-naphtalenedicarboxylate (NDC)[63] or 2,2'-bipyridine-5,5-dicarboxylate (BPyDC)[64-71] linkers, which were particularly applied for catalytic reactions. However, due to the small pore windows of 8 Å, the selection of substrates with regard to the accessibility in post-synthetic modification or catalytic approaches is limited.

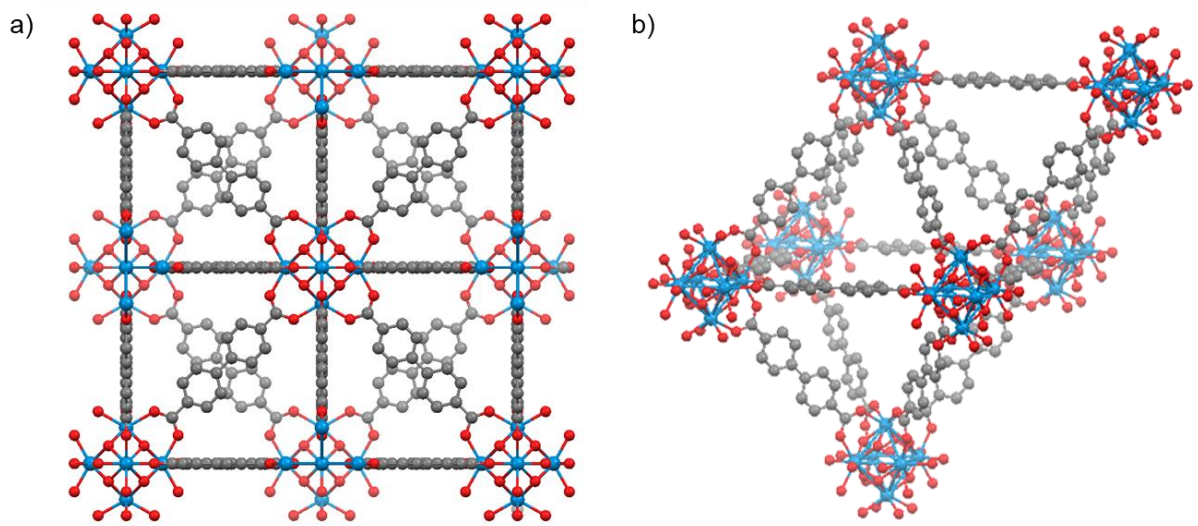

Figure 6. Schematic representation of the UiO-67 structure showing a single octahedral and tetrahedral pore; blue: Zr, grey: C, red: O.[55]

1.4 Mixed-linker metal-organic frameworks

The concept of mixed-component metal-organic frameworks (MC-MOFs)[72], also termed as MIXMOFs[73], multivariate MOFs (MTV-MOFs)[74] or coordination co-polymers[75], describes the synthesis of framework materials containing at least two types of different linkers or different metals, which feature the same coordination geometry and connectivity. Usually, the direct synthesis of MC-MOFs leads to a homogeneous distribution of the different components within the framework (Figure 7a, b). In contrast, core-shell structures, in which the outside of the MOF differs chemically from the center, can be achieved through epitaxial growth or *via* post-synthetic modification (Figure 7c, d). An overview of different synthetic strategies to control the structural arrangement of the components is discussed in detail by Bitzer and Kleist.[76] By using different approaches and distributions of components, the properties can be

adjusted for specific applications. Since only the mixed-linker approach was used in this work, only this concept will be described in detail in the present thesis.

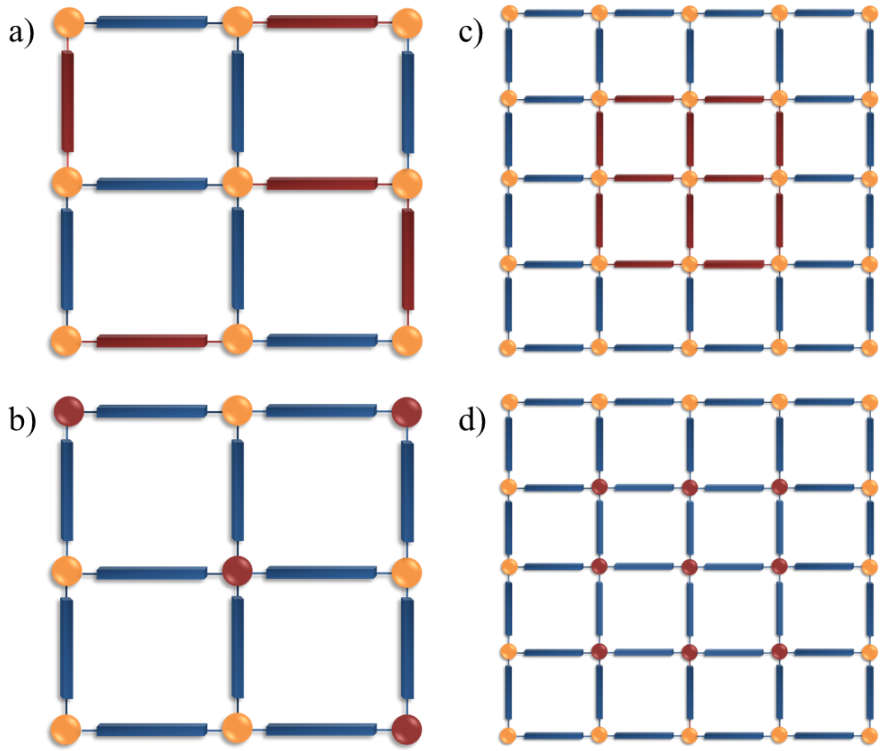

Figure 7. The different categories of mixed-component MOFs: mixed-linker MOFs with statistically distributed linkers (a) or with core-shell structure (c), mixed-metal MOFs with statistically distributed metals (b) or with core-shell structure (d).

Metal-organic frameworks containing more than one type of linker can be synthesized by using different linkers with similar lengths, donor groups and solubilities resulting in a single phase MC-MOF. In 2009, the first direct synthesis of a mixed-linker MOF-5 was published by Kleist *et al.*, in which a defined amount of benzene-1,4-dicarboxylate (BDC) linker was substituted by 2-aminobenzene-1,4-dicarboxylate (ABDC).[73,77] Shortly afterwards, the group of Yaghi presented a MOF-5-type structure that contained up to eight distinct linkers in one material.[74] At the same time, a mixed-linker MIL-53(Al) with defined ratios of BDC and ABDC linker was prepared forming the MOF $Al(OH)(BDC)_{1-x}(ABDC)_x$ (x = 0.1, 0.5, 0.9).[78] The formation of a mixed-linker MOF could also be achieved *via* a two-step process, a so-called post-synthetic modification (*cf.* chapter 1.5). The chemical modification of a pre-formed MOF is usually incomplete and, thus, results in a mixed-linker MOF. Wang and Cohen published the first report of post-synthetic modification on IRMOF-3, where 80% of the amine groups were partially modified with acetic anhydride (Scheme 1).[79]

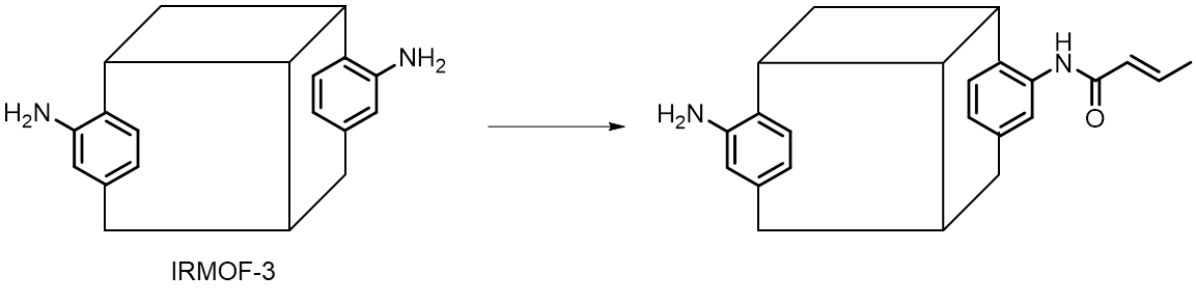

Scheme 1. Partial post-synthetic modification of IRMOF-3 with acetic anhydride by Wang and Cohen. Adapted with permission from [79]. Copyright 2007 American Chemical Society.

In the meantime, various mixed-linker MOFs have been published based on the structures of, *e.g.*, MOF-5[73,74,77,80], MIL-53(Al)[78,81-84], UiO-66/67[64,65,67,68,71] or DUT-5[45,46]. These materials featured tunable properties that allowed the synthesis of tailored materials for applications like gas adsorption, gas separation or heterogeneous catalysis. Gotthardt *et al.* have synthesized a mixed-linker MIL-53(Al)-NH_2 material with defined amounts of amine groups, which were used for post-synthetic modification and subsequent palladium immobilization. Due to the lower amine content, the materials featured a higher porosity resulting in a better accessibility of substrate molecules during the catalytic process.[85]

Several characterization methods can be used to obtain a qualitative proof for the incorporation of the different linkers into the framework structure. Powder X-ray diffraction, which represents one of the most important standard techniques, is used to show that single phases are present.[86,87] Kleist *et al.*[77,78] and the group of Kitagawa[88] could identify the linker distribution by the use of high-resolution XRD methods using the Vegard's law[89]. Further qualitative analysis can be done *via* IR spectroscopy[90,91], TG analysis[46,85], XPS[92,93], XAS[94] or solid state NMR spectroscopy of digested samples[45,81,95]. Liquid phase NMR spectroscopy has become the routine method to determine linker ratios qualitatively as well as quantitatively for mixed-linker MOFs.[65,74,85]

1.5 Post-synthetic modification (PSM)

Altering the physical and chemical properties of metal-organic frameworks *via* functionalization of their pores might be beneficial for several applications. So far, functional groups have been incorporated into MOFs using functionalized organic linkers during the direct solvothermal synthesis. This 'prefunctionalization' has resulted in MOF materials bearing *e.g.*, -NH_2, -Br, -CH_3 or other 'simple' substituents.[74] However, the variety of functional groups, which can be introduced *via* direct synthesis, is limited due to the fact that not all

functionalized groups are compatible with the reaction conditions such as high temperatures or pressures, which are required to obtain the desired crystalline phases. Furthermore, due to steric hindrances, the incorporation of larger and/or complex functional side groups at the organic linker could prevent the formation of the targeted framework structure or lead to a completely different topology, since the functionalities are able to coordinate to the framework metal centers.

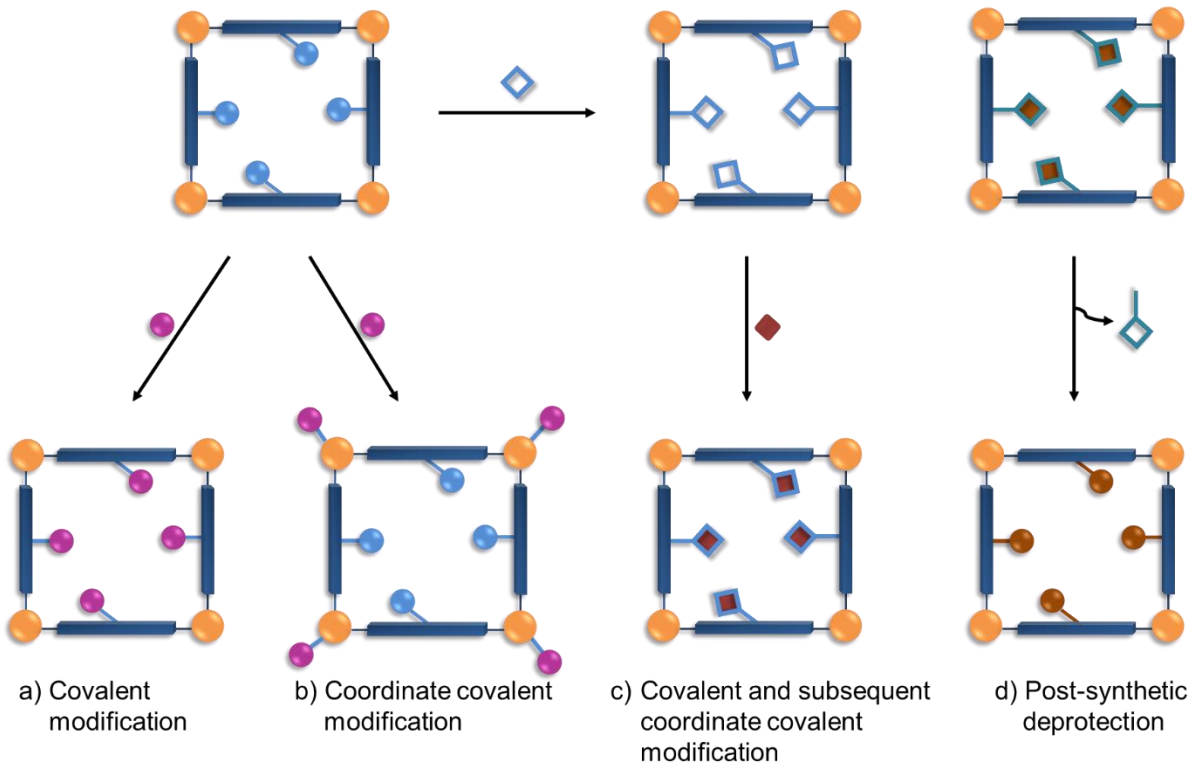

Figure 8. Representation of the covalent modification (a), coordinate covalent modification (b), the combination of covalent and covalent coordinate modification (c) (reproduced from [96] with permission from The Royal Society of Chemistry) and the post-synthetic deprotection (d). (Adapted with permission from [97]. Copyright 2012 American Chemical Society).

Since the 1990s, post-synthetic modification (PSM), which describes the chemical modification of MOFs after it has been synthesized, has become a groundbreaking method to functionalize MOFs. In the meantime, a large number of reviews have been published by the group of Cohen and others.[96-101] The post-synthetic modification approach enables a better control over the type and the number of incorporated functional groups into the framework. The 'postfunctionalization' is generally achieved without affecting the overall stability of the framework.

The strategies of post-synthetic modification can be divided into two main categories (Figure 8). 'Covalent modification' is defined as the chemical modification of the organic linker of the MOF (Figure 8a), by which a wide range of complex groups can be introduced into the metal-organic frameworks. In the case of a 'coordinate covalent modification', also called dative PSM, either a coordinating ligand can be introduced into the framework to bind to unsaturated metal nodes of the secondary building unit (Figure 8b) or a metal can be incorporated onto a chelating linker. Furthermore, covalent and coordinate modification can be used in a tandem reaction (Figure 8c). In a first step, the organic linker can be modified to obtain a chelating side group that can be metalated in a second step. Another known method is the post-synthetic deprotection (PSD), which cleaves the chemical bond within the framework resulting in a chemical functionality providing different properties (Figure 8d).

1.5.1 Post-synthetic modification of amine-functionalized MOFs

Among all functionalities, amine groups incorporated into the MOF structure are most commonly used for PSM reactions due to their wealth of possible chemical transformations. Amine functionalities can be easily incorporated into the framework without disrupting the formation process and do not participate in the coordination to the SBU. Wang and Cohen performed the first detailed study of a PSM reaction using amine-tagged IRMOF-3 with acetic anhydride resulting in an amide group (*cf.* Scheme 1).[79] Afterwards, several articles were published, which described the PSM of amine-functionalized MOFs with anhydrides.[102-106] Garibay *et al.* modified MIL-53(Al)-NH_2 with various anhydrides and showed that a partial modification of the amine groups was obtained *via* NMR spectroscopy (Scheme 2). The modification with succinic anhydride and maleic anhydride resulted in 40-43% conversion, whereas the modification with formic anhydride yielded a conversion of 95%.[103]

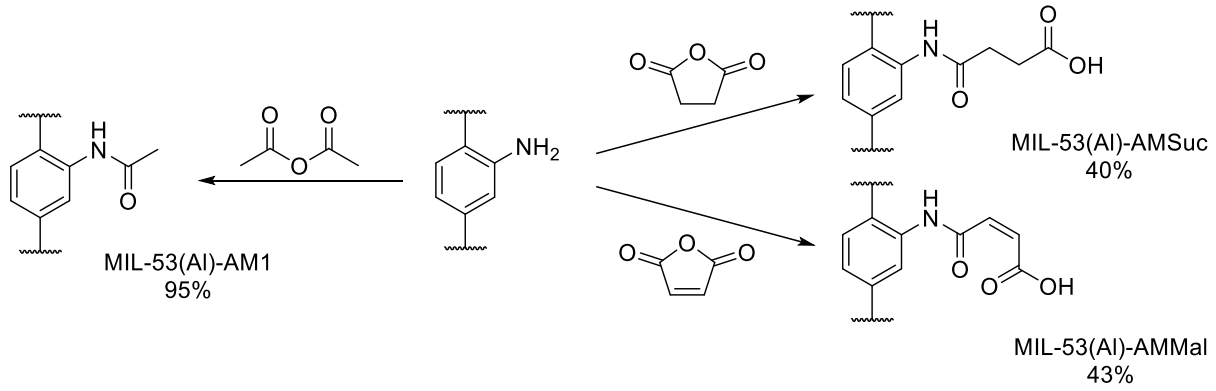

Scheme 2. Post-synthetic modification reactions of MIL-53(Al)-NH_2 performed by Garibay et al.[103]

Apart from the PSM reaction with anhydrides, Sánchez Costa *et al.* presented the synthesis of MOF-LIC-1, whose amine functionalities were used for a PSM reaction with isocyanates.[107] Volkringer *et al*. transformed the amine groups of MIL-53(Al)-NH_2 into isocyanates or isothiocyanates, which were converted into urea or thiourea groups in a second step.[108] A further commonly used group of reactants for post-synthetic modification approaches are aldehydes. Haneda *et al*. performed the transformation of an amine-tagged MOF with an acetaldehyde into an imine group.[109] A tandem condensation-reduction process was executed by Burrows and Kenaan. The primary amine of IRMOF-3 was modified with an aldehyde, which was reduced with $NaBH_3CN$ to a secondary amine to improve the stability of the functionalized MOF.[110] In a report of Rosseinsky, the combination of covalent and dative modification was used on IRMOF-3. The reaction between the amine groups and salicylaldehyde in toluene resulted in a Schiff base group. ^{1}H NMR analysis revealed that after 7 days reaction time 40% of the amine groups were modified. The obtained IRMOF-3-Sal was metalated with $VO(acac)_2 \bullet H_2O$.[111]

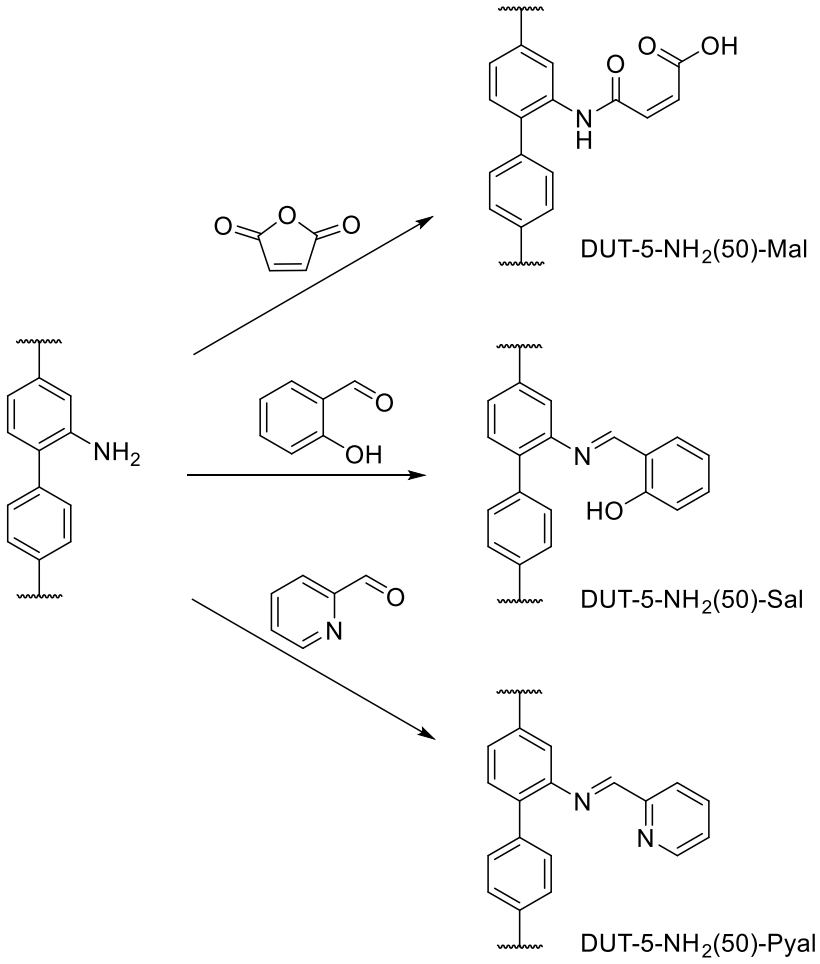

Scheme 3. Post-synthetic modification reactions of MIXDUT-5-amine(50) with maleic anhydride, salicylaldehyde and 2-pyridinecarboxaldehyde by Gotthardt et al.[46]

Schiff bases are easily synthesized and the resulting chelates form complexes with almost all metal ions, which are interesting for catalytic applications. Based on the work of Rosseinsky, several reports have followed up, which described the formation of chelating groups to generate engineered metal sites within the framework materials (*cf.* chapter 1.5.3 for more details).

Aldehydes like salicylaldehyde or 2-pyridinecarboxaldehyde are frequently used for PSM reactions of metal-organic frameworks producing bidentate side groups, which can be used for a subsequent metal immobilization. Gotthardt *et al.* used mixed-linker DUT-5-NH_2(50) materials for the post-synthetic modification with maleic anhydride, salicylaldehyde and 2-pyridinecarboxaldehyde resulting in bidentate ligands without changing the framework structure or significantly decreasing the porosity of the materials (Scheme 3).[46]

1.5.2 Post-synthetic modification of MOFs *via* click reaction

Recently, click reactions between terminal alkynes and azides have emerged as an interesting approach due to their capability of introducing complex organic or organometallic compounds into the framework structure (Scheme 4). Click reactions are generally performed according to the Cu(I)-catalyzed Huisgen 1,3-dipolar cycloaddition (CuAAC)[112], which yields 1,2,3-triazoles, but catalyst-free variants of this reaction are also known[112].

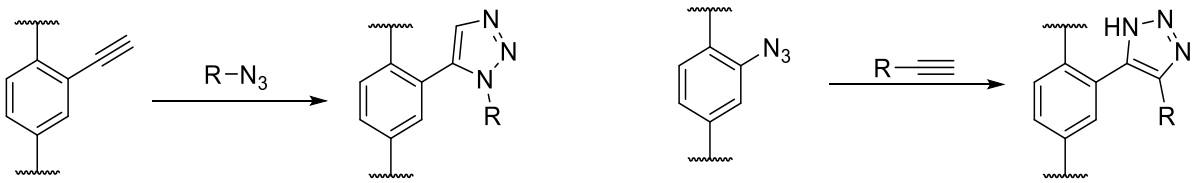

Scheme 4. Post-synthetic modification of alkyne- and azide-functionalized MOF materials via click reactions

Click reactions on MOFs have first been studied by Goto *et al*. in 2008, where N_3-MOF-16 bearing azide functionalities was clicked with different alkynes. The reaction was monitored *via* IR spectroscopy under observation of the stretching bands of the azides and alkynes functionalities. The formation of the corresponding triazole derivative was proven *via* ^{1}H NMR spectroscopy.[113] Gadzikwa *et al*. reported click chemistry on an alkyne-functionalized Zn-MOF. The alkyne groups were protected with tetramethysilane (TMS), which was first removed post-synthetically using a fluoride source. Afterwards, the free alkyne groups were modified with the fluorescent dye ethidium bromide monoazide (Scheme 5a).[114] Savonnet *et al.* performed a one-pot synthesis of DMOF-NH_2, which was converted to an azide-bearing MOF and subsequently modified *via* copper-catalyzed click chemistry with phenylacetylene. The

resulting frameworks showed decreased porosity, which the authors explained by a slight decomposition of the framework. However, a direct conversion of the amine to the azide and subsequently to the triazole seems to be a promising approach (Scheme 4b).[115] The click modification of UiO-67-N_3 with different alkyne compounds was carried out by Yi *et al*. and the resulting materials were used as catalysts in the Knoevenagel condensation. The authors reported that the azide-functionalized 4,4'-biphenyldicarboxylate linker underwent an *in situ* thermocyclization forming a carbazole during the synthesis.[116] This observation has been found also by Gotthardt *et al*. during the synthesis of DUT-5-N_3. Consequently, post-synthetic click reactions of 2-alkyne-4-biphenyldicarboxylate functionalized MOFs should be more efficient. Gotthardt *et al.* applied DUT-5-alkyne(50) in a copper-catalyzed click reaction with 2-pyridine azide. However, characterization results revealed a very low porosity and, thus, the material might be not stable under the used reaction conditions.[46]

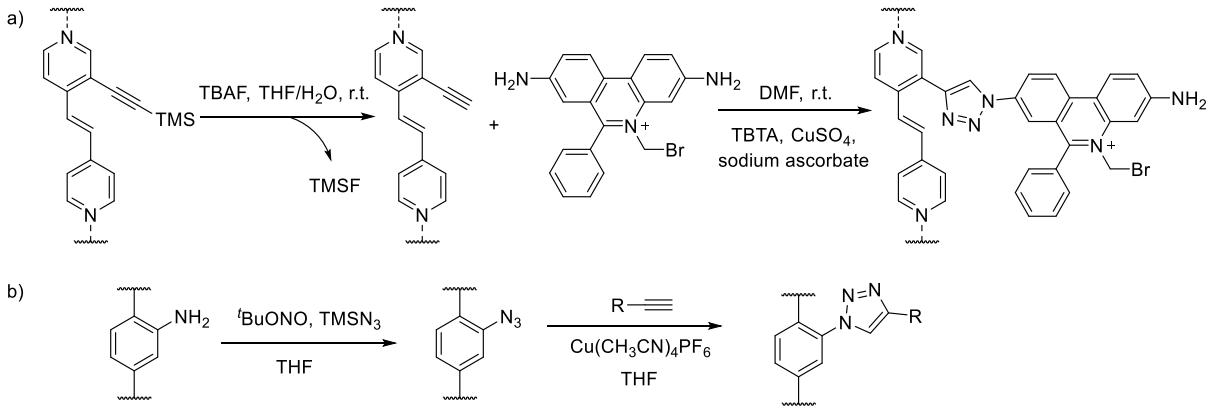

Scheme 5. Post-synthetic modification of alkyne-functionalized MOF via click chemistry by Gadzikwa et al.[114] (a) and one-pot PSM reaction of DMOF-NH_2 by Savonnet et al.[115] (b).

1.5.3 Immobilization of metals on metal-organic frameworks

The incorporation of defined metal complexes *via* post-synthetic modification approaches can be carried out using two different strategies.[117] One approach includes the use of chelating linker molecules, which are available for direct immobilization of additional metal ions. This strategy was introduced by the group of Lin using an axially chiral bridging ligand (*R*)-6,6'-dichloro-2,2'-dihydroxy-1,1'-binaphthyl-4,4'-bipyridine (**1**), whose dihydroxy functional groups were metalated with $Ti(O^iPr)_4$.[118] Furthermore, metal-containing MOF materials have been developed by using chelating linker molecules containing thioether (**2**)[119], *N*-heterocyclic carbene (**3**)[120], or bipyridine (**4**, **5**)[41,121] or porphyrine (**6**) moieties[122,123] (Figure 9).

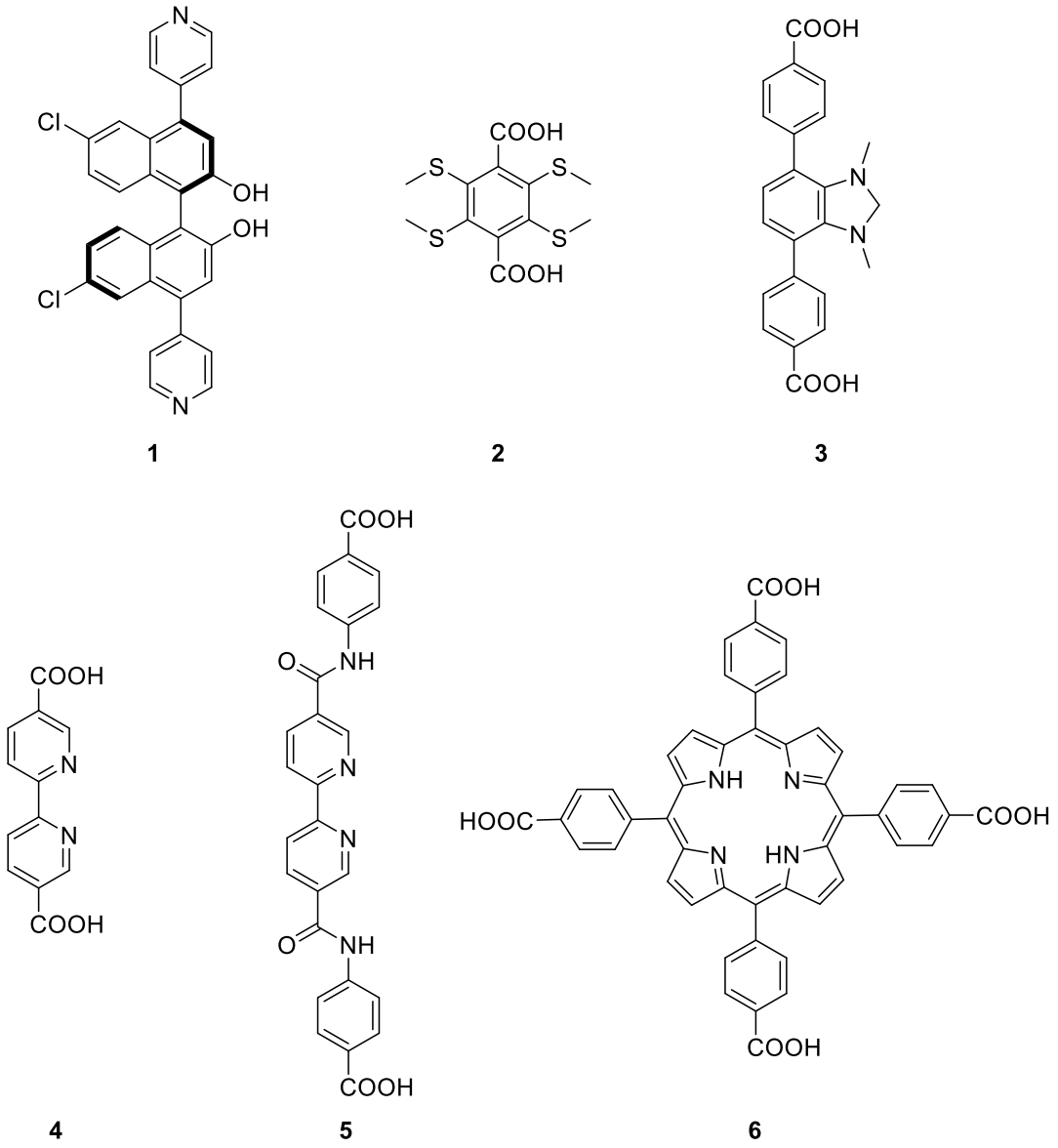

Figure 9. Organic linkers with potential metal binding sites used for post-synthetic modification approaches. Reproduced from [117] with permission from The Royal Society of Chemistry.

Since 2,2'-bipyridine-5,5'-dicarboxylic acid (**5**) represents a robust and rigid chelating linker, it has been applied in various works. 2,2'-Bipyridine-5,5'-dicarboxylate (abbreviated as BPyDC, bpy or bipy) was first applied in the framework synthesis of MOF-253, which was used for the post-synthetic complexation of palladium and copper ions.[41,52-54,124] Martín-Matute and co-workers reported the immobilization of $[Ru(bpy)Cl_3(dmso)]$ within the MOF-253 structure (Scheme 6). They prepared two samples, in which the BPyDC linkers were loaded with either 7 mol% or 13 mol% of ruthenium. While the product with the lower ruthenium loading retained its porosity with S_{BET} = 1145 m^2/g, the material containing 13 mol% ruthenium had a very low BET surface area of 80 m^2/g. The ruthenium-containing MOF-253 materials were then used to catalyze oxidation reaction of alcohols.[51] UiO-67

containing BPyDC linkers in single- or mixed-linker variants have also been used for post-synthetic metalation approaches and applied in heterogeneous catalysis.[64,65] UiO-67 materials with incorporated Ir-, Re-, Ru-, and Rh-bipyridine complexes have been used for various photocatalytic reactions.[66,68,125] In addition, molybdenum or iridium were incorporated into a gallium-based metal-organic framework (COMOC-4), which was applied as heterogeneous catalyst for aerobic oxidation reactions.[126,127]

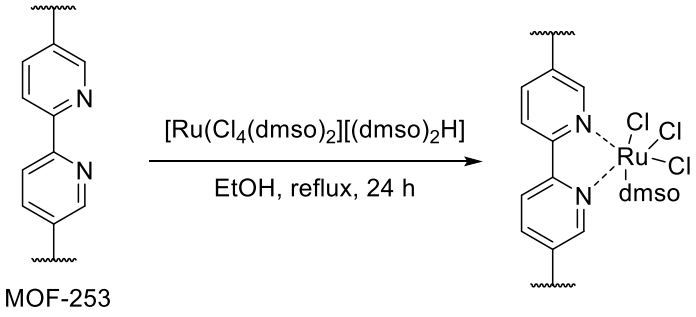

Scheme 6. Schematic representation of ruthenium complexation in MOF-253 performed by Carson et al.[51]

Another strategy represents the post-synthetic introduction of chelating side groups into the framework. As mentioned before, the cornerstone of this strategy was laid by Rosseinsky and co-workers by forming a Schiff base complex *via* two-step post-synthetic modification.[111] Doonan *et al*. performed the modification of UMCM-1-NH_2 with 2-pyridinecarboxaldehyde and metalated the MOF using $PdCl_2(CH_3CN)_2$. After the two-step PSM reaction, the BET surface area dropped from 3200 to 1700 m^2/g and the palladium incorporation was examined by X-ray absorption spectroscopy (XAS).[128] Liu *et al*. inserted nickel to a series of mixed-linker zinc-based MOFs using an imino-pyridine nickel complex.[129] UiO-66- and UiO-67-NH_2 was treated with aldehydes, which were subsequently used for the immobilization of copper[130], palladium[131] or cobalt[132] ions. The formation of *N,N,N*-pincer ligands within the frameworks of IRMOF-3 and UiO-66-NH_2 was employed by the group of Corma, which were then used for the immobilization of iridium. The resulting iridium-based catalysts were subsequently applied in the hydrogenation of aromatic compounds.[133,134]

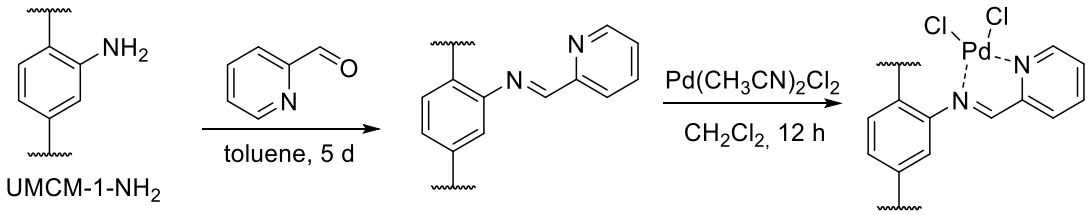

Scheme 7. Two-step post-synthetic modification of UMCM-1-NH₂ by Doonan et al.[128]

Beside Schiff base reactions between aldehydes and amines, treatment of amine groups with cyclic anhydrides, which results in salicylate and pyrazine dicarboxylate chelating groups, was reported as an alternative approach by Tanabe and Cohen (Scheme 8). Both modified MOFs were subsequently used to immobilize iron and copper using $Fe(acac)_3$ and $Cu(acac)_2$ as precursor salts. Atomic absorption spectroscopy (AAS) revealed a metal content of 0.77 wt% of Fe^{3+} and 1.76 wt% of Cu^{2+}, which corresponded to ≈50% metalation of the available chelating groups within the frameworks.[104] Gotthardt *et al*. modified amine-containing MIL-53(Al) with maleic anhydride, which was used for a subsequent palladium immobilization. The obtained palladium-containing MIL-53(Al) materials were used as heterogeneous catalysts in Heck-type C-C coupling reactions.[85,135]

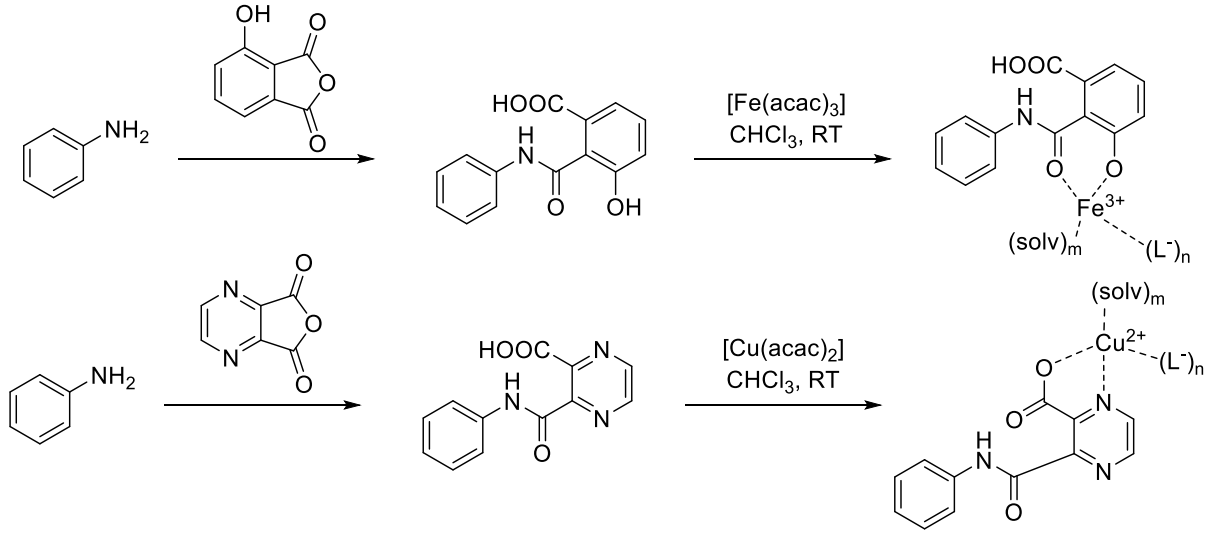

Scheme 8. Post-synthetic modification of UMCM-1-NH₂ by Tanabe and Cohen.[104]

1.6 Applications of metal-organic frameworks in catalysis

1.6.1 Incorporation of active centers in metal-organic frameworks

Due to their high crystallinity, porosity and structural diversity, metal-organic frameworks are promising materials for various applications like catalysis, gas separation or adsorption[136,137] or biomedicine[138], as well as for applications in the field of porous magnets[139] or luminescent sensors[140]. Catalysis was one of the earliest proposed as well as demonstrated applications for metal-organic frameworks.[141,142] In the meantime, a large variety of reviews exist, which provide extensive insight on the catalytic potential of MOF-based catalyst materials.[143-157] In contrast to other porous materials, metal-organic frameworks offer many advantages, especially as single-site catalysts. In particular, they can combine the advantages of heterogeneous and homogeneous catalysis. On the one hand, they are well recyclable after catalytic runs and, on the other hand, they might behave like well-defined homogeneous metal complexes. Nevertheless, highly robust structures with high thermal and chemical stability are required, which can tolerate the conditions during catalytic reactions.

As mentioned above, metal-organic frameworks can be tailored for specific applications. Thus, catalyst materials can be generated with well-defined active sites within the framework *via* different strategies. Various possibilities to locate catalytically active sites at various positions within the framework can be exploited, which are schematically illustrated in Figure 10. Five different approaches can be distinguished: encapsulation of nanoparticles in the pores (**I**), unsaturated metal sites (**II**), functionalized open metal sites (**III**), functionalized linker molecules (**IV**) and modified linker molecules containing transition metal complexes (**V**).[157] Except for the encapsulation of nanoparticles (**I**), these approaches (**II** – **V**) result in single-site catalysts.

I) Metal-organic frameworks are able to act as a host matrix without any covalent interaction for guest species like enzymes, metal complexes or nanoparticles (MNPs). In the case of MNPs incorporated in MOFs, there are numerous studies on different framework structures.[158-160] Different methods have been used for the incorporation including the approaches "ship-in-a-bottle" or "bottle-around ship"[160,161], chemical vapor deposition (CVD) techniques[162-164], liquid-phase impregnation[165-168] or solid grinding with organometallic complexes[169]. Although synergistic effects between MNPs and MOFs have been observed, transport limitations can occur due to restricted diffusion within the framework.[170]

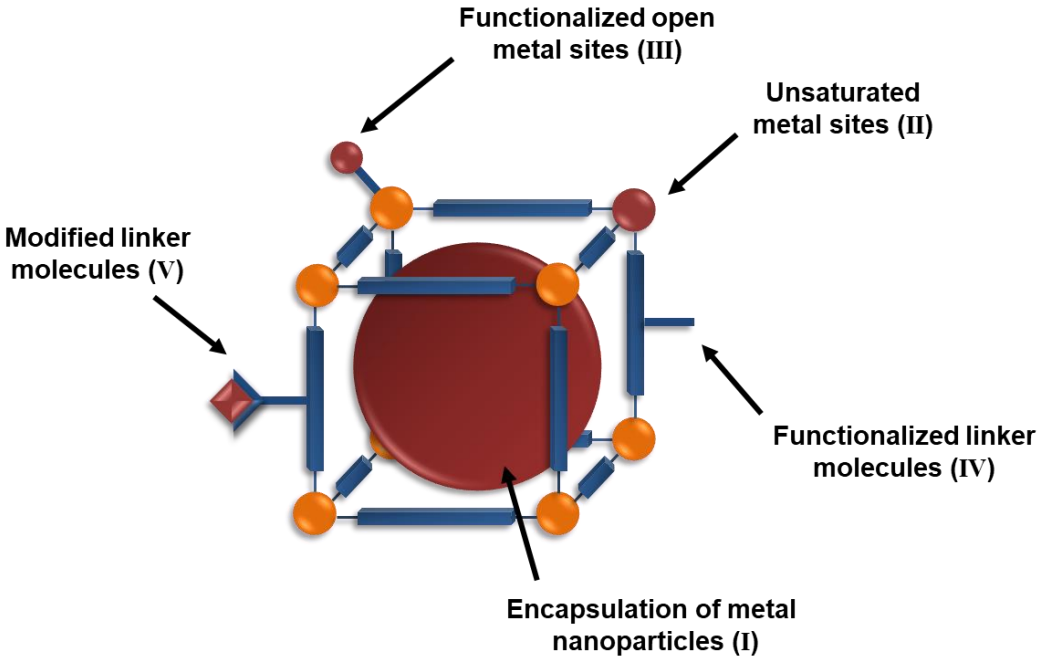

Figure 10. Different strategies for the incorporation of active sites inside a metal-organic framework.

II) The metal ions in MOF lattices require free coordination sites to be catalytically active. These unsaturated active sites are usually occupied by solvent molecules, which can be removed upon heating. HKUST-1, which possesses open Cu^{2+} sites upon the removal of coordinated water molecules, is a classic example for the utilization of unsaturated metal centers in catalysis.[171,172] In addition, MIL-101(Cr), which consists of Cr^{3+} octahedral clusters, showed a superior activity in catalysis than HKUST-1 due to the higher Lewis acidity of Cr^{3+} compared to Cu^{2+}.[173] Unsaturated active sites can also be generated by engineering structural defects into the framework structure.[174] The group of De Vos showed that the use of trifluoroacetic acid (TFA) and HCl for the synthesis of UiO-66 resulted in a highly crystalline material, in which the BDC linkers were partially substituted by TFA. The resulting material was highly active in several Lewis acid catalyzed reactions.[175]

III) Unsaturated metal sites within the framework structure allow for post-synthetic modification with catalytically active species (coordinate covalent modification, *cf.* chapter 1.5). Organic molecules, such as amine groups[176] or chiral molecules[177] can be used to coordinate to the unsaturated metal sites. Additionally, metal complexes can be employed to obtain heterogeneous single-site catalysts.[178-181]

IV) Metal-organic frameworks bearing simple functionalized linker molecules may also be catalytically active. Functional groups, such as amine[182], amide[183], pyridyl[184] or

sulfoxy[185,186], can be used as active sites for organocatalysis and they can be introduced *via* direct synthesis into the framework structure. Brønsted acid catalysts have been synthesized using MIL-101(Cr) with sulfonic acid as well as carboxylic acid groups, which showed high catalytic activity in hydrolysis or ring-opening reactions.[186,187] Basic catalysts can be obtained by using pyridyl, amide or amine groups incorporated into metal-organic frameworks, and such systems have been employed in Knoevenagel condensation or transesterification reactions.[155] Liu *et al.* presented a new MIL-101 material, which was dually functionalized with amine and sulfone groups possessing a basic and an acid active site within one material that was then used to catalyze a one-pot deacetalization Knoevenagel condensation (Scheme 9).[92]

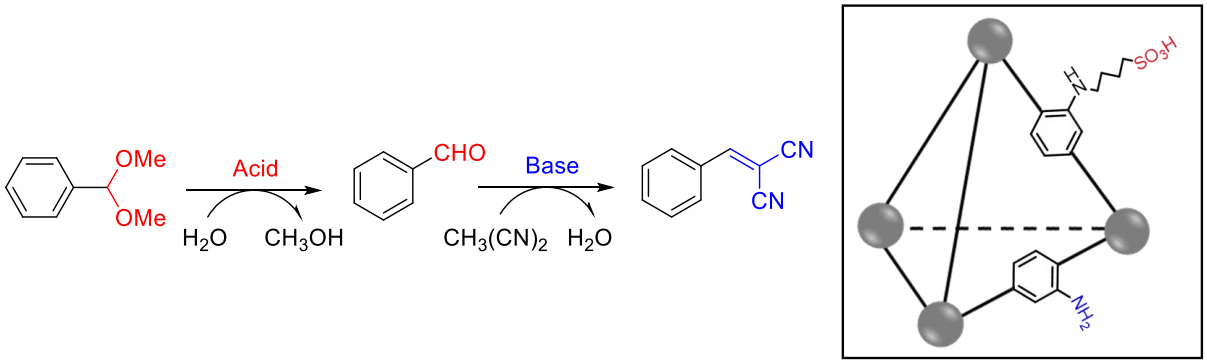

Scheme 9. Tandem deacetalization and Knoevenagel condensation catalyzed by dually functionalized UiO-66 reported by the group of Gao. Adapted with permission from [92], Copyright 2016 American Chemical Society.

In addition to the acidic and basic catalysis over MOFs, asymmetric catalysis can be performed by using chiral bridging ligands, such as BINOL (1,1'-bi-2-naphtol), as linker to form MOFs.[118,188]

V) The insertion of catalytically active metal centers requires the introduction of chelating moieties into the MOF structure either *via* the utilization of chelating linkers for the direct synthesis or *via* post-synthetic introduction of chelating side groups into the framework. Since synthetic strategies and various examples of metal-functionalized MOF materials have been discussed in chapter 1.5.3, this topic will be not explicitly discussed in this chapter. Various metal-organic frameworks, which were metalated at chelating moieties *via* post-synthetic modification reactions, have already been applied as catalysts in different chemical syntheses, such as C-C coupling [52,64,85,135] or oxidation reactions[189].

1.6.2 Metal-organic frameworks as catalysts in oxidation reactions

Selective oxidation reactions are of key importance for the chemical industry, since chemicals or intermediates such as alcohols, epoxides, aldehydes, ketones and organic acids are produced, which are starting materials for many synthetic routes.[190] Among oxidizing agents, hydrogen peroxide, organic hydroperoxides and molecular oxygen are the most important ones avoiding toxic stoichiometric oxidants due to the green chemistry.[191,192] Hydrogen peroxide has a high oxygen content and forms water as the only byproduct, which makes this reagent to an almost perfect oxidant. Nevertheless, the lack of miscibility in organic solvents and the high costs should be considered. Contrary, organic hydroperoxides are soluble in most organic solvents, but they are relatively expensive and form additional organic waste products. Molecular oxygen is environmental friendly and cheaper, however, highly active transition metal catalysts are required for the activation of this oxidizing agent.[193] Metal-organic frameworks are suitable catalyst materials to overcome this issue, since highly active single-site metal centers are available, which are dispersed over a very large surface area.[194]

1.6.2.1 Epoxidation reactions

The conversion of olefins into epoxides is industrially important for a wide range of industrial applications as feedstocks for high added value products. Various examples for the olefin epoxidation are known using metal-organic frameworks with different transition metals. A copper-catalyzed reaction was reported by Brown *et al*.[195] They used $[Cu(H_2btec)(bpy)]_\infty$ (H_4btec = 1,2,4,5-benzenetetracarboxylic acid) as catalyst for the epoxidation of cyclohexene and styrene with *tert*-butyl hydroperoxide (TBHP) as oxidant resulting in 65% conversion of cyclohexene and 24% of styrene with high turnover numbers up to ≈1900 (Scheme 10a). A titanium-based material was applied as catalyst in the epoxidation of propylene and other alkenes, where it showed a high selectivity towards the epoxide in combination with TBHP.[196] Leus *et al.* employed vanadium-containing MIL-47 in the cyclohexene epoxidation, also with TBHP as oxidant (Scheme 10b). With a conversion up to 50%, the heterogeneous vanadium catalyst showed similar catalytic activity as the homogeneous vanadium complex $VO(acac)_2$.[197] An iron-based MIL-101 has been reported as heterogeneous catalyst for the oxidation of alkenes using hydrogen peroxide as oxidant. Different alkenes were used including limonene, α-pinene, styrene, stilbene, etc., resulting in high epoxide selectivities.[198]

Manganese exhibits a high activity for the alkene epoxidation, which has its origin in the Jacobsen epoxidation reaction pioneered by Eric N. Jacobsen[199] and Tsutomu Katsuki[200]

using a manganese(III)-salen catalyst. Hupp and co-workers synthesized a metal-organic framework compound featuring chiral (salen)Mn struts, which showed to be an effective catalyst for asymmetric epoxidation reactions.[201] Bhunia *et al.* reported the formation of a 1D coordination polymer with Mn–salen units, which were applied as catalysts in the epoxidation of *trans*-stilbene using molecular oxygen as oxidant.[202] Furthermore, Bhattacharjee *et al.* immobilized a manganese(II) acetylacetonate complex into IRMOF-3 *via* a one-step post-synthetic route and used it as heterogeneous catalyst for the epoxidation of cyclohexene, cyclooctene and styrene with pivalaldehyde and oxygen as oxidant (Scheme 10c).[203]

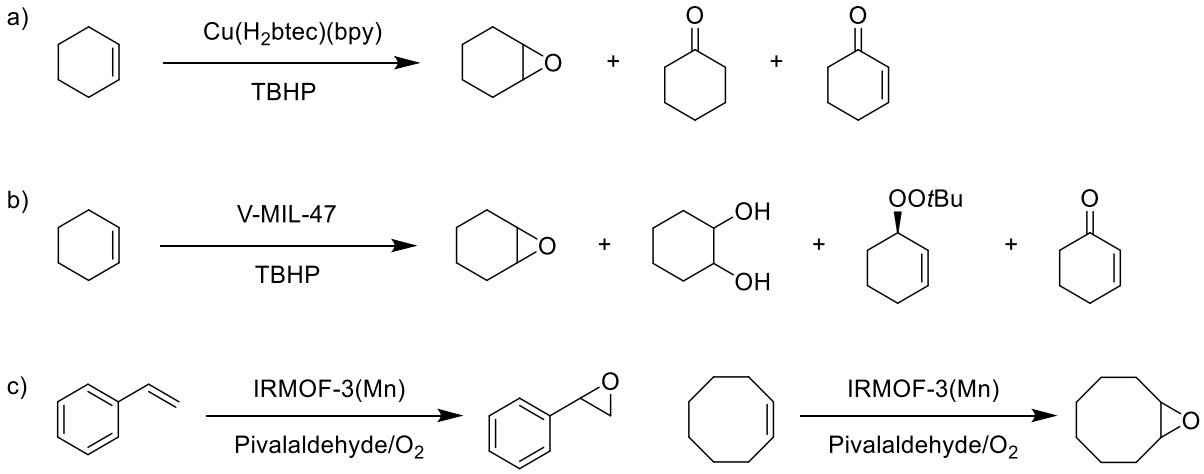

Scheme 10. Epoxidation of olefins catalyzed by copper[195], vanadium[197] and manganese[203].

Cobalt-based metal-organic frameworks have been reported as promising catalysts for the oxidation of cyclohexene using TBHP.[204,205] In the presence of molecular oxygen, Beier *et al.* performed the epoxidation of stilbene using STA-12(Co) as the catalyst, resulting in stilbene oxide as the main product and benzaldehyde as the only side product.[206] Mechanistic studies were executed using *in situ* electron paramagnetic resonance (EPR) and X-ray absorption spectroscopy (XAS) analysis. The studies showed that benzaldehyde exhibited a promoting effect with regard to the activation of the active site (Scheme 11, step **1**). The activated Co^{II} sites react with oxygen resulting in Co-superoxo radicals (step **2**). Further reaction with stilbene affords an intermediate complex (step **3**), which forms stilbene oxide in the next step (step **4**). In step **5,** the regeneration of the catalyst from the Co^{III} species proceeds through the oxidation of the amide solvent, which indicated a strong influence of the solvent.

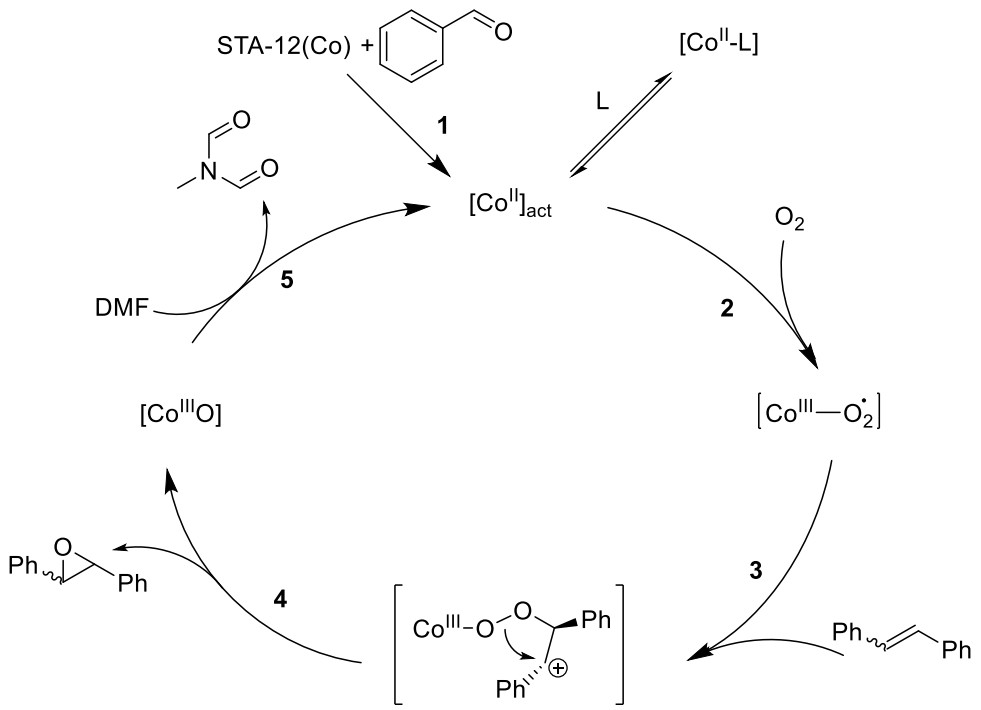

Scheme 11. Proposed reaction mechanism for the epoxidation of stilbene catalyzed by cobalt reported by Beier et al. Adapted from [206]. Copyright © 2012 Wiley-VCH Verlag GmbH & Co. KGaA Weinheim.

1.6.2.2 Alcohol oxidation reactions

The catalytic oxidation of primary or secondary alcohols to aldehydes or ketones represents one of the most frequently used oxidation reactions in the organic chemistry. Due to their properties and chemical reactivity, the resulting carbonyl compounds are appropriate starting materials for various synthetic methods.[194] Llabrés i Xamena *et al.* presented a palladium-containing MOF material, which was applied in the aerobic oxidation of cinnamyl alcohol resulting in a total conversion after 20 h with a 74% selectivity to cinnamylaldehyde. Nevertheless, it was shown that the palladium catalyst also promoted undesirable side reactions, like polymerization and C=C double-bond isomerization, which explained the low selectivity of the reaction.[207] Proch et al. used Pt@MOF-177 as a catalysts in the solvent- and base-free oxidation of different allylic and aliphatic alcohols at room-temperature with air as oxidant and the authors obtained high selectivities (Scheme 24a). Recycling tests showed that the XRD patterns were no longer similar to the patterns of MOF-177 after the first test run and the catalyst showed almost no activity in the second run. The authors explained this by the now inaccessible platinum particles in the destroyed host.[208] Haruta and co-workers used several MOFs, such as MOF-5, MIL-53(Al) or $Cu_3(BTC)_2$, for the insertion of gold nanoparticles inside the pore structures and used them as catalysts for the oxidation of benzyl alcohol and 1-phenylalcohol. The obtained results showed that the selectivity towards methyl benzoate was much higher than for

benzaldehyde.[169] The previously mentioned MOF-253-Ru synthesized by the group of Martín-Matute was employed in the oxidation of primary alcohols resulting in high conversions up to 99%.[51] Considering the observed transport limitations and also the high cost of the noble metals of these examples, the use of cheaper non-noble metals became more and more popular as catalysts in alcohol oxidation. Copper-catalyzed oxidation reactions were performed by the group of Garcia using $Cu_3(BTC)_2$ combined with TEMPO as co-catalyst, which proved to be an effective and reusable heterogeneous catalyst for the oxidation of benzyl alcohol under mild reaction conditions (Scheme 24b).[209]

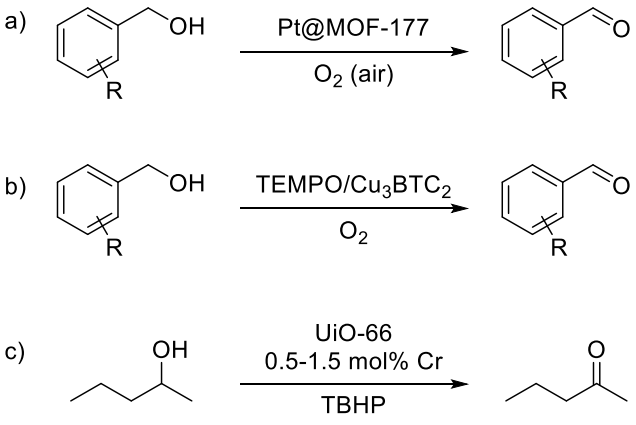

Scheme 12. Alcohol oxidation reactions catalyzed by platinum[208], copper[209] and chromium[210].

Hou *et al*. applied a post-synthetically modified copper-containing UiO-66, in which three different of copper(II) salts were immobilized, in the aerobic oxidation of primary aromatic alcohols using molecular oxygen as oxidant. Despite the same metal loading, UiO-66-Sal-$CuCl_2$ provided the highest conversion of 99% and selectivity of 99% compared to the immobilized $Cu(OAc)_2$ and $Cu(NO_3)_2$ salts.[130] Cohen and co-workers synthesized a chromium-containing UiO-66 material *via* post-synthetic deprotection (PSD) and post-synthetic exchange (PSE) (Scheme 24c). The obtained materials were applied in the oxidation of various alcohol substrates using a catalyst loading of 0.5 – 1.0 mol%.[210] However, as the above examples show, there are only a few examples, in which catalytically active single-site centers have been introduced into MOF structures *via* post-synthetic modification and applied as heterogeneous catalysts in oxidation reactions.

2 Motivation

Metal-organic frameworks represent an interesting class of materials for applications in catalysis due to their broad variety of accessible structures and remarkable properties. Their chemical and structural opportunities make them potential candidates for developing highly active and selective catalyst systems. The concepts of mixed-linker MOFs and post-synthetic modification (PSM) enable the synthesis of MOF materials with tailor-made properties adjusted for targeted applications. Thus, by a combination of these methods, metal-organic frameworks with well-defined and uniform metal sites can be developed, which facilitate a controlled metal distribution within the framework structure. The aim of the presented thesis was to design novel single-site catalyst materials based on metal-organic frameworks and to investigate those new catalyst materials in relevant test reactions in liquid-phase.

The first part of this work included the synthesis of mixed-linker DUT-5 materials with functionalized linkers, whose functional groups should be used to introduce well-defined metal complexes into the pores of these framework materials *via* post-synthetic modification approaches. First, mixed-linker DUT-5 bearing various amounts of 2,2'-bipyridine-5,5'-dicarboxylate (BPyDC) linkers should be prepared, whose bipyridine moieties should be subsequently used for the direct immobilization of metal ions, such as palladium, nickel, copper, cobalt and manganese (Scheme 13, structure **A**). Next, amine-functionalized carboxylate linkers should be applied for the synthesis of functionalized mixed-linker MIL-53 and DUT-5 structures. Mixed-linker MIL-53 containing equal amounts of 1,4-benzenedicarboxylate (BDC) and 2-aminobenzyl-1,4-dicarboxylate (ABDC) linkers should be synthesized and post-synthetically modified (Scheme 13, structure **B**). Furthermore, DUT-5 materials with 10% of 2-amino-4,4'-biphenyldicarboxylate (ABPDC) and 5% of 2,2'-diamino-4,4'-biphenyldicarboxylate (dABPDC) should be prepared (Scheme 13, structures **C** and **D**). The amine groups of the resulting materials should be modified with anhydrides and aldehydes to obtain chelating side groups, which should be subsequently applied for immobilization of cobalt and manganese ions. In addition, a mixed-linker DUT-5 material containing 10% of 2-ethinyl-4,4'-biphenyldicarboxylate linkers should be prepared, whose alkyne groups should be modified *via* inorganic click reaction (iClick) with a gold azide compound (Scheme 13, structure **E**).

The resulting materials should be thoroughly characterized using various characterization techniques. Thus, the formation of crystalline MOF structure as well as the absence of undesired

phases should be proven using powder X-ray diffraction (PXRD), while the presence of undesired guest molecules in the pores should be excluded *via* ATR-IR spectroscopy. Furthermore, ATR-IR spectroscopy should be also used to verify qualitatively the incorporation of the functional groups. N_2 physisorption analysis should be performed to determine the specific surface areas and the pore volumes. NMR spectroscopy should be used to quantify the incorporated functionalized linkers of the mixed-linker MOF materials as well as the modification degree of the side groups. The metal content of the immobilized complexes should be determined *via* inductively coupled plasma optical emission spectroscopy (ICP-OES) measurements. X-ray absorption spectroscopy (XAS) should be performed to obtain information regarding the oxidation states and the local chemical environment of the immobilized metal centers. Thus, efforts should be made to prove the absence of undesired metallic or oxidic nanoparticles within the pore systems, in particular.

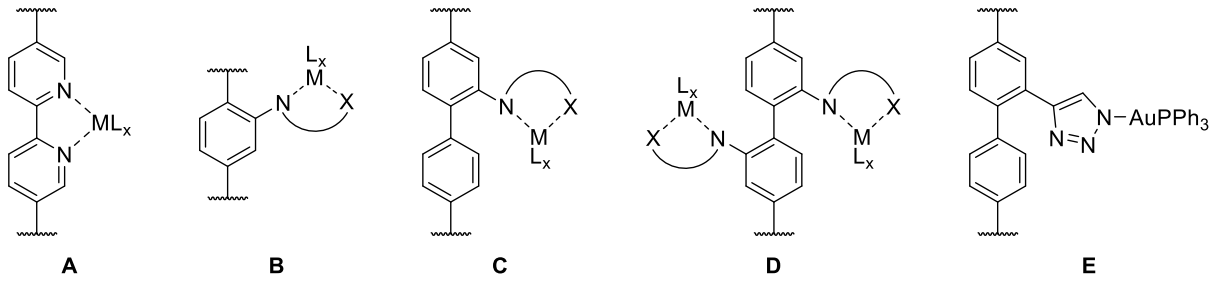

Scheme 13. Schematic representation of the targeted MOF based catalyst materials synthesized via post-synthetic modification.

In the second part of this work, the novel MOF materials should be applied as heterogeneous single-site catalysts in aerobic oxidation test reactions using air as oxidizing agent. The influence of different reaction parameters on conversion, yield and selectivity should be evaluated. Heterogeneity tests should be performed by recycling and hot filtrations experiments. First, the manganese-containing MIL-53 material should be tested in the aerobic epoxidation of α-pinene and its catalytic activity should be compared to its homogeneous counterpart. The cobalt- and manganese-containing DUT-5 materials should be applied in the aerobic epoxidation of *trans*-stilbene as well as in the oxidation of benzyl alcohol. Thereby, the activities and the selectivities of the different DUT-5 catalysts should compare with regard to the positioning of the metal centers.

3 Design of novel heterogeneous single-site catalysts *via* the post-synthetic immobilization of metal complexes

3.1 2,2'-Bipyridine containing DUT-5 materials

2,2'-Bipyridine is considered as one of the most widely used bidentate chelating ligand in transition metal coordination chemistry.[211] Its robust redox stability and the easy of functionalization made 2,2'-bipyridine popular for the design and synthesis of metal-bipyridine complexes. In this chapter, well-defined heterogeneous single-site catalysts with DUT-5 structure were synthesized using 2,2'-bipyridine-5,5'-dicarboxylate (BPyDC) as chelating linker. The mixed-linker approach was applied to control the metal loading. In the first section (chapter 3.1.1), the synthesis of DUT-5 bearing 0%, 10%, 25% and 100% 2,2'-bipyridine-5,5'-dicarboxylate linkers, respectively, is described. In the subsequent section (chapter 3.1.2), the synthesized DUT-5-BPyDC(10) materials were used for the immobilization of metals using palladium, manganese, nickel, copper and cobalt ions. All materials were thoroughly characterized using PXRD, ATR-IR, N_2 physisorption, TG, ^{1}H NMR, ^{13}C CP MAS NMR, ICP-OES and XAS after each synthetic step.

3.1.1 Synthesis and characterization of mixed-linker DUT-5-BPyDC

Mixed-linker metal-organic frameworks based on DUT-5 materials were synthesized under solvothermal conditions according to the literature procedure (Scheme 14).[40,46] The reaction of $AlCl_3 \cdot 6\ H_2O$ with the commercially available linker molecules 4,4'-biphenyldicarboxylic acid (H_2BPDC) and 2,2'-bipyridine-5,5'-dicarboxylic acid (H_2BPyDC) resulted in DUT-5 [Al(OH)(BPDC)], DUT-5-BPyDC(10) [$Al(OH)(BPDC)_{0.9}(BPyDC)_{0.1}$], DUT-5-BPyDC(25) [$(Al(OH)(BPDC)_{0.75}(BPyDC)_{0.25}$] and DUT-5-BPyDC(100) [Al(OH)(BPyDC)]. The syntheses were performed in a closed vessel under solvothermal conditions at 120 °C for 24 h.

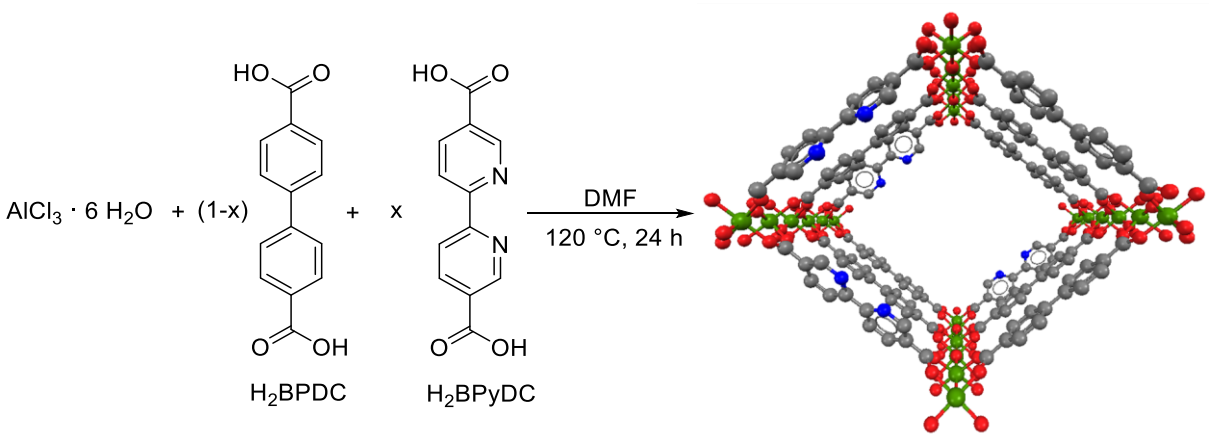

Scheme 14. Synthesis of mixed-linker DUT-5-BPyDC(x) (x = 0, 10, 25, 100); green: Al, red: O, grey: C, blue: N.

Powder X-ray diffraction (PXRD) measurements revealed similar reflection patterns for all materials (Figure 11). The incorporation of additional functionalized linkers did not prevent the framework formation and, thus, the structure of the bipyridine-containing mixed-linker materials proved to be isoreticular to DUT-5.

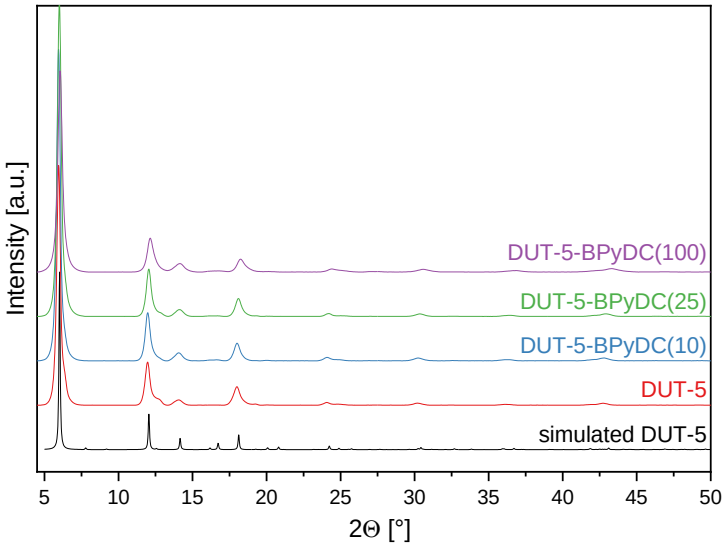

Figure 11. Powder X-ray diffraction patterns of DUT-5, mixed-linker DUT-5-BPyDC and DUT-5-BPyDC(100) materials.

ATR-IR spectroscopy was used to make sure that the pore systems were free from unreacted linkers or solvent molecules. To prevent the precipitation of unreacted linker molecules, the hot solvent was removed from the solid immediately after the reaction procedure and the obtained frameworks were washed with hot DMF. The resulting spectra demonstrated that no residual linkers (corresponding C=O stretching bands expected at around 1685 cm^{-1}) or to DMF (corresponding C=O stretching expected at around 1650 cm^{-1}) were visible (Figure 12a). This

observation proved that the pores were not blocked by any guest molecules and accessible for the following immobilization of metals. Moreover, ATR-IR was used to qualitatively prove the successful incorporation of the 2,2'-bipyridine functionalities based on the aromatic C=N vibrations at 1364 cm^{-1} corresponding to the bipyridine moiety (Figure 12b). The intensity of this band was more pronounced with increasing amount of the bipyridine linker amount.

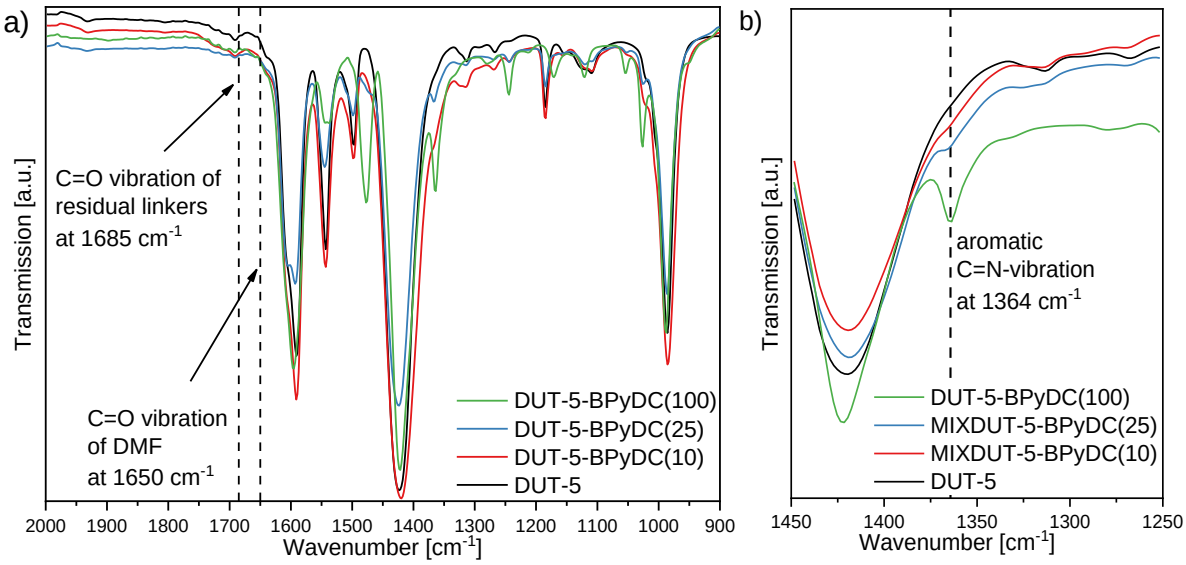

Figure 12. ATR-IR spectra of DUT-5, mixed-linker DUT-5-BPyDC and DUT-5-BPyDC(100) materials.

The results of nitrogen physisorption measurements showed that all materials were obtained with very high porosity (Table 1), which matched the specific surface area of S_{BET} = 1880 m^2/g and a pore volume of 0.81 cm^3/g for DUT-5[46] and S_{BET} = 2160 m^2/g and a pore volume of 0.89 cm^3/g for MOF-253[41] very well. A slight increase of the specific surface area with increasing bipyridine amounts was observed.

Table 1. BET surface areas (S_{BET}), total pore volumes (tpv) and micropore volumes (mpv) of DUT-5, mixed-linker DUT-5-BPyDC and DUT-5-BPyDC(100) materials.

Entry	Material	S_{BET} [m^2/g]	tpv [cm^3/g]	mpv [cm^3/g]
1	DUT-5	1880	0.81	0.61
2	DUT-5-BPyDC(10)	1920	0.77	0.67
3	DUT-5-BPyDC(25)	1980	0.78	0.62
4	DUT-5-BPyDC(100)	2000	0.88	0.76

Thermogravimetric analysis performed in air revealed that the framework decomposition started at 380 °C for all materials (Figure 13a). However, a shift of the minima in the DTA curves (Figure 13b) towards lower temperatures from 580 to 520 °C was observed for higher amounts of bipyridine functionalization, which confirmed the incorporation of both 4,4'-biphenyldicarboxylate and 2,2'-bipyridine-5,5'-dicarboxylate linkers qualitatively as well as the statistically distribution of the linkers within the framework structure.

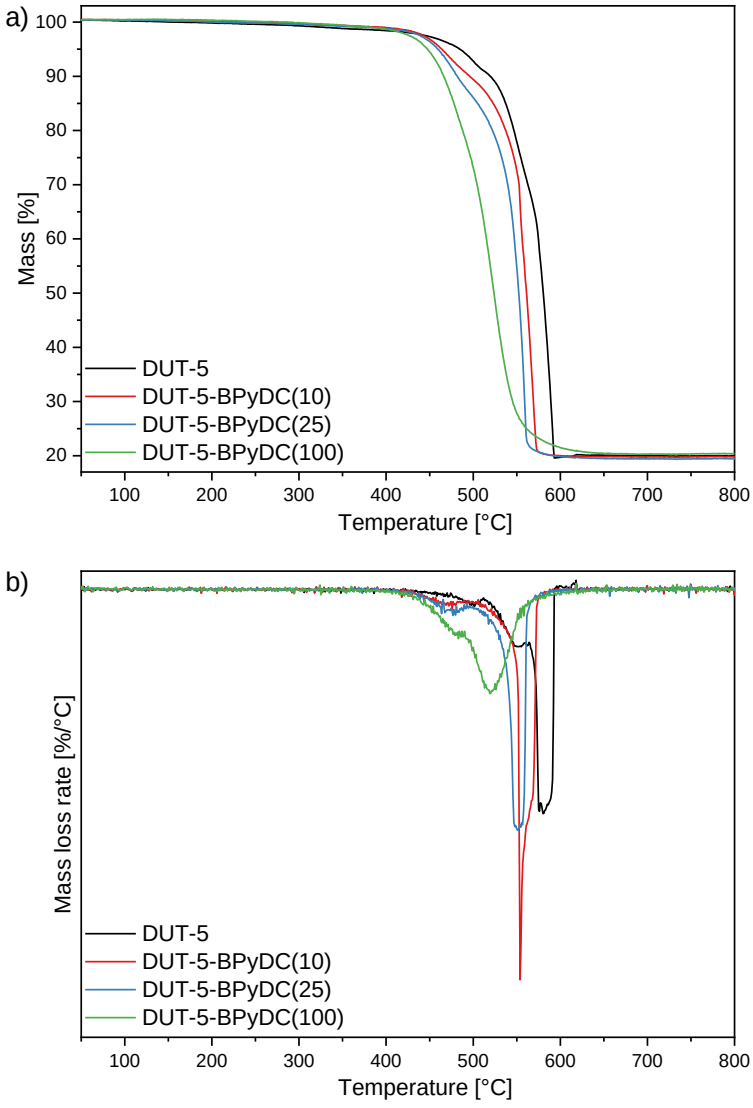

Figure 13. Thermogravimetric analysis (a) and derivative thermogravimetric analysis (b) of DUT-5, mixed-linker DUT-5-BPyDC and DUT-5-BPyDC(100) materials carried out in atmosphere.

For a further proof of the incorporation of the bipyridine linker molecules, solid state ^{13}C NMR spectra were recorded (Figure 14a). Five signals were found for the unfunctionalized DUT-5 material. The peaks at 125 and 130 ppm could be assigned to the carbon atoms of the aromatic rings and the peak at 172 ppm corresponded to the carbon atoms of the carboxylate groups.

With increasing substitution of 4,4'-biphenyldicarboxylate by 2,2'-bipyridine-5,5'-dicarboxylate linkers, new signals were visible such as the peak of the carbon atom next to the nitrogen at 152 ppm (Figure 14a, peak 9).

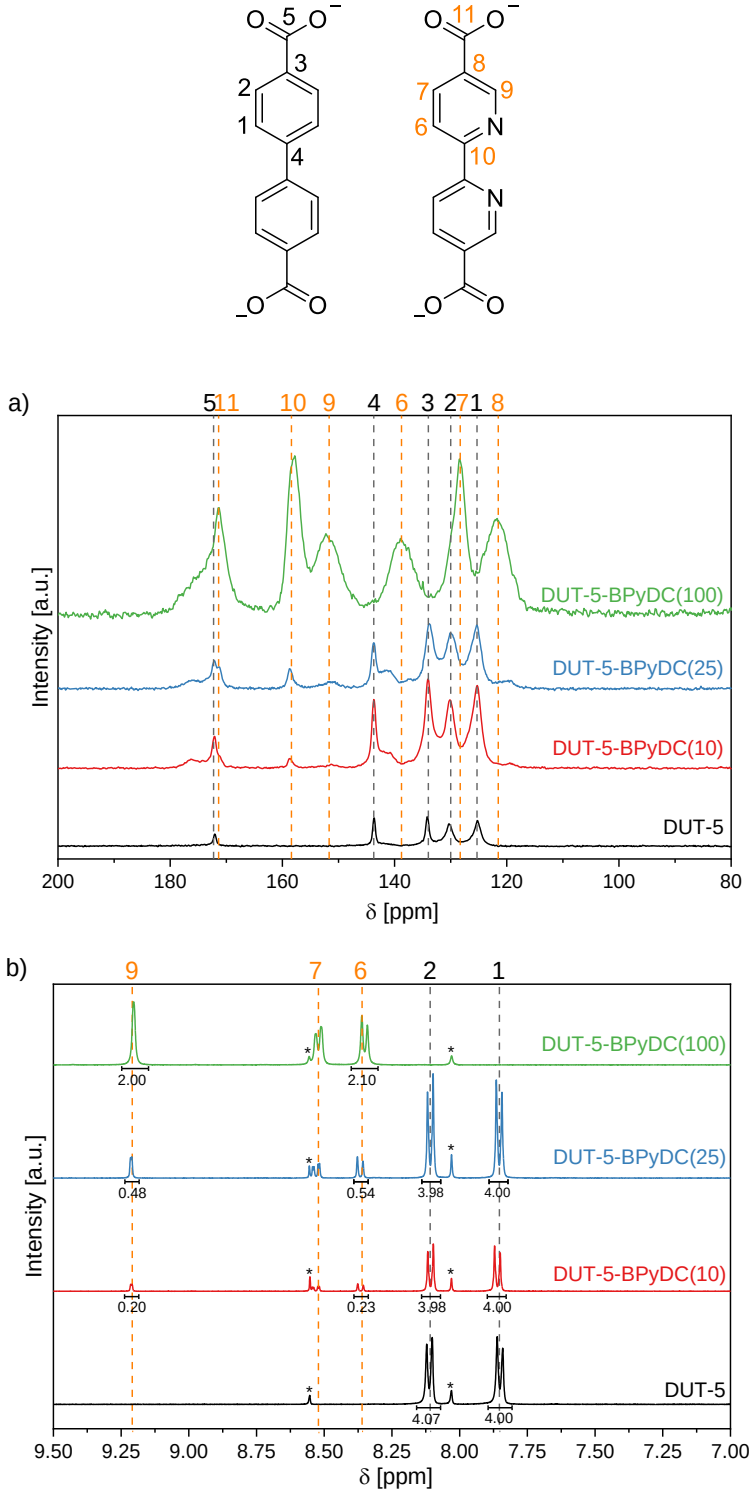

Figure 14. Solid state ^{13}C CP MAS NMR (a) and liquid phase ^{1}H NMR spectra (b) of DUT-5, mixed-linker DUT-5-BPyDC and DUT-5-BPyDC(100) materials.

Solid state NMR spectroscopy was used to obtain qualitative information about the linker ratio. For quantitative investigations, liquid phase ^{1}H NMR spectroscopy measurements of digested samples were performed (Figure 14b). The spectra were referenced to *N*,*N*-dimethylformamide-d_7 at 8.03 ppm. It should be noted that a signal of formate (8.55 ppm, designated with *) was found in the spectra, which was presumably formed during the synthesis that might be caused by the decomposition of DMF. Since unreacted linker molecules were not observed in the ATR-IR spectra, the observed peaks could be directly referred to the protons of the linker molecules incorporated in the framework. For DUT-5, two doublets were observed, which corresponded to four protons. Furthermore, one singlet and two doublets, which were assigned to two protons, were detected for DUT-5-BPyDC(100). The determined linker ratio *via* peak integration matched with the applied linker ratio during synthesis. For DUT-5-BPyDC(10), an amount of 11% and for DUT-5-BPyDC(25), an amount of 26% bipyridine linker were determined.

The results in this chapter showed that the synthesis of mixed-linker DUT-5 materials with adjustable amounts of bipyridine was successfully established. In the next step, the obtained bipyridine containing materials were post-synthetically metalated using different transition metal ions followed by thorough characterization.

3.1.2 Immobilization of metal complexes at DUT-5-BPyDC

DUT-5-BPyDC(10) was chosen for the immobilization of metals due to the lower content of bipyridine and, hence, pore blocking should be inhibited or minimized and a good distribution of the metal complexes within the framework should be attained. The synthesis of the transition metal-containing DUT-5-BPyDC(10) materials shown in Scheme 15 was performed using the acetate or nitrate salts of palladium, manganese, nickel, copper and cobalt as precursor. The metal salts were immobilized by using a lower amount of metal precursors (0.9 equivalents) than available bipyridine sites, since higher concentrations of metal precursor could be led to the formation of undesired nanoparticles or clusters in the pores of the framework. The reaction was carried out at room temperature for 6 h in a laboratory shaker without stirring the reaction mixture.

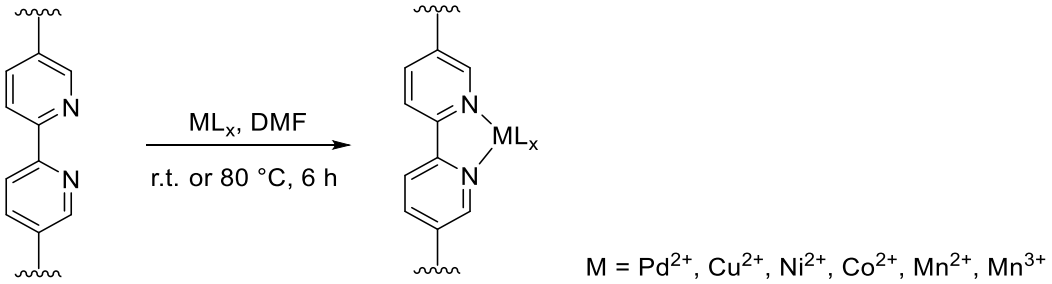

Scheme 15. Schematic representation of the immobilization of metals in DUT-5-BPyDC(10) with M = Pd^{2+}, Cu^{2+}, Ni^{2+}, Co^{2+}, Mn^{2+} and Mn^{3+}.

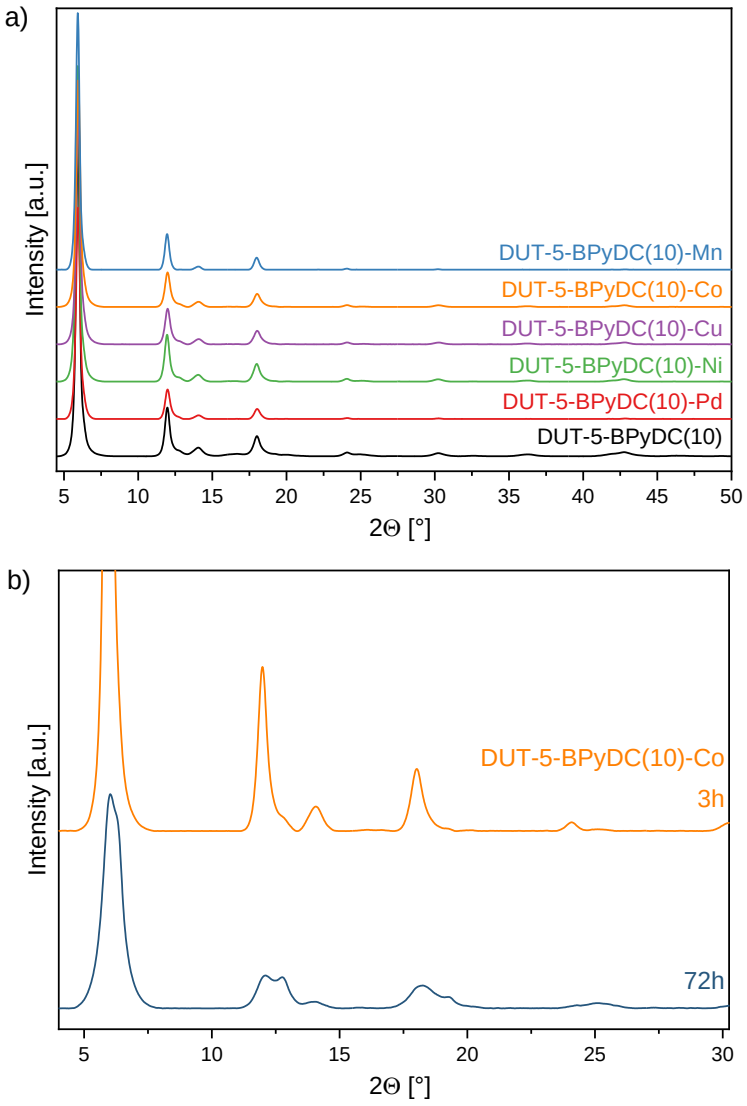

Figure 15. Powder X-ray diffraction patterns of metal-containing DUT-5-BPyDC(10) materials (a) and comparison of DUT-5-BPyDC(10)-Co after3 h and 72 h drying (b).

Powder X-ray diffraction measurements showed that the DUT-5 structure was retained after the metal immobilization without loss of crystallinity (Figure 15). In order to rule out the formation of undesired nanoparticles during the drying process of the framework materials, PXRD measurements of DUT-5-BPyDC(10)-Co were performed after 3 and 72 h drying at 130 °C in air atmosphere. After 72 hours, a decreased crystallinity and additional reflections from undesired crystalline phases were observed, whereas the sample dried for 3 hours showed a phase pure pattern. ATR-IR measurements of the samples were performed to ensure that DMF was removed completely after 3 h drying, which was confirmed by the spectra shown in Figure 16.

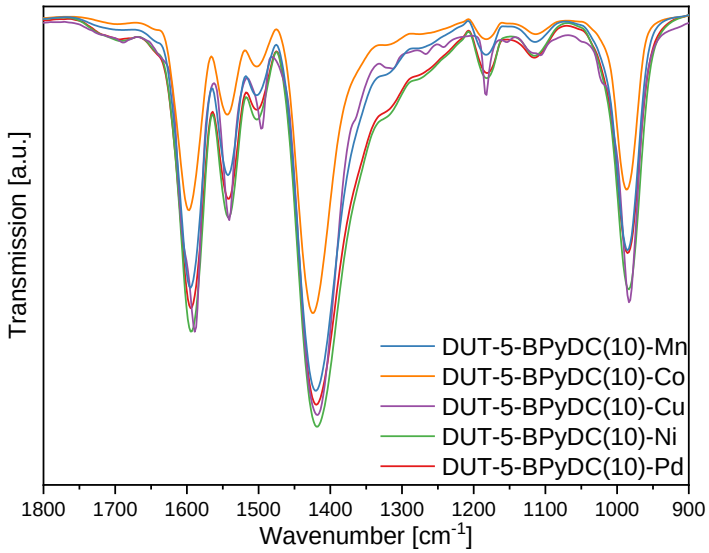

Figure 16. ATR-IR spectra of metal-containing DUT-5-BPyDC(10) materials.

N_2 physisorption measurements confirmed that all materials were obtained with high porosity and accessible micropore volumes after metal incorporation (Table 2). A slight decrease of the specific surface areas was observed after the incorporation of the metal ions. Consequently, the pore systems were not blocked by undesired metal particles and were easily accessible for catalytic applications.

The metal loading of the DUT-5 materials was determined *via* inductively coupled plasma optical emission spectroscopy (ICP-OES, Table 2). The obtained results showed that the bipyridine groups were only partially used for the complexation of the metal ions. The highest metal content was achieved for DUT-5-BPyDC(10)-Pd with 0.88 wt% (Table 2, Entry 2) and for DUT-5-BPyDC(10)-Ni with 0.85 wt% (Table 2, Entry 3), which corresponded to 26% and 45% loading of the bipyridine moieties, respectively. The remaining materials revealed a low

metal loading of 0.10 wt% to 0.18 wt% corresponding to 5 – 9% loading of the bipyridine linkers (Table 2, Entry 4 – 6). To increase the metal content for the latter materials, an optimization of the reaction conditions was performed using DUT-5-BPyDC(10)-Co. First, the reaction time for the immobilization of cobalt was increased from 6 h to 24 h or 72 h. The obtained metal content varied between 0.07 – 0.10 wt%. Hence, the reaction time had only a negligible influence on the metal loading. Furthermore, the reaction temperature was increased from room temperature to 80 °C resulting in a cobalt content of 0.44 wt% (23% loading of bipyridine). Nevertheless, even though elevated reaction temperatures of 80 °C seemed more promising for the synthesis of catalyst materials, they were only applied for the cobalt immobilization in this work, all other metal species were immobilized at room temperature.

To compare the influence of the oxidation state in catalytic applications in oxidation reactions (*cf.* chapter 4.2), DUT-5-BPyDC(10)-Mn^{3+} was synthesized containing manganese in the oxidation state +3. According to PXRD and ATR-IR measurements, the DUT-5 structure was retained. The specific surface area decreased to 1530 m^2/g after immobilization of manganese(III) and a higher metal content of 0.47 wt% corresponding to 27% loading of the bipyridine linkers was obtained (Table 2, Entry 7), which was significantly higher than the manganese(II) content of DUT-5-BPyDC(10)-Mn^{2+} (0.10 wt% or 5% loading of the bipyridine linkers).

Table 2. Specific surface areas (S_{BET}), total pore volumes (tpv), micropore volumes (mpv) and metal loadings of the metal-containing DUT-5-BPyDC(10) materials.

Entry	Sample	S_{BET} [m^2/g]	tpv [cm^3/g]	mpv [cm^3/g]	metal loading* [wt%]
1	DUT-5-BPyDC(10)	1880	0.77	0.67	-
2	DUT-5-BPyDC(10)-Pd	1620	0.73	0.59	0.88
3	DUT-5-BPyDC(10)-Ni	1730	0.76	0.63	0.85
4	DUT-5-BPyDC(10)-Cu	1700	0.75	0.62	0.18
5	DUT-5-BPyDC(10)-Co	1870	0.75	0.62	0.10
6	DUT-5-BPyDC(10)-Mn^{2+}	1810	0.78	0.65	0.10
7	DUT-5-BPyDC(10)-Mn^{3+}	1530	0.67	0.55	0.47

* Metal loading of materials synthesized at room temperature for 6 h.

Single-site catalysts proved to be more reactive than bulk catalysts due to the uniform nature and atomic distribution of the active metal centers. To elucidate the structure of these active centers and the catalytic mechanisms in the subsequent catalytic applications (*cf.* chapter 4), a

detailed characterization of the metal centers was necessary. Since common techniques are not suitable to provide a detailed insight into the local chemical environment of the immobilized metal complexes, X-ray absorption spectra were recorded. X-ray absorption near edge structure (XANES) spectroscopy was used to get information about the oxidation state and the geometry of the metal centers, while extended X-ray absorption fine structure (EXAFS) spectroscopy was used to analyze the local environment of the metal centers, especially to distinguish the well-defined complexes from undesired metallic or oxidic nanoparticles within the pore systems. For this purpose, different fits were performed, in which the presence of the corresponding metal bipyridine complexes (denoted as $4O_L$ $2N_{BPyDC}$) and the formation of small oxidized nanoparticles (denoted as $4O_L$ $2N_{BPyDC}$ + MO_x) were examined. The measurements and analysis of the bipyridine-containing DUT-5 materials after metal incorporation were performed at DESY Hamburg and analyzed in collaboration with Alba Titze-Alonso within her master thesis.[212]

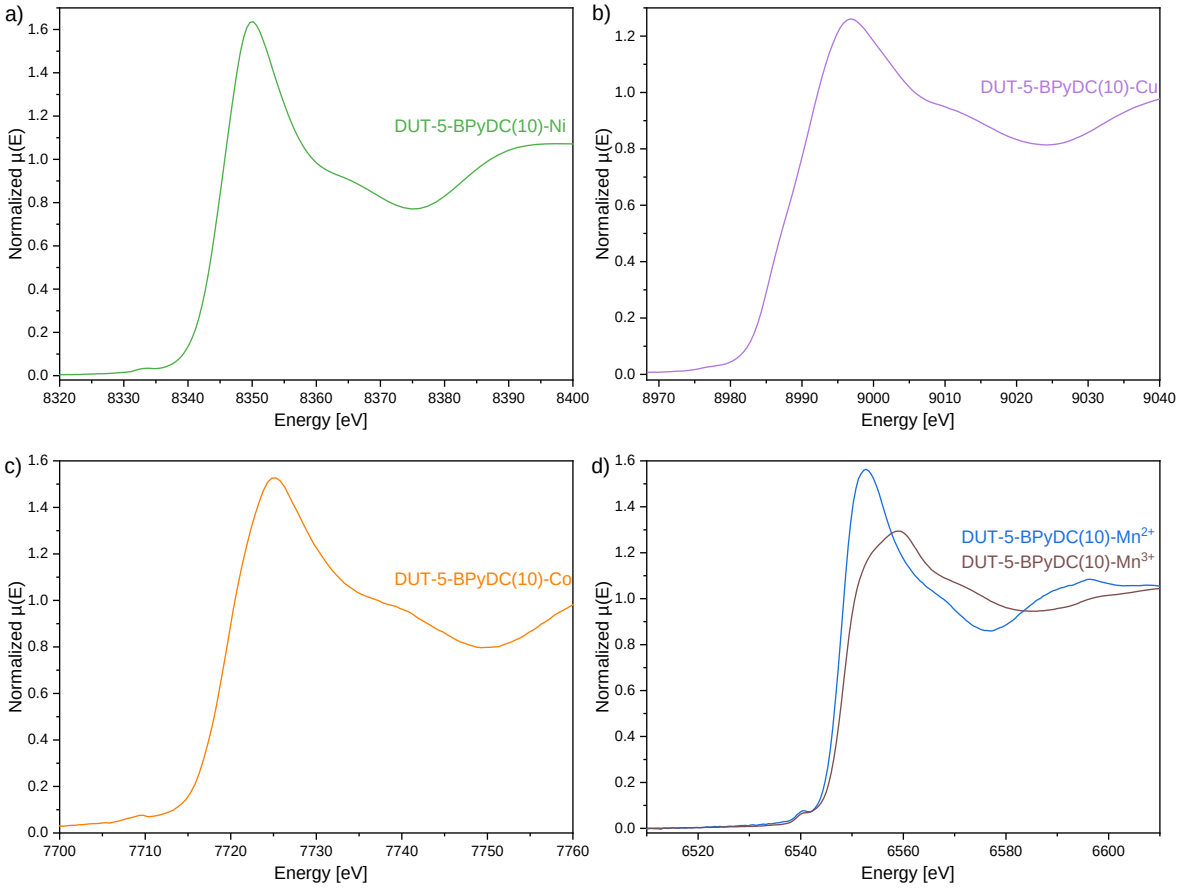

Figure 17. XANES spectra of the DUT-5 materials after metal immobilization at the Ni K-edge (a), Cu K-edge (b), Co K-edge (c) and the Mn K-edge (d).

The XANES spectra at the K-edges of the metals (with M = Ni, Cu, Co, Mn) of the metal containing DUT-5 materials revealed the expected oxidation state for all materials. For the

nickel material (Figure 17a), three characteristic features for Ni^{2+} were observed, which proved the obtained oxidation state of +2 for the nickel complex within the framework. The pre-edge peak at 8333 eV, the position of the absorption edge defined by the maximum of the first derivative at 8346 eV as well as the white line at 8350 eV, which is characteristic in the XANES profile of $Ni(OAc)_2$[213], matched very well with the XANES analysis for DUT-5-BPyDC(10)-Ni. DUT-5-BPyDC(10)-Cu exhibited a weak pre-edge peak at 8978 eV, which indicated an octahedral geometry of the Cu^{2+} ions. The white line position at 8997 eV was close to the reported value for Cu^{2+} ions of CuO[214] at 8996 eV (Figure 17b). The curve of DUT-5-BPyDC(10)-Co showed a smooth shoulder at 7740 eV, which was similar to the curve of $Co(NO_3)_2$[215] (Figure 17c). Furthermore, with regard to the maximum of the first derivative, a shift of 6 eV from the edge position between DUT-5-BPyDC(10)-Mn^{2+} and DUT-5-BPyDC(10)-Mn^{3+} was observed, whereas a shift of 3 eV is known for MnO[216] and Mn_2O_3[217] (Figure 17d). The white line position of the DUT-5-BPyDC(10)-Mn^{2+} material was around 6552 eV and of the DUT-5-BPyDC(10)-Mn^{3+}material around 6560 eV, which was in good agreement with the values for Mn^{2+} ions of MnO and Mn^{3+} ions of Mn_2O_3 and, thus, indicating that the oxidation states of the Mn ions were retained during the immobilization process.

With respect to the EXAFS analysis, the Fourier-transformed spectra of all materials revealed that the first complex shell showed a high intensity in contrast to the higher shells, which indicated that the metals were exclusively present in the form of the desired complexes (Figure 18 and Figure A1). The corresponding fitting parameters and results of the EXAFS analysis of the first shell are listed in Table A1 – A5. In the first shell, two different distances with two and four neighbors, respectively, could be fitted, which could be assigned to two nitrogen of the bipyridine linker and four oxygen neighbor atoms belonging to the ligands of the complex. Thus, these values are in good agreement with the desired complex. The fits of the metal complexes with an additional metal shell from the corresponding metal oxides showed no significant amount of metal backscatters from an oxidic phase. The plotted k-space and q-space EXAFS spectra of all materials are shown in Figure A2 – A6.

As mentioned above, reflections from additional phases were obtained *via* PXRD patterns of the samples after drying for 72 h. The EXAFS analysis could confirm the formation of CoO in the structure of DUT-5-BPyDC(10)-Co in this case. The fit values included the 6 oxygen atoms at 2.06 Å and Co neighbors at 2.10 Å of the CoO phase, which indicated the formation of very small CoO nanoparticles insight the pores. A comparison of the cobalt materials dried after 3 h and 72 h is shown in the Fourier-transformed EXAFS spectra in Figure 19.

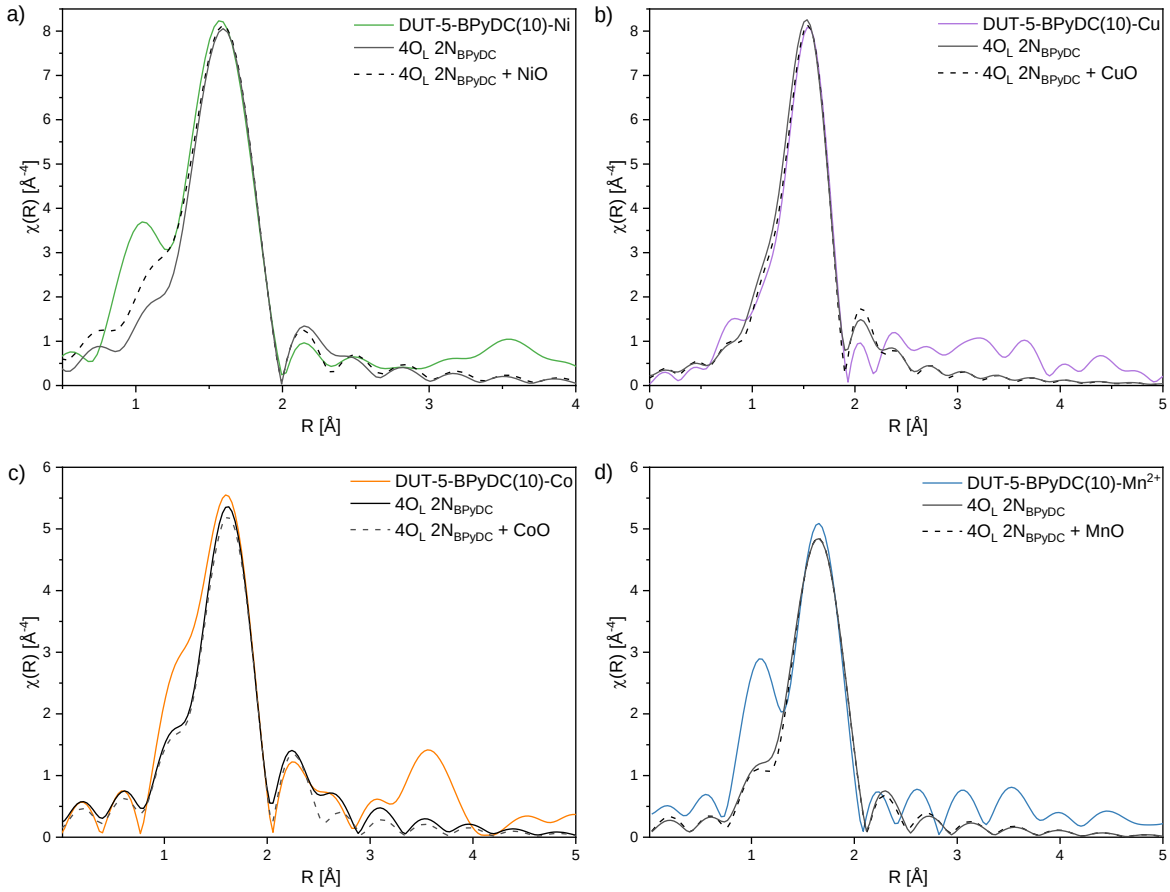

Figure 18. Experimental Fourier-transformed EXAFS spectra, the fit of the first complex shell and the fit of the first complex shell with the corresponding metal oxide of DUT-5-BPyDC(10)-Ni (a), DUT-5-BPyDC(10)-Cu (b), DUT-5-BPyDC(10)-Co (c), and DUT-5-BPyDC(10)-Mn^{2+} (d).

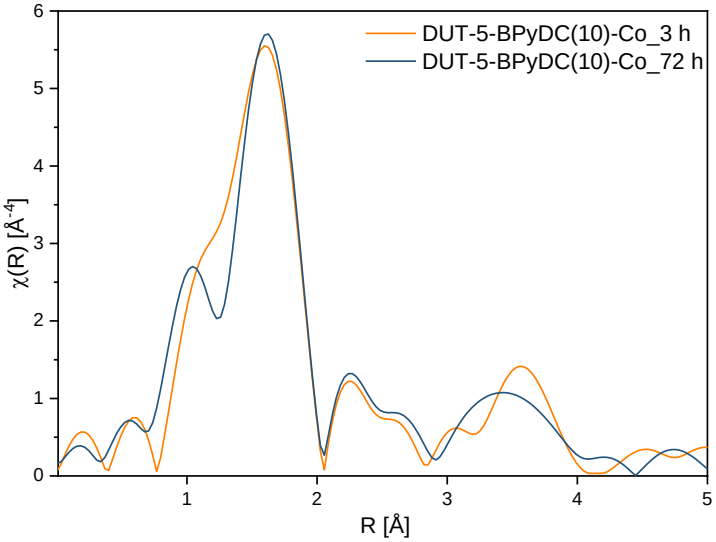

Figure 19. Comparison of Fourier-transformed EXAFS spectra of DUT-5-BPyDC(10)-Co materials dried after 3 h and 72 h.

3.2 Amine containing framework materials

As mentioned in chapter 1.5.1, amine functionalities are frequently used for post-synthetic modification strategies due to their ability to undergo a variety of organic transformations. In the first part of this section (chapter 3.2.1), an amine-functionalized MIL-53(Al) material was post-synthetically modified with maleic anhydride resulting in a chelating side group, which was then used for the immobilization of manganese ions. The obtained manganese-containing MIL-53 material was successfully tested as catalyst in the oxidation of α-pinene (see chapter 4.1). Nevertheless, MIL-53 materials exhibit small pore dimensions (8.5 Å × 8.5 Å) and, thus, their relevance for potential applications is limited. In contrast, DUT-5 seems to be an ideal alternative to overcome the limitations of MIL-53 due to its elongated linker molecules. The larger pore dimensions (22.7 Å ×19.2 Å) facilitate the design of promising catalyst materials for fine chemical reactions. Therefore, the reaction between amine-functionalized DUT-5 materials and various aldehydes using salicylaldehyde, 2-pyridinecaboxaldehyde and 2-imidazolecarboxaldehyde resulting in Schiff base complexes is described in the next section (chapter 3.2.2). The formed materials were subsequently used for the immobilization of cobalt and manganese ions and were further applied in the catalytic test reactions (see chapter 4.2 and 4.3). All materials were characterized in detail using PXRD, ATR-IR and N_2 physisorption. ^{1}H NMR spectroscopy was used to determine both the linker ratios and the modification degrees. The metal loadings of the catalysts were determined by ICP-OES analysis. To ensure that the pores of the resulting frameworks were still accessible for substrate molecules after post-synthetic modification, the mixed-linker concept was applied, which guaranteed a homogeneous distribution of complexes within the framework and a low concentration of catalytically active sites within the framework structure.

3.2.1 Synthesis and characterization of MIL-53-NH_2

The preparation of the aluminum-based MIL-53-NH_2(50) [$Al(OH)(BDC)_{0.5}(ABDC)_{0.5}$] material was performed according to the reported literature procedure from Gotthardt *et al.*[85] The reaction between aluminum nitrate and equal amounts of 1,4-benzenedicarboxlic acid (H_2BDC) and 2-aminobenzyl-1,4-dicarboxylic acid (H_2ABDC) was carried out at ambient pressure and 90 °C using a water/DMF solvent mixture (Scheme 16).

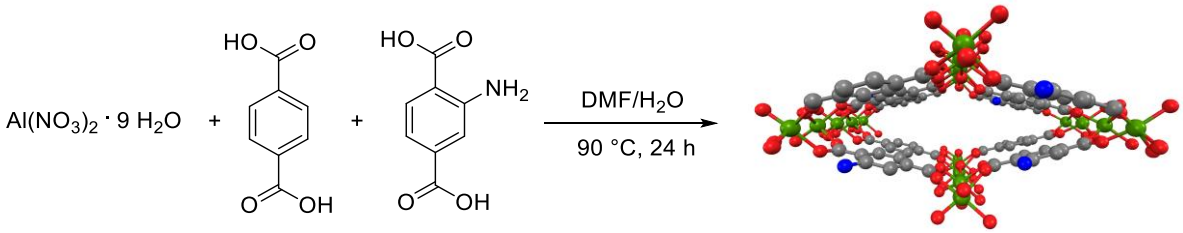

Scheme 16. Schematic representation of the synthesis of MIL-53-NH₂(50), green: Al, red: O, grey: C, blue: N.

In the next step, the obtained amine-functionalized MIL-53 material was used for a two-step post-synthetic modification reaction (Scheme 17). First, the amine groups were modified with maleic anhydride, which underwent a ring-opening reaction resulting in the formation of an amide (MIL-53-NH₂(50)-Mal). The obtained chelating side group was modified using manganese(III) acetate at 60 °C. To prevent the formation of undesired nanoparticles in the pores of the framework, 0.9 equivalents of manganese precursor were used based on the number of chelating side groups.

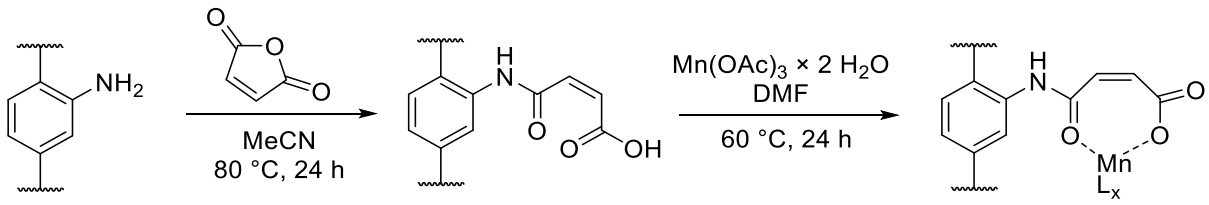

Scheme 17. Schematic representation of the two-step PSM reaction of MIL-53-NH₂(50) with maleic anhydride and manganese(III) acetate.

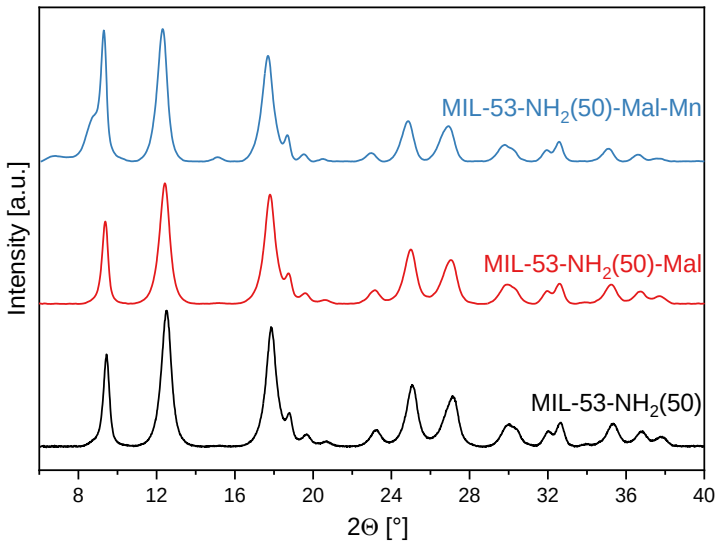

Figure 20. Powder X-ray diffraction patterns of MIL-53-NH₂(50), MIL-53-NH₂(50)-Mal and MIL-53-NH₂(50)-Mal-Mn.

The powder X-ray diffraction patterns revealed that the structure was retained during the modification process. The patterns were similar to the reported structure of MIL-53(Al)-*lt* with minor deviations, which could be caused by a small breathing effect after the introduction of both the chelating side groups or the manganese ions.[28]

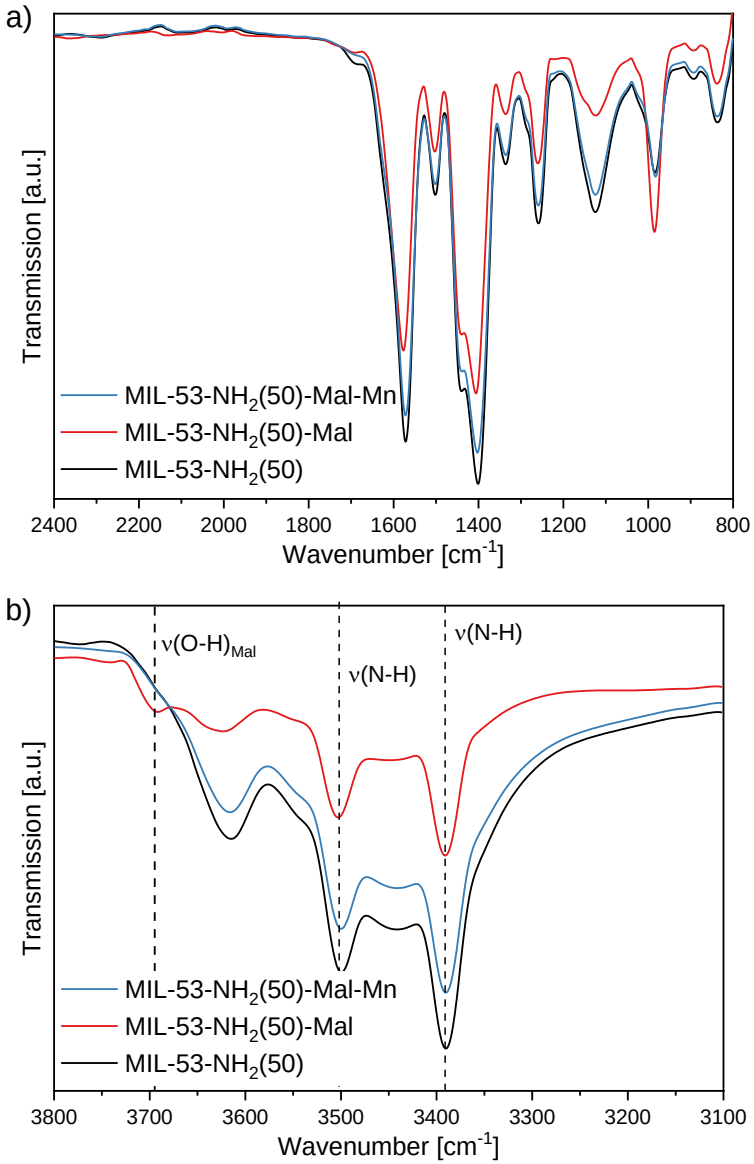

Figure 21. ATR-IR spectra of MIL-53-NH₂(50), MIL-53-NH₂(50)-Mal and MIL-53-NH₂(50)-Mal-Mn.

The ATR-IR spectra revealed that the pores were free from residual guest molecules after synthesis. No C=O bands at 1685 cm^{-1} (expected for the free acid molecules) and at 1650 cm^{-1} (expected for DMF) were observed (Figure 21a). Furthermore, the IR spectra of the modified MIL-53 materials provided a qualitative statement about the successful incorporation of the functional groups, which could be proven by the N–H stretching vibrations of the amine groups

at 3500 cm^{-1} and 3389 cm^{-1} and the O–H stretching vibrations of the maleate side groups at 3692 cm^{-1} (Figure 21b). Moreover, there were no peaks, which belonged to the vibrations of residual maleic anhydride indicating a successful modification of the amine groups and the removal of excess substrate.

Adsorption isotherms showed a step at low relative pressure due to the breathing effect, which indicated the transition from a narrow to a large pore form. After modification with maleic anhydride, the step shifted to higher relative pressures. The subsequent immobilization of manganese did not cause other major effects on the shape of the isotherms (Figure 22).

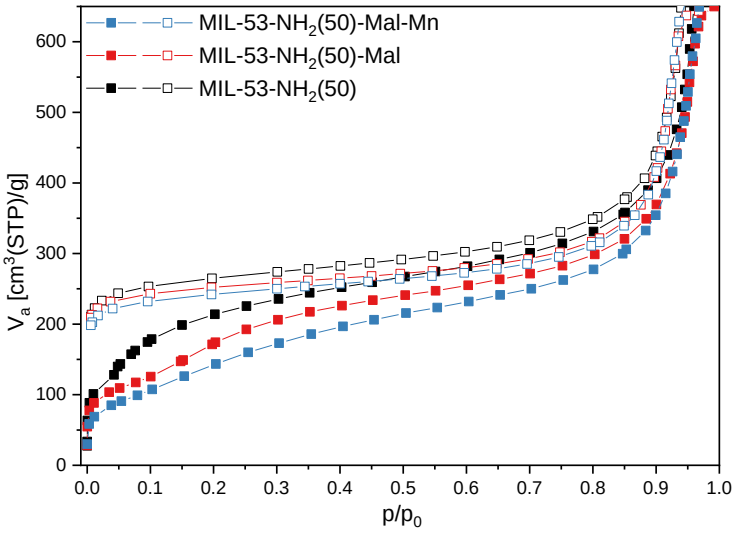

Figure 22. Adsorption and desorption isotherms of MIL-53-NH_2(50), MIL-53-NH_2(50)-Mal and MIL-53-NH_2(50)-Mal-Mn.

The materials still revealed acceptable specific surface areas after post-synthetic modification (Table 3). The specific surface area decreased from 840 to 380 m^2/g, which proved the successful modification of MIL-53-NH_2(50).

Table 3. Specific surface areas (S_{BET}), total pore volumes (tpv) and micropore volumes (mpv) of MIL-53-NH_2(50), MIL-53-NH_2(50)-Mal and MIL-53-NH_2(50)-Mal-Mn analyzed by N_2 physisorption measurements. Manganese content of MIL-53-NH_2(50)-Mal-Mn determined by AAS measurements.

Entry	Sample	S_{BET} [m^2/g]	mpv [cm^3/g]	metal loading [wt%]
1	MIL-53-NH_2(50)	840	0.23	-
2	MIL-53-NH_2(50)-Mal	480	0.21	-
3	MIL-53-NH_2(50)-Mal-Mn	380	0.15	0.90

^{1}H NMR spectroscopic measurements were performed using digested samples before and after the PSM reactions (Figure 23). The integration of the peaks proved the presence of the two linker molecules in the desired ratio (1:1) and revealed a modification degree of approx. 7% of the amine groups. Consequently, the post-synthetically modified MIL-53-NH$_2$(50) was loaded with 0.9 wt% of manganese, which corresponded to a completely complexation of the maleate groups (Table 3, Entry 3).

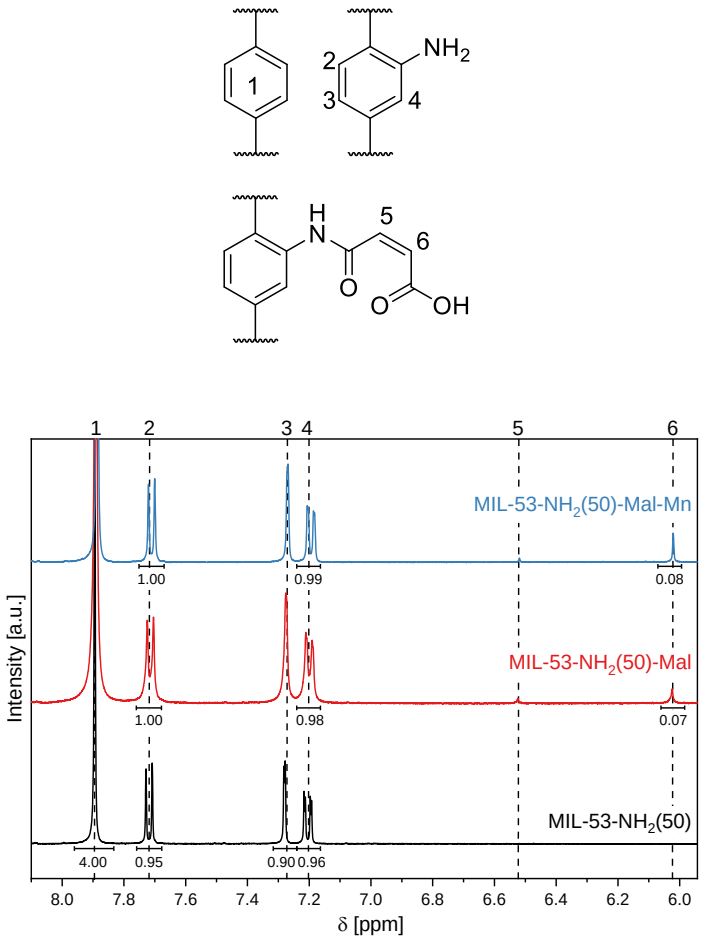

Figure 23. ^{1}H NMR spectra of digested MIL-53-NH$_2$(50) samples after post-synthetic modification.

3.2.2 Synthesis and characterization of mixed-linker DUT-5-NH$_2$

The position of the catalytically active sites in the metal-organic frameworks can play an important role in catalytic reactions. It is known that the direct synthesis of mixed-linker frameworks usually results in a statistic distribution of the different linker molecules, which leads to randomly distributed active sites after post-synthetic modification, consequently. Using difunctionalized linker molecules, the spatial proximity of the active sites could be enforced,

which might enable better synergistic effects. In this work, amine-functionalized 4,4'-biphenyldicarboxylate linkers were selected bearing one or two amine groups on one linker.

The synthesis of the mixed-linker DUT-5 materials containing amine functionalities were carried out by using of 4,4'-biphenyldicarboxylic acid (H_2BPDC) in combination with 2-aminobiphenyldicarboxylic acid (H_2ABPDC) or 2,2'-diamino-4,4'-biphenyldicarboxylic acid (H_2dABPDC), resulting in DUT-5-NH_2(10) [Al(OH)(BPDC)$_{0.9}$(ABPDC)$_{0.1}$] or DUT-5-$(NH_2)_2$(5) [Al(OH)(BPDC)$_{0.95}$(dAPBDC)$_{0.05}$]. The syntheses, which are shown in Scheme 18, were performed analogously to the synthesis procedure of DUT-5-BPyDC(10) (Chapter 3.1.1). The amine-functionalized linker molecules were provided by the group of Professor Bräse (Karlsruhe Institute of Technology).

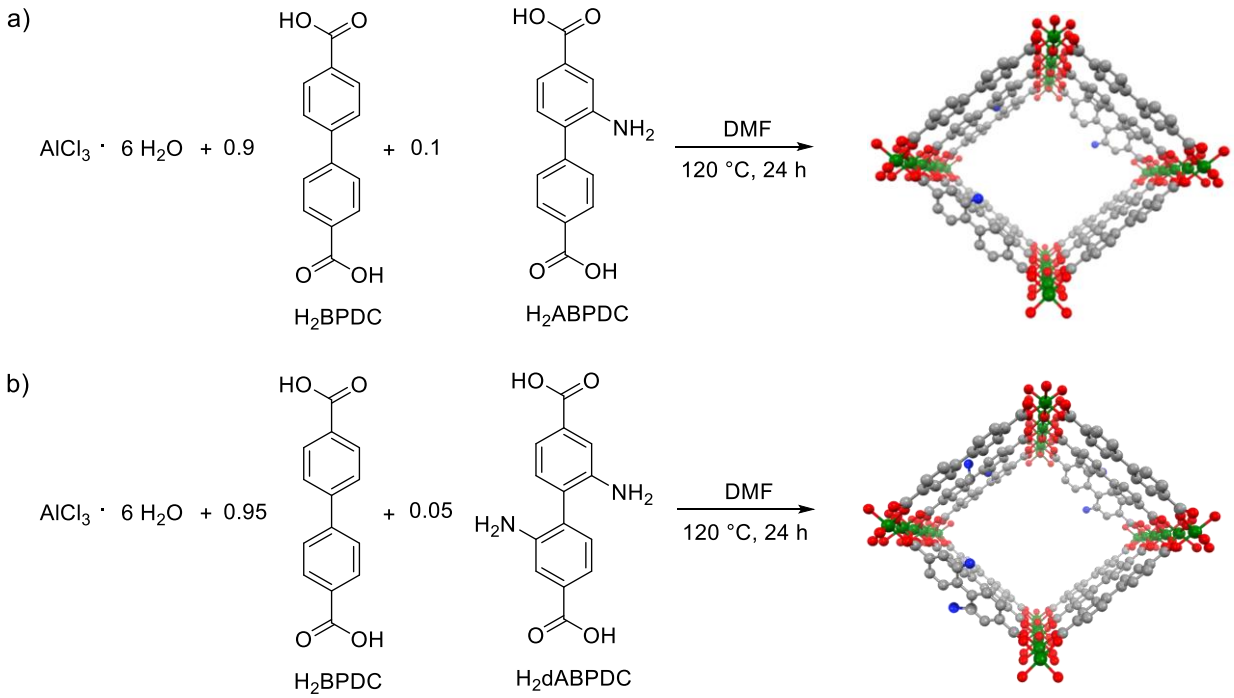

Scheme 18. Schematic representation of the synthesis of DUT-5-NH_2(10) (a) and DUT-5-$(NH_2)_2$(5) (b).

Results of the powder X-ray diffraction measurements showed that the amine-functionalized DUT-5 materials were isoreticular to DUT-5 (Figure 24a). C=O bands that belonged to solvent or unreacted linker molecules could not be detected in the ATR-IR spectra, which revealed that the pores were free for post-synthetic modification reactions. Due to the low amine content, the characteristic bands of the incorporated amine groups could not be observed, which would be usually expected at 3500 cm^{-1} and 3389 cm^{-1}.

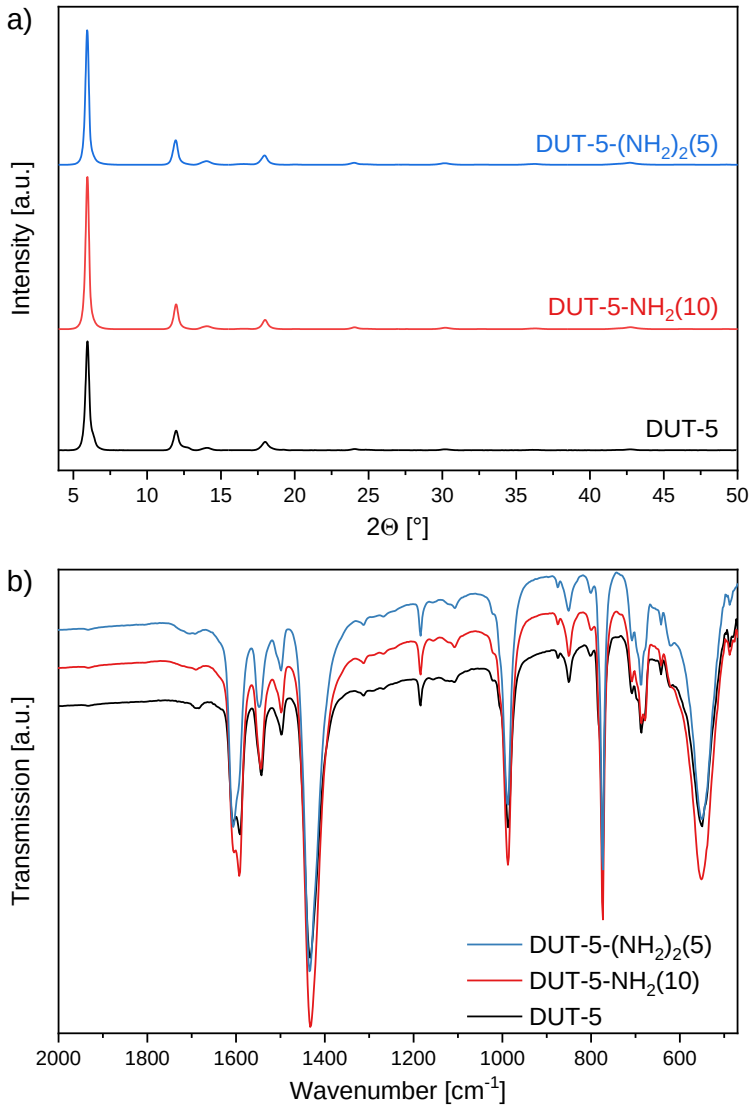

Figure 24. Powder X-ray diffraction patterns (a) and ATR-IR spectra (b) of amine-functionalized DUT-5 materials.

N_2 physisorption measurements showed that highly porous materials were obtained with a specific surface area around 1900 m^2/g, a total pore volume around 0.90 cm^3/g and a micropore volume around 0.66 cm^3/g on average (Table 4).

Table 4. Specific surface areas (S_{BET}), total pore volumes (tpv) and micropore volumes (mpv) of amine-functionalized DUT-5 materials analyzed by N_2 physisorption measurements.

Entry		S_{BET} [m^2/g]	tpv [cm^3/g]	mpv [cm^3/g]
1	DUT-5	1880	0.81	0.61
2	DUT-5-NH_2(10)	1860	0.85	0.66
3	DUT-5-$(NH_2)_2$(5)	1910	0.94	0.69

For quantitative analysis, ^{1}H NMR spectroscopy was recorded using digested samples in NaOD and DMF-d_7 (Figure 25). The results showed that 8% of 2-amino-4,4'-biphenyldicarboxylate could be incorporated into DUT-5-NH_2(10).

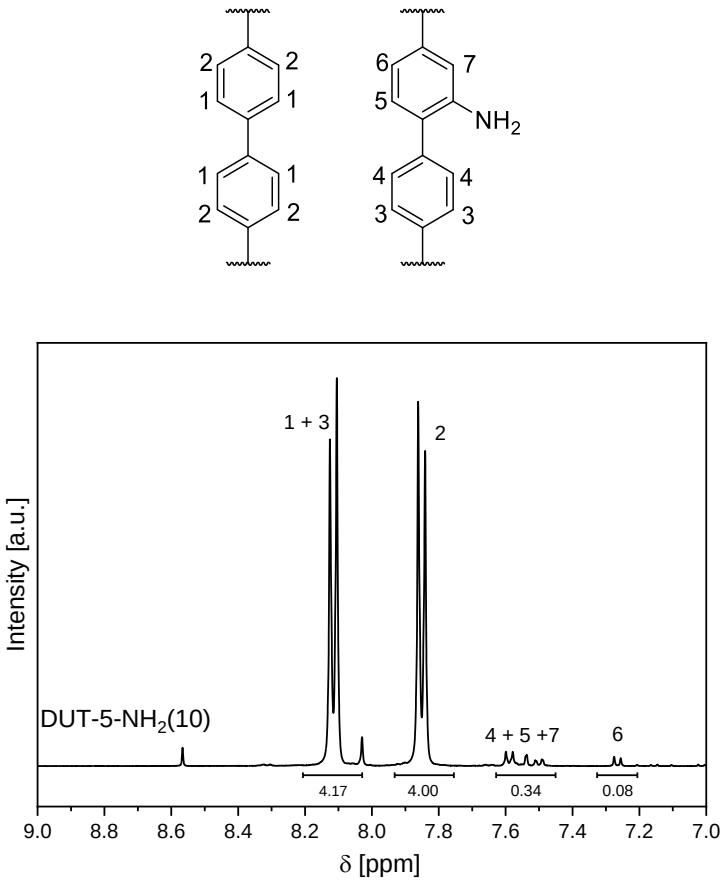

Figure 25. ^{1}H NMR spectrum of digested DUT-5-NH_2(10) material.

The amount of the amine groups of the difunctionalized DUT-5 materials was too low to determine the amine content. Therefore, a reference material (DUT-5-$(NH_2)_2$(25)) containing a theoretical amount of 25% of 2,2'-diamino-4,4'-biphenyldicarboxylate linker was synthesized. Figure 26 shows the ^{1}H NMR spectrum of DUT-5-$(NH_2)_2$(25), which revealed an amine content of 15% indicating a lower percentage of the functionalized linker after the synthetis. Consequently, since only small signals of the peaks were observed, which belonged to the protons of 2,2'-diamino-4,4'-biphenyldicarboxylate linkers, the amount of diamine-functionalized linker might also be ≤5% for DUT-5-$(NH_2)_2$(5).

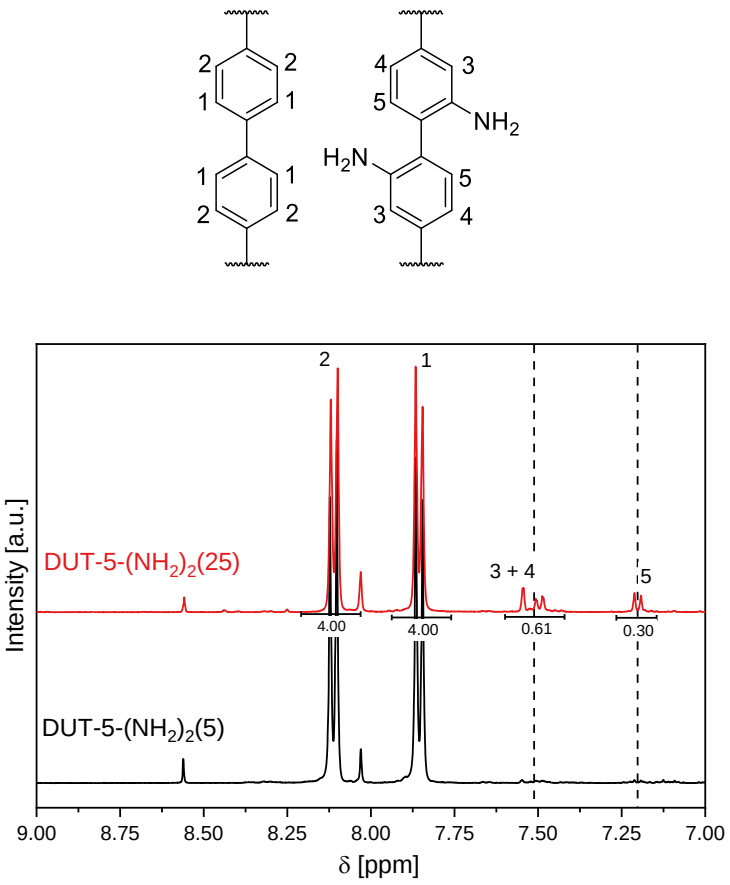

Figure 26. ^{1}H NMR spectra of digested DUT-5-$(NH_2)_2$ materials.

3.2.2.1 Post-synthetic modification of DUT-5-NH_2 *via* Schiff base reaction

Bidentate Schiff base compounds are easy to synthesize in liquid phase under mild conditions, which are usually required for the reactions with metal-organic frameworks, and can coordinate to almost all metal ions. In the meantime, the efficiency of Schiff base complexes as highly active catalysts is well-known in homogeneous as well as in heterogeneous catalysis.[218]

The mono- and difunctionalized DUT-5-NH_2 materials were post-synthetically modified *via* Schiff base reactions. To achieve a higher modification degree, the materials were activated under vacuum to remove guest molecules like, *e.g*, H_2O or DMF. Salicylaldehyde, 2-pyridine-carboxaldehyde and 2-imidazolecarboxaldehyde were used to obtain different chelating side groups within the framework. The PSM reactions were performed by using acetic acid as a catalyst at 60 °C in a laboratory shaker.

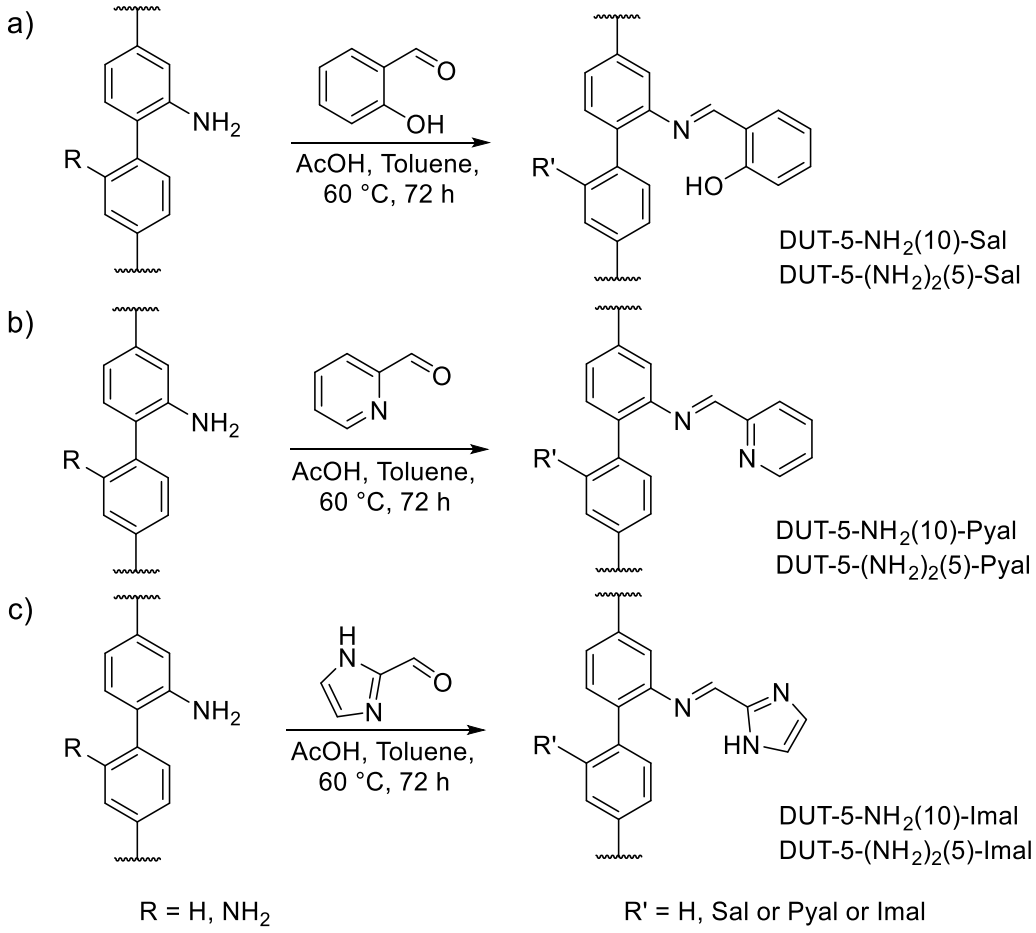

Scheme 19. Schematic representation of the post-synthetic modification of DUT-5-NH₂(10) and DUT-5-(NH₂)₂(5) with salicylaldehyde, 2-pyridinecarboxaldehyde or 2-imidazolaldehyde.

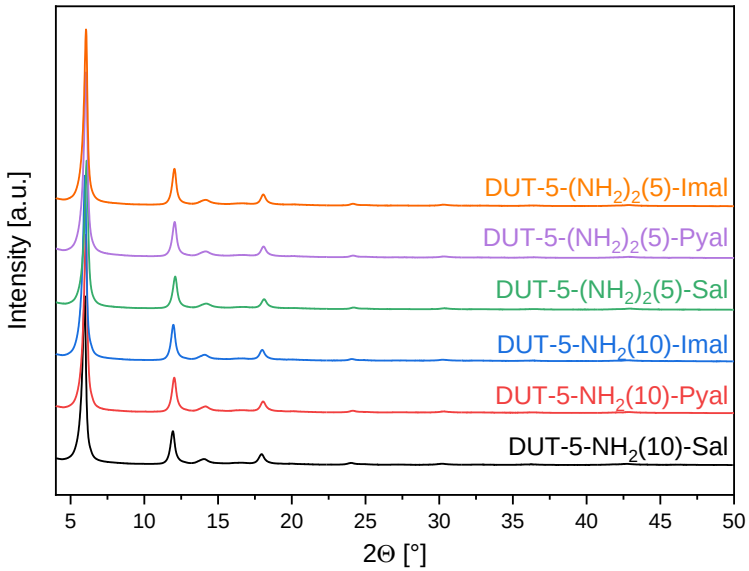

Figure 27. Powder X-ray diffraction patterns of amine-functionalized DUT-5 materials after post-synthetic modification.

The analysis of the powder X-ray diffraction patterns and ATR-IR spectra showed that all materials were retained during the post-synthetic modification process (Figure 27). In addition,

bands, which belonged to free aldehydes, were not observed in the ATR-IR spectra (Figure 28). Thus, undesired molecules within the pores could be excluded.

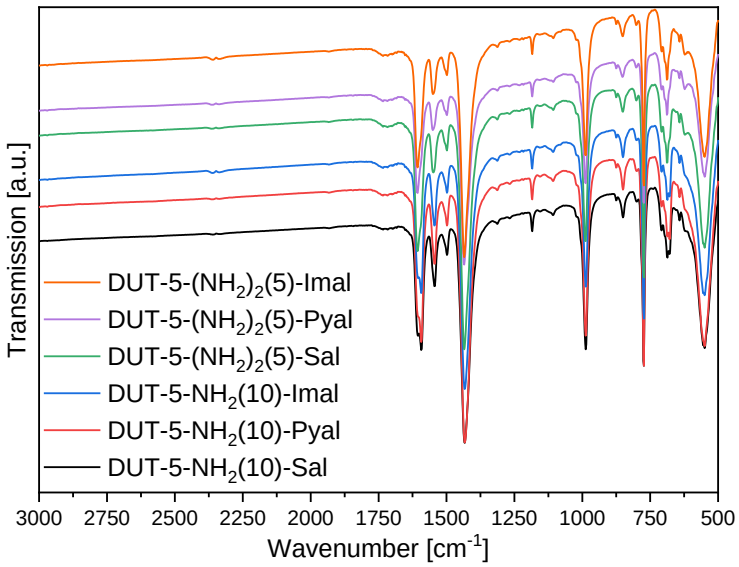

Figure 28. ATR-IR spectra of amine-functionalized DUT-5 materials after post-synthetic modification.

Nitrogen physisorption results revealed that the amine-functionalized DUT-5 materials were obtained with high specific surface areas after post-synthetic modification. Surface areas and porosity did not change significantly due to the low modification degree.

Table 5. Specific surface areas (S_{BET}), total pore volumes (tpv) and micropore volumes (mpv) of amine-functionalized DUT-5 materials after post-synthetic modification.

Entry		S_{BET} [m^2/g]	tpv [cm^3/g]	mpv [cm^3/g]
1	DUT-5-NH_2(10)-Sal	1810	0.84	0.65
2	DUT-5-NH_2(10)-Pyal	1820	0.83	0.65
3	DUT-5-NH_2(10)-Imal	1810	0.81	0.65
4	DUT-5-$(NH_2)_2$(5)-Sal	1910	0.91	0.69
5	DUT-5-$(NH_2)_2$(5)-Pyal	1930	0.93	0.71
6	DUT-5-$(NH_2)_2$(5)-Imal	1930	0.93	0.67

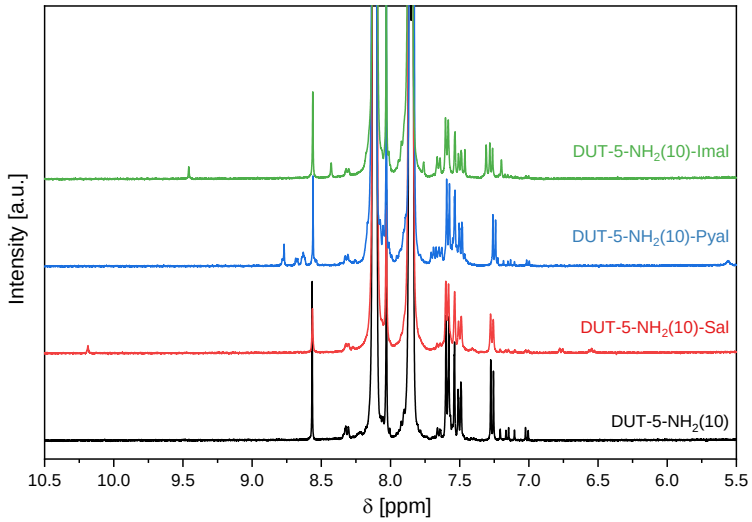

Figure 29. ^{1}H NMR spectra of digested monofunctionalized DUT-5-NH₂(10) materials after post-synthetic modification.

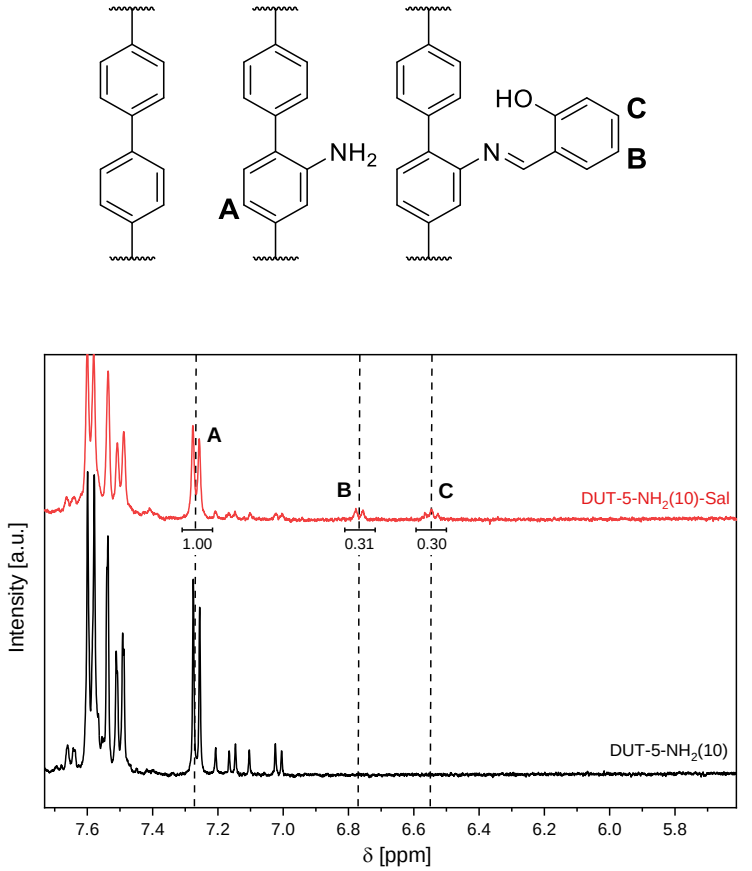

Figure 30. ^{1}H NMR spectra of digested DUT-5-NH₂(10-Sal.

^{1}H NMR spectroscopy measurements were performed to determine the modification degree. The results showed that only a partial modification of the amine groups was obtained (Figure 29). For DUT-5-NH₂(10)-Sal, new peaks were observed at 6.76 (peak **B**) and 6.54 ppm (peak

C), which could be assigned to two carbon atoms of the phenyl ring of the side group. Thus, a modification degree of 30% could be calculated from the ratio of the integrals of these peaks and the integral of peak (peak **A**) corresponding to the unmodified amine-functionalized linker (Figure 30). However, the modification degree for the other materials could not be determined quantitatively, since a peak assignment was difficult due to the strong overlap of the signals.

3.2.2.2 Immobilization of metal complexes at modified DUT-5-NH_2

After the successful modification of the amine groups in the DUT-5 structure, the materials were subsequently used for the immobilization of cobalt ions. Furthermore, manganese(II) and manganese(III) ions were incorporated into DUT-5-NH_2(10)-Sal. The immobilization of the metal ions was carried out using 0.9 equivalents of the metal precursor with regard to the modification degree of the side groups at 80 °C in DMF for 6 hours. Since the modification degree was determined only for DUT-5-NH_2(10)-Sal, a similar modification degree of 30% was assumed for all materials. $Co(NO_3)_2 \cdot 6\ H_2O$, $Mn(CH_3COO)_2$ and $Mn(CH_3COO)_3 \cdot 2\ H_2O$ were applied as precursor salts.

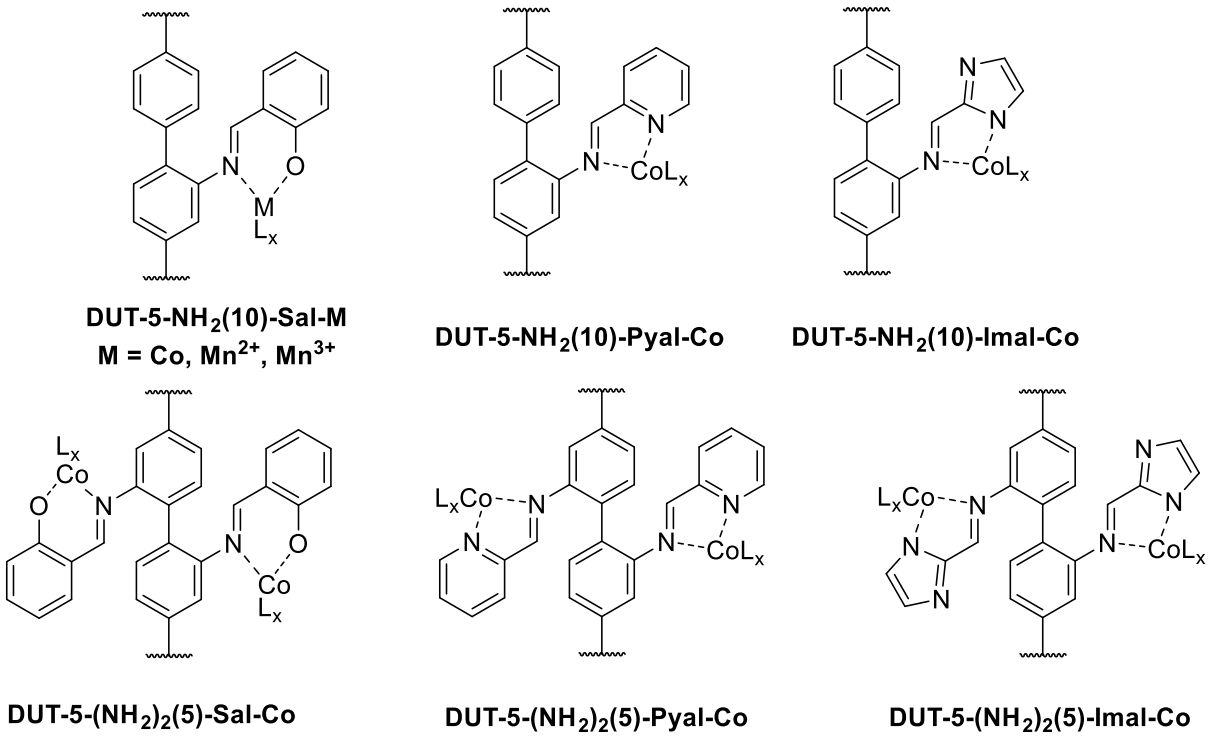

Figure 31. Schematic representation of metal containing DUT-5 materials.

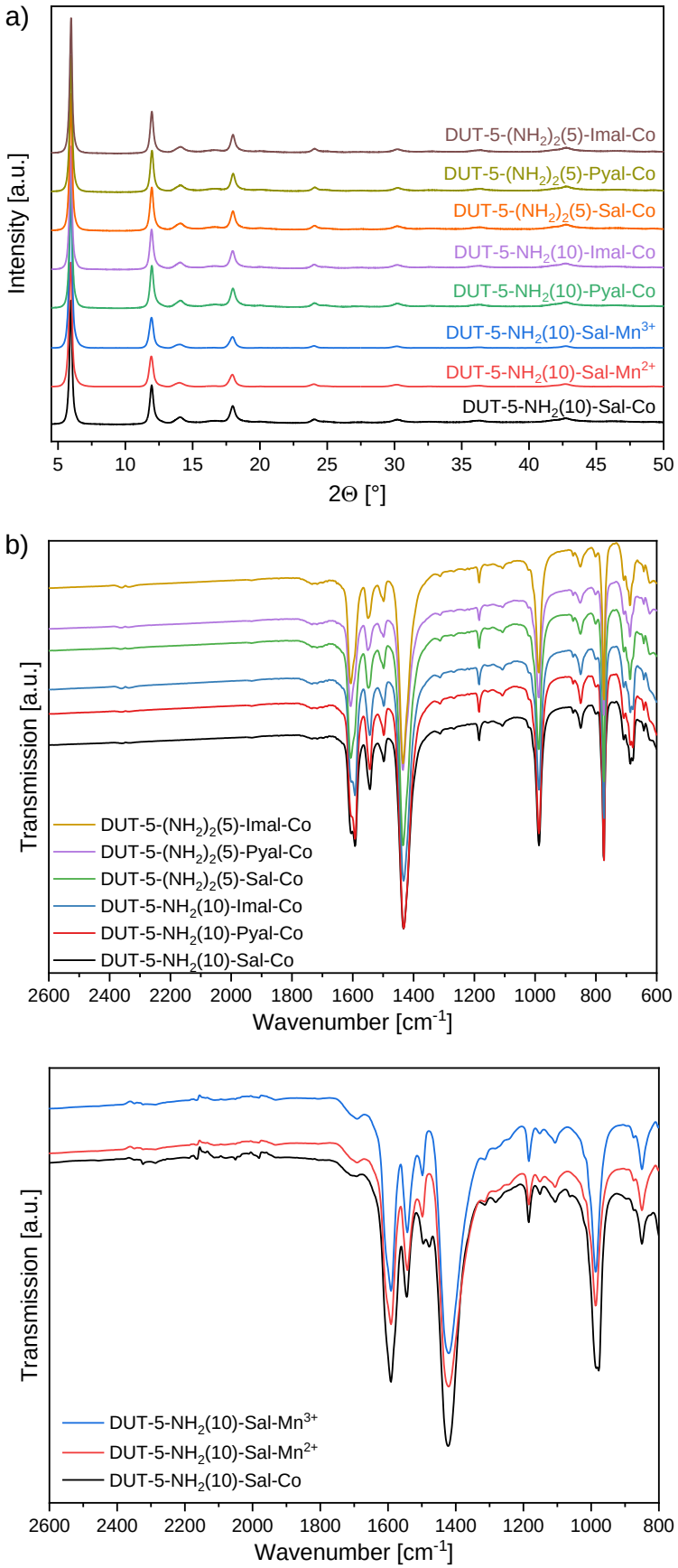

Figure 32. Powder X-ray diffraction patterns (a) and ATR-IR spectra (b) of amine-functionalized DUT-5 materials after immobilization of metals.

The structure of the metal containing materials proved to be isoreticular to the DUT-5 structure, which was confirmed by the X-ray diffraction measurements (Figure 32a). ATR-IR spectroscopy showed bands similar to the DUT-5 spectrum (Figure 32b). Thus, the immobilization of the metals did not destroy the framework structure.

ICP-OES analysis showed that the chelating moieties were partially occupied with the metal ions (Table 5). The metal loading was 0.14 – 0.29 wt% on average. For DUT-5-NH_2(10)-Sal-Co, 70% of the available side groups were loaded with cobalt. Since the modification degrees of the other materials could not be determined, consequently the amount of immobilized chelating side groups could not also be determined.

The porosity of the materials was retained during the immobilization. High specific surface areas were obtained for the materials, which indicated that no undesired nanoparticles should be formed. The pore systems of the framework were still accessible for substrate molecules, which is required for the further catalytic application. EXAFS studies (*cf.* chapter 3.1.2) could not performed for these samples within the present work.

Table 6. Specific surface areas (S_{BET}), total pore volumes (tpv), micropore volumes (mpv) and metal content of DUT-5 materials after immobilization of metals.

Entry		S_{BET} [m^2/g]	tpv [cm^3/g]	mpv [cm^3/g]	metal loading [wt%]
1	DUT-5-NH_2(10)-Sal-Co	1760	0.78	0.63	0.14
2	DUT-5-NH_2(10)-Pyal-Co	1850	0.82	0.67	0.16
3	DUT-5-NH_2(10)-Imal-Co	1810	0.81	0.65	0.23
4	DUT-5-$(NH_2)_2$(5)-Sal-Co	1920	0.90	0.69	0.20
5	DUT-5-$(NH_2)_2$(5)-Pyal-Co	1900	0.94	0.70	0.25
6	DUT-5-$(NH_2)_2$(5)-Imal-Co	1960	0.92	0.70	0.29

Cobalt and manganese containing catalyst materials were established by utilizing the different chelating moieties. Various characterization methods showed comparable results for both the mono- and the difunctionalized DUT-5 materials. In order to determine a possible influence of the spatial proximity of the active centers in the framework materials, the catalysts were applied in selective oxidation reactions.

3.3 Alkyne-functionalized DUT-5 materials

3.3.1 Synthesis of mixed-linker DUT-5-C_2H(10) and post-synthetic modification *via* iClick reaction

Recently, in terms of click chemistry, the use of metal azides or metal-alkynes resulting in inorganic click reactions (iClick) has gained great attention.[219-223] With regard to metal-organic framework chemistry, the approach of iClick reactions seems very promising due to its capability of introducing complex organic or organometallic compounds into the framework structure. In this chapter, alkyne-functionalized DUT-5 materials were applied in iClick reactions using gold(I)-azide as reaction component. The gold(I)-azide compound was provided by the group of Professor Roesky (Karlsruhe Institute of Technology).

The synthesis of the mixed-linker alkyne-containing DUT-5 material was performed according to the synthetic procedures described in the previous sections. Under solvothermal conditions 10% of the 4,4'-biphenyldicarboxylic acid (H_2BPDC) linkers were replaced by 2-ethynyl-4,4'-biphenyldicarboxylic acid (H_2EBPDC) resulting in DUT-5-C_2H(10) [Al(OH)(BPDC)$_{0.9}$(EBPDC)$_{0.1}$].

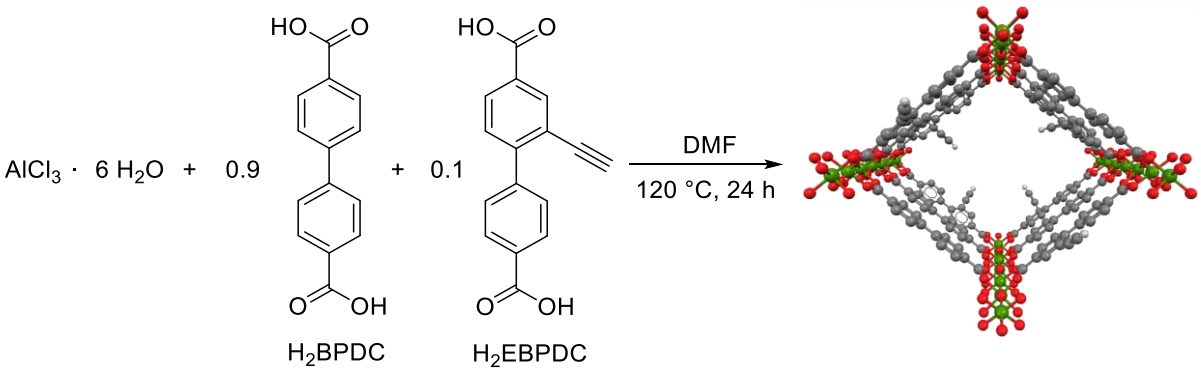

Scheme 20. Schematic representation of the synthesis of DUT-5-C_2H(10).

After thorough characterization of DUT-5-C_2H(10), the alkyne groups were modified with the gold(I)-azide N_3AuPPh_3 *via* inorganic click (iClick) reaction resulting in DUT-5-C_2H(10)-[(triazole)$AuPPh_3$]. The PSM reaction was performed in a laboratory shaker for 48 h at room temperature according to the literature procedure by Partyka *et al.*[219] The use of toluene as solvent led to a suspension of the gold(I)-azide compound. Thus, another reaction was performed in dichloromethane, where the precursor was completely dissolved.

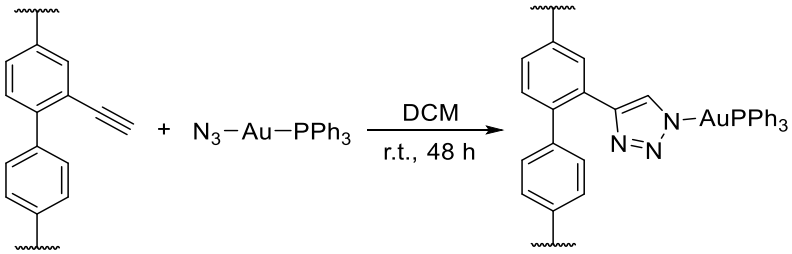

Scheme 21. Schematic representation of the post-synthetic modification of DUT-5-C_2H(10) with gold(I)-azide.

ATR-IR spectroscopy measurements revealed an azide band at 2061 cm^{-1} indicating that unreacted azide precursor was present in the pores of the gold-containing DUT-5-C_2H(10) material, which was synthesized in toluene. In contrast, the reaction performed in dichloromethane exhibited free pores without any guest molecules. Powder X-ray diffraction pattern showed that the structure of DUT-5 was maintained during post-synthetic modification.

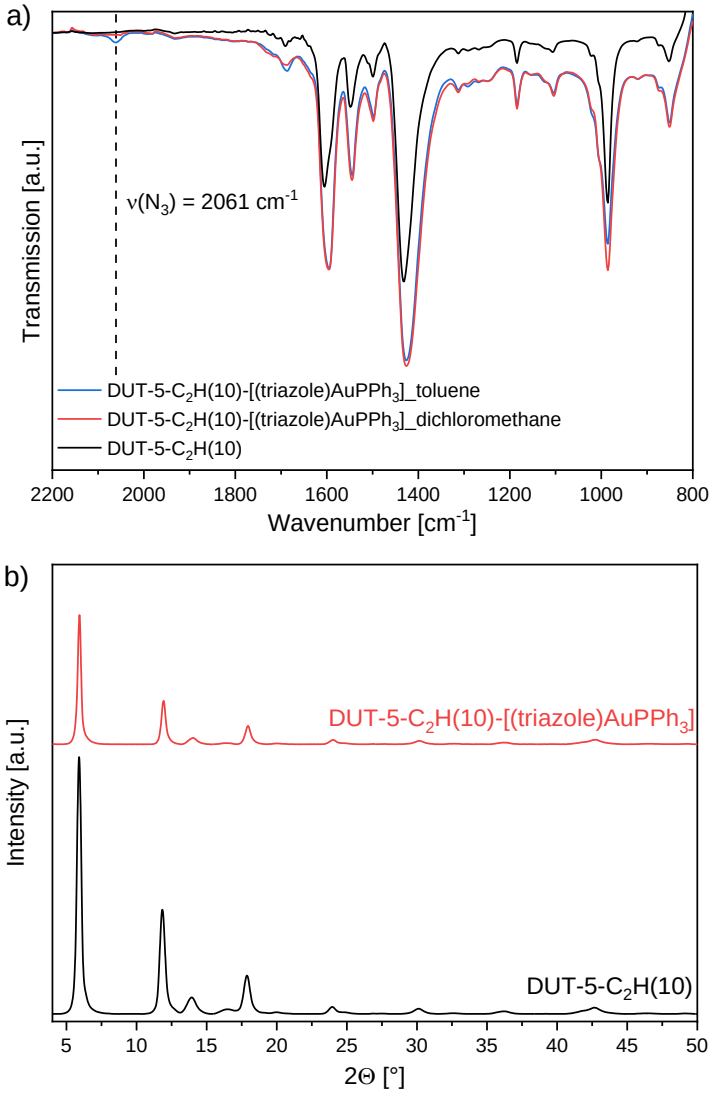

Figure 33. ATR-IR spectra (a) and powder X-ray diffraction patterns (b) of DUT-5-C_2H(10) before and after post-synthetic modification.

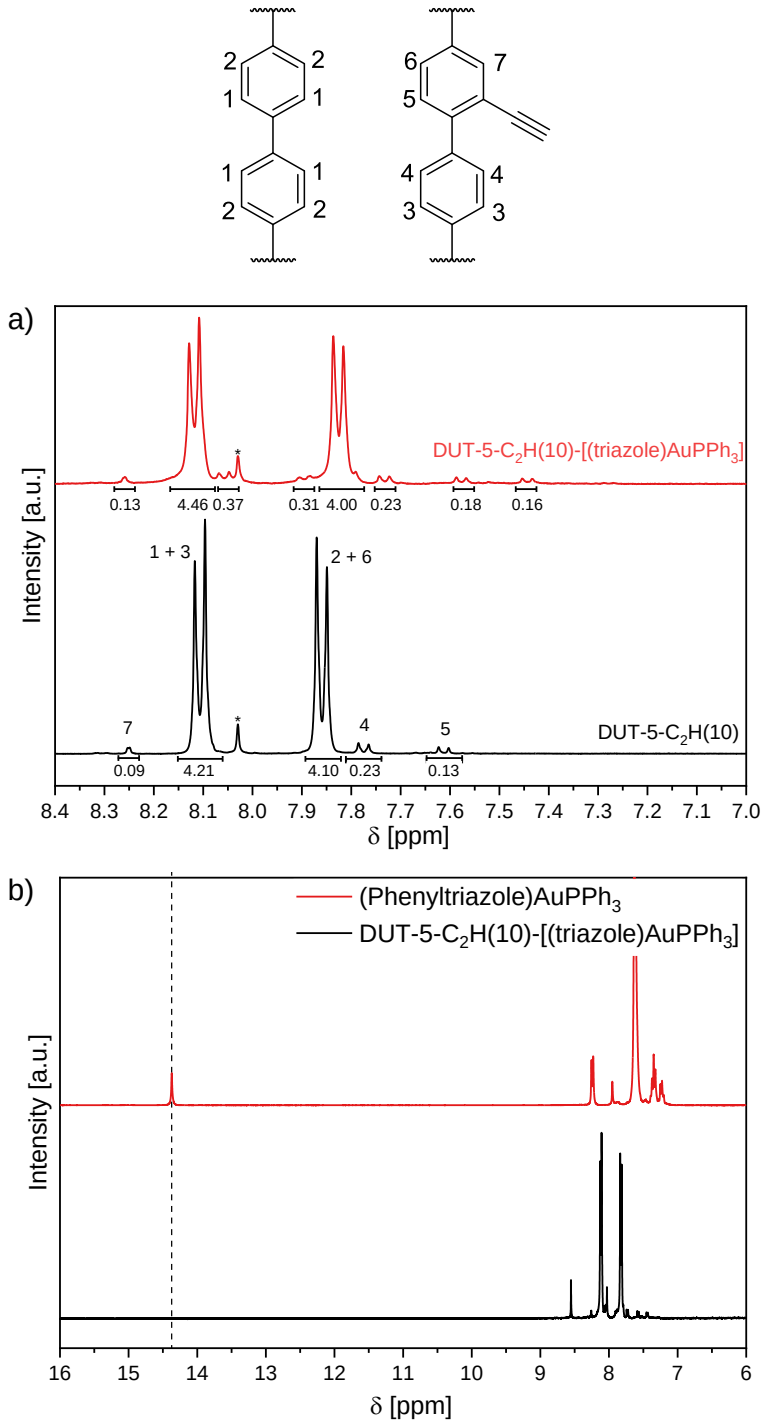

Figure 34. ^{1}H NMR spectra of digested alkyne-functionalized DUT-5 materials after post-synthetic modification.

^{1}H NMR spectra of the DUT-5-C_2H(10) materials were recorded before and after the PSM reaction (Figure 34a). For DUT-5-C_2H(10), 11% of alkyne groups were found in the structure, which matched very well with the used amount of alkyne-functionalized linkers during synthesis. A quantification of the modification degree of the modified DUT-5-C_2H(10) material was expected to be difficult due to the strong overlap of the peaks of the side group with the

peaks of the linker molecules. However, new peaks were observed after the PSM reaction, which confirmed the presence of modified alkyne groups of the framework.

Furthermore, Partyka *et al.* reported that the reaction between phenylacetylene and N_3AuPPh_3 resulted in a product in which the 1,2,3-triazolato ligand was bound through the carbon, which was confirmed by the *N-H* peak at $\delta = 14.3$ ppm in the ^1H NMR spectrum. However, the spectrum of the modified DUT-5 material revealed no *N-H* peak, which might indicate a gold-nitrogen bound. Nevertheless, an exchange of the *N-H* proton with the deuterated proton of sodium deuteriumoxide (NaOD) could not be ruled out (Figure 34b).

DUT-5-C_2H(10) showed a high porosity with a specific surface area of 1600 m^2/g and a total pore volume of 0.76 cm^3/g. After post-synthetic modification, the specific surface area decreased to 1200 m^2/g (Table 7).

In the case of a complete modification, a gold loading of 6.34 wt% would be obtained. For DUT-5-C_2H(10)-[(triazolate)$AuPPh_3$], a gold loading of 3.64 wt% was determined from ICP-OES analysis. Consequently, a modification degree of 57% of the alkyne groups could be calculated.

Table 7. Specific surface areas (S_{BET}), total pore volumes (tpv) and micropore volumes (mpv) of DUT-5-C_2H(10) before and after post-synthetic modification and determined gold content of DUT-5-C_2H(10)-[(triazolate)$AuPPh_3$].

Entry		S_{BET} [m^2/g]	tpv [cm^3/g]	Metal loading [wt%]
1	DUT-5-C_2H(10)	1600	0.76	-
2	DUT-5-C_2H(10)-[(triazole)AuPPh3]	1200	0.63	3.64

XANES analysis at the Au L_3-edge showed that the oxidation state of +1 was retained throughout the post-synthetic modification process (Figure 35a). With regard to the spectra of the gold-containing DUT-5 material and metallic gold, a shift of the edge position of 1.2 eV at the maximum of the first derivative was observed indicating the presence of Au^+. Since the observed white line at 11925 eV corresponded to Au^+, the presence of Au^{3+} (white line at 11920 eV) was excluded. The formed gold complex at the side group of the linker could be confirmed using Fourier-transformed EXAFS analysis. The best fit was obtained for the expected (triazole)$AuPPh_3$ complex (denoted as $1N_{Triazole}$ $1P_{PPh_3}$), since the fit with Au neighbors from a metallic gold crystal structure showed a very low coordination number with high error bars (Figure 35b and Table A6).[212]

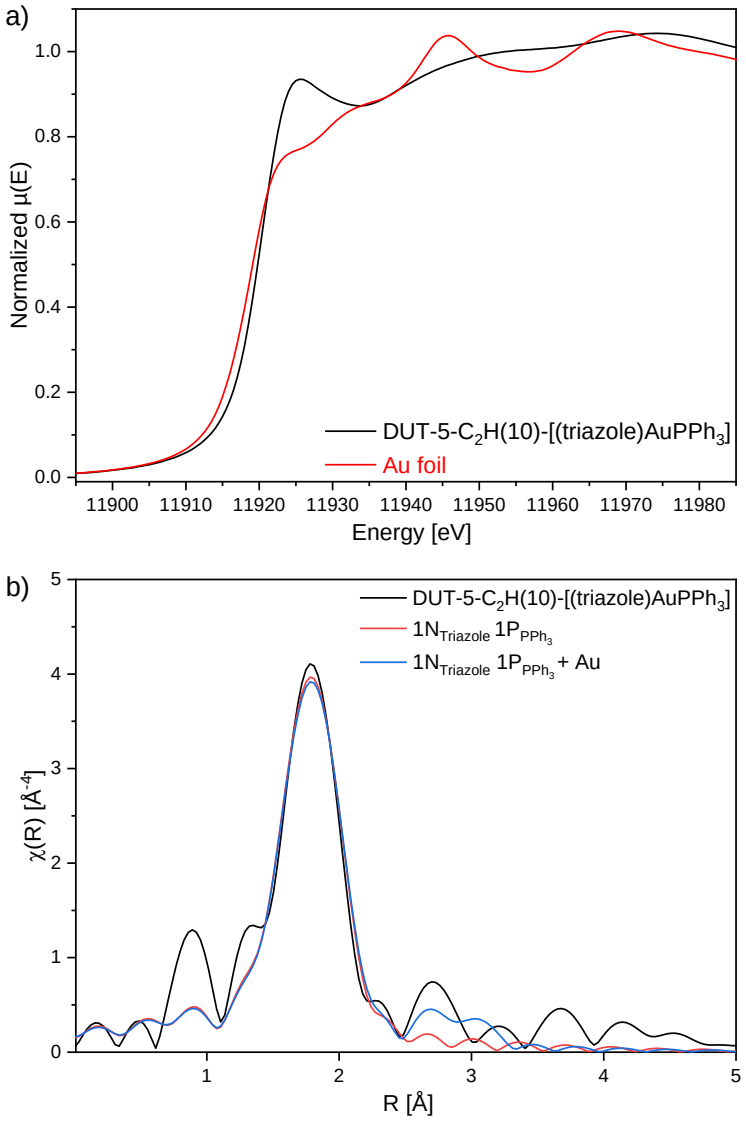

Figure 35. Au L_3-edge XANES spectra (a) and Fourier-transformed experimental EXAFS spectra with the comparison of the fits (b) of DUT-5-C_2H(10)-[(triaziole)AuPPh$_3$].

Fluorescence microscopy measurements proved that the gold containing DUT-5 materials showed fluorescence behavior. To ensure that the fluorescence originated from the gold compound, microscopic images of DUT-5-C_2H(10) were also recorded. As depicted in Figure 36a, a low intensity of the fluorescence was detected, whereas the intensity of the gold-functionalized DUT-5 materials were significantly higher. These results proved the successfully incorporation of the gold triazolate complex.

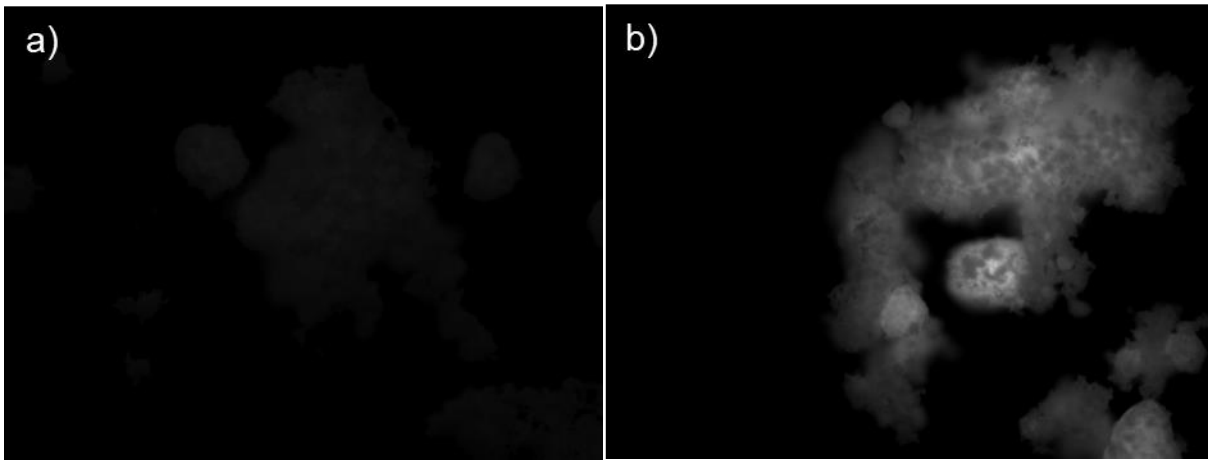

Figure 36. Fluorescence light microscopic images of DUT-5-$C_2H(10)$, exposure time = 400 ms (a) and DUT-5-$C_2H(10)$-[(triazole)$AuPPh_3$], exposure time = 400 ms (b).

The click reaction between alkyne-modified DUT-5 materials and gold azides offers a broad opportunity for the use of various metal azides to introduce covalently bound metal species into the framework pores, which represent promising materials for various applications, in particular for heterogeneous catalysis.

4 Application of MOF-based single-site catalysts in liquid phase reactions

4.1 Aerobic epoxidation of α-pinene

The development of sustainable catalytic processes for chemical reactions using renewable raw materials has become a major focus, *e.g.* in the synthesis of oxygen containing compounds. Among these processes, the oxidation of monoterpenes like α-pinene produces valuable fine chemicals. Recently, numerous catalytic systems have been applied in the oxidation of α-pinene by using different reaction conditions. In collaboration with Y. Raupp and Prof. M. Meier (Karlsruhe Institute of Technology), the synthesized MIL-53(Al)-NH_2(50)-Mal-Mn material (see chapter 3.2.1) was used as heterogeneous catalyst in the aerobic oxidation of α–pinene. The catalytic reaction of α-pinene with molecular oxygen resulted in pinene oxide as the main product with small amounts of verbenone and verbenol as the side products (Scheme 22). First, the influence of different reaction parameters on conversion, yield and selectivity were evaluated using Mn(III) acetate as a homogeneous catalyst by the group of Prof. Meier. High temperatures of 130 °C, an oxidant flow rate of 50 ml/min, a low catalyst concentration (0.25 mol%) and a toluene/DMF solvent mixture have been found as the most favorable reaction conditions. Subsequently, the optimized reaction conditions were applied to the manganese-containing MIL-53(Al)-NH_2(10)-Mal-Mn material and the obtained results will be briefly discussed in this chapter.

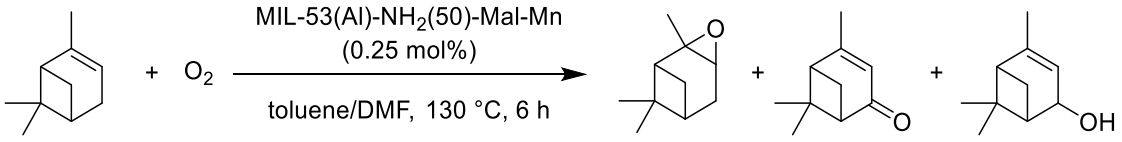

Scheme 22. Catalytic oxidation of α-pinene by MIL-53(Al)-NH_2(50)-Mal-Mn resulting in pinene oxide as the main product, verbenone and verbenol as the side products.

The oxidation of α-pinene using the homogeneous catalyst Mn(III) acetate and air as oxidant resulted in a conversion of 62% with a yield of 40% pinene oxide, 4% verbenone and 3% verbenol. Toluene was exchanged by diethyl carbonate (DEC) to prevent side reactions with toluene. Diethyl carbonate was used as sustainable alternative for toluene, however, pure DEC without DMF resulted in poor conversion and yield. The use of a DEC/DMF solvent mixture

in a ratio of 9:1 resulted in 38% conversion and 23% pinene oxide yield using 1.0 mol% manganese(III) acetate.

After thorough investigations of different reaction parameters with the homogeneous manganese catalyst, the optimized reaction conditions were applied in the α-pinene oxidation with MIL-53(Al)-NH_2(50)-Mal-Mn as heterogeneous catalyst to facilitate a direct comparison of the catalyst performances. A conversion of 31% α-pinene and a yield of 17% pinene oxide were achieved using 0.5 mol% MOF catalyst, which proved to be similar to its homogeneous counterpart (Figure 37a). The selectivities to pinene oxide (55%), verbenone (7%) and verbenol (6%) were also comparable.

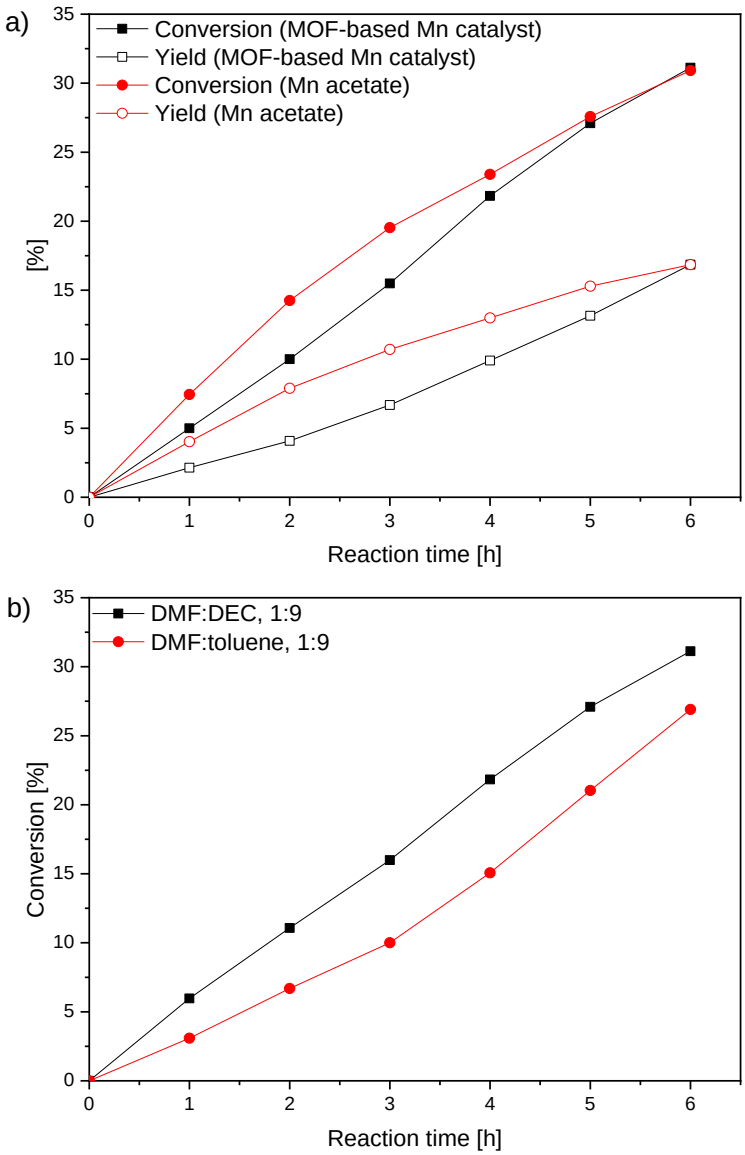

Figure 37. Conversion and yield of the aerobic oxidation of α-pinene catalyzed by MIL-53(Al)-NH_2(50)-Mal-Mn and homogeneous Mn(III) acetate (a) and solvent effect on the conversion using MIL-53(Al)-NH_2(50)-Mal-Mn (b).

The effect of the solvent was tested applying the heterogeneous manganese-containing MOF. Using the solvent mixture of DEC/DMF, the conversion of α-pinene was higher than the conversion achieved with the solvent mixture of toluene/DMF (27%) (Figure 37b).

Heterogeneity and recycling tests were performed to investigate the reusability of MIL-53(Al)-NH_2(50)-Mal-Mn. The solid catalyst was filtered from the reaction mixture, washed, dried at room temperature und reused another four times in α-pinene oxidations under the same conditions. As depicted in Figure 38a, the catalyst was active for at least five reaction runs without significant loss of activity. In the five consecutive runs, an overall turnover number (TON) of 166 was obtained.

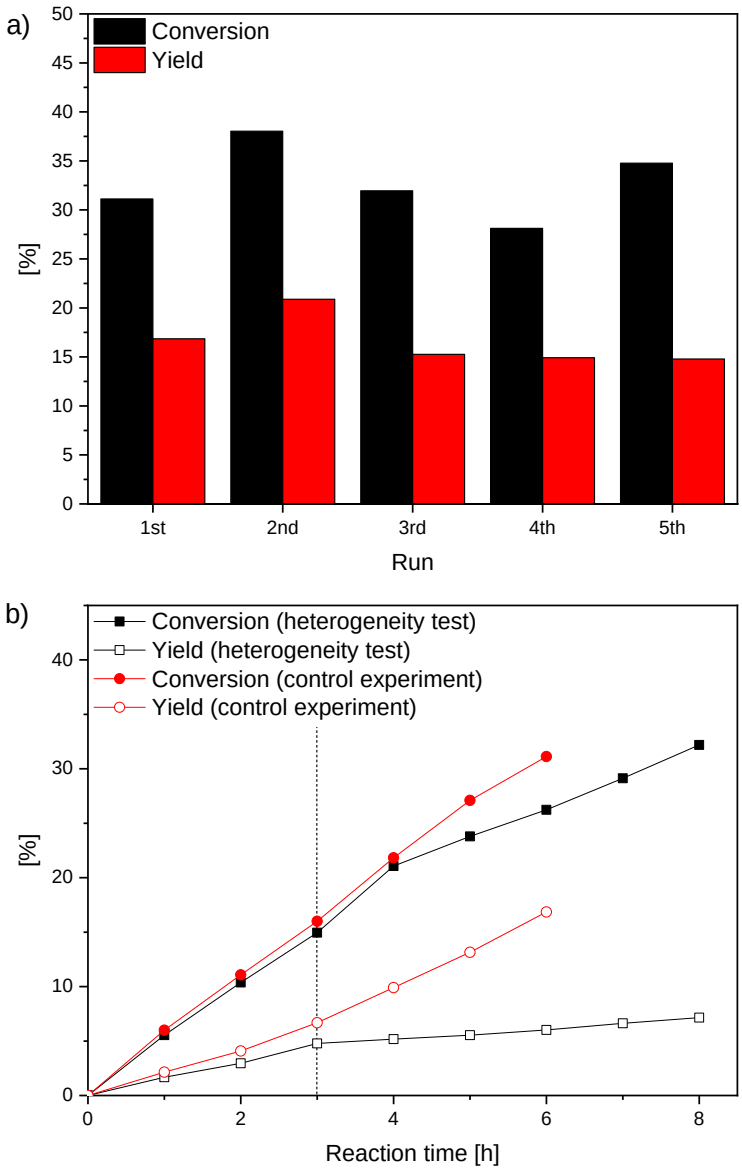

Figure 38. Conversion and yield in five runs of the aerobic α-pinene oxidation (a) and comparison of conversion and yield with and without catalyst removal after 2.5 h (as indicated by vertical line) (b).

Furthermore, for a rigorous proof of heterogeneity, hot filtration tests were carried out by filtering the solid catalyst from the hot reaction mixture after 3 h and continuing the reaction for another 5 h (Figure 38b). At the same time, a control experiment was performed by leaving the catalyst in the reaction mixture. The results showed that conversion and yield further increased slightly after filtration. The activity after filtration might be caused by small solid particles, which could not be removed by filtration from the reaction mixture, although minor amounts of homogeneous species could not be completely ruled out. Nevertheless, compared to the control experiment, the reaction rate was much lower and, thus, the reaction proved to be catalyzed *via* a heterogeneous pathway.

To conclude, considering the recyclability of the catalyst, the heterogenization of homogeneous catalysts could be achieved by using metal-organic frameworks and, thus, the resulting single-site catalyst can be considered as a promising catalyst material for aerobic oxidation reactions under green conditions.

4.2 Aerobic epoxidation of *trans*-stilbene

The cobalt- and manganese-containing DUT-5 materials (syntheses described in chapter 3.1.2 and 3.2.2.2) were applied in the aerobic oxidation of *trans*-stilbene (Scheme 23). In a typical reaction, *trans*-stilbene oxide was obtained as the main product and benzaldehyde as a side product using air as the oxidizing agent in DMF as solvent. DUT-5-BPyDC(10)-Co and DUT-5-BPyDC(10)-Mn^{2+} were used to investigate the influence of various reaction parameters such as temperature, oxidant flow rate, catalyst concentration and substrate concentration. The activities of the catalyst materials DUT-5-BPyDC(10)-Mn^{3+}, DUT-5-NH_2(10)-Sal-Co, DUT-5-NH_2(10)-Sal-Mn^{2+} and DUT-5-NH_2(10)-Sal-Mn^{3+} were compared under optimized conditions. Conversions, yields and selectivities were evaluated by variation of one reaction parameter at a time, whereas the others remained unchanged, and the quantification was done by GC analysis using biphenyl as an internal standard.

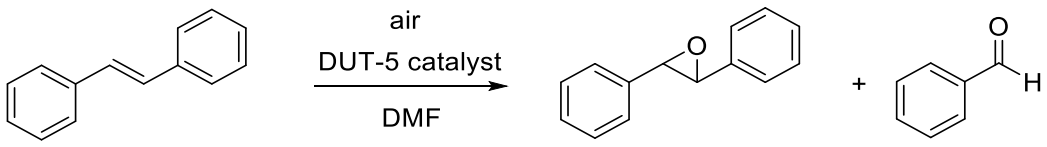

Scheme 23. Aerobic epoxidation of trans-stilbene catalyzed by metal-containing DUT-5 resulting in trans-stilbene oxide (main product) and benzaldehyde (side product).

First, a reaction without the solid catalyst was performed as a blank test at 150 °C for 24 h with a continuous air flow through the solution (200 ml/min), which resulted in 12% *trans*-stilbene conversion and 10% product formation (Table 8, Entry 1). A blank test using a bipyridine-containing DUT-5 without further metal immobilization was also carried out, which gave 9% conversion and 6% yield (Table 8, Entry 2). In contrast, the reaction catalyzed with DUT-5-BPyDC(10)-Co led to a much higher conversion of 93% (Figure 39) and with DUT-5-BPyDC(10)-Mn to 32% (Figure 40) indicating that the formation of *tans*-stilbene oxide was truly induced by the metal-containing DUT-5 materials.

Table 8. Blank tests of the epoxidation of trans-stilbene. Reaction conditions: 24 h, 150 °C, air flow (200 ml/min), trans-stilbene (1 mmol), DMF (60 ml).

Entry	Material	Conversion [%]	Yield [%]	Selectivity [%]
1	-	12	10	76
2	DUT-5-BPyDC(10)	9	6	68

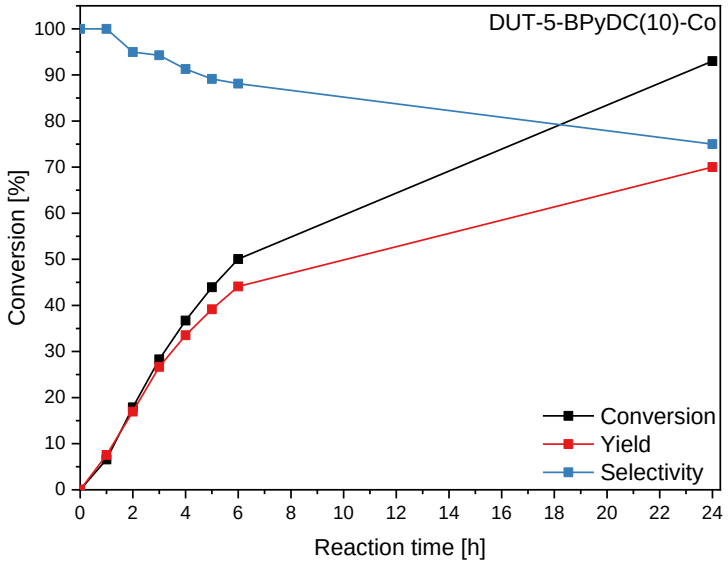

Figure 39. Conversion, yield and selectivity of the epoxidation of trans-stilbene catalyzed by DUT-5-BpyDC(10)-Co. Reaction conditions: 24 h, 150 °C, catalyst amount (0.02 mol% of cobalt), air flow (200 ml/min), trans-stilbene (1 mmol), DMF (60 ml).

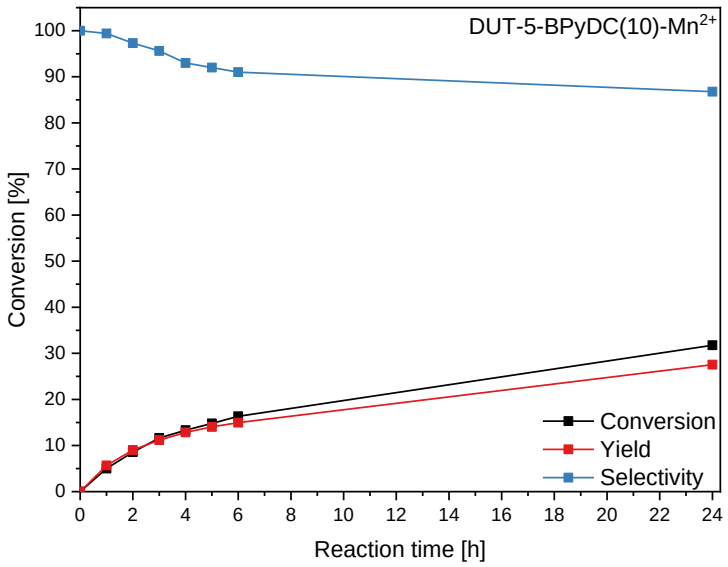

Figure 40. Conversion, yield and selectivity of the epoxidation of trans-stilbene catalyzed by DUT-5-BPyDC(10)-Mn^{2+}. Reaction conditions: 24 h, 150 °C, catalyst amount (0.02 mol% of manganese), air flow (200 ml/min), trans-stilbene (1 mmol), DMF (60 ml).

The impact of various reaction temperatures was studied using temperatures of 90, 110, 130 and 150 °C. The conversion of *trans*-stilbene increased at higher temperatures due to an increased reaction rate. After 24 h at 90 °C, conversion and yield were 51% and 46%, whereas these values reached to 93% and 70% at 150 °C using DUT-5-BPyDC(10)-Co (Table 9). Higher temperatures led to the additional formation of benzaldehyde (10% at 150 °C) as a side product, which caused a decreased selectivity. For the DUT-5-BPyDC(10)-Mn^{2+} catalyst, conversion and yield increased from 5% and 4% at 90 °C to 32% and 28%, respectively, at 150 °C (Table 10). The formation of benzaldehyde was not observed in detectable amounts *via* GC analysis.

Table 9. Influence of the temperature on the epoxidation of trans-stilbene catalyzed by DUT-5-BPyDC(10)-Co. Reaction conditions: 24 h, catalyst amount (0.02 mol% of cobalt), air flow (200 ml/min), trans-stilbene (1 mmol), DMF (60 ml).

Entry	Temperature [°C]	Conversion [%]	Yield [%]	Selectivity [%]
1	90	51	46	89
2	110	80	71	88
3	130	89	72	81
4	150	93	79	75

Table 10. Influence of the temperature on the epoxidation of trans-stilbene catalyzed by DUT-5-BPyDC(10)-Mn^{2+}. Reaction conditions: 24 h, catalyst amount (0.02 mol% of manganese), air flow (200 ml/min), trans-stilbene (1 mmol), DMF (60 ml).

Entry	Temperature [°C]	Conversion [%]	Yield [%]	Selectivity [%]
1	90	5	4	76
2	110	11	9	78
3	130	16	14	90
4	150	32	28	87

Next, the influence of the air flow rate was tested by using flow rates of 100, 200 and 300 ml/min. The conversion of *trans*-stilbene with DUT-5-BPyDC(10)-Co as catalyst was evaluated after 6 hours, since the conversion after 24 h was almost complete (Figure 41). The conversion increased from 31 to 50% and the yield from 28 to 44%, respectively, by increasing the air flow from 100 to 200 ml/min. However, a further increase of the flow rate to 300 ml/min did neither enhance the conversion nor the yield. For DUT-5-BPyDC(10)-Mn^{2+}, only slight differences were observed after 24 h by increasing the air flow rate (Figure 42).

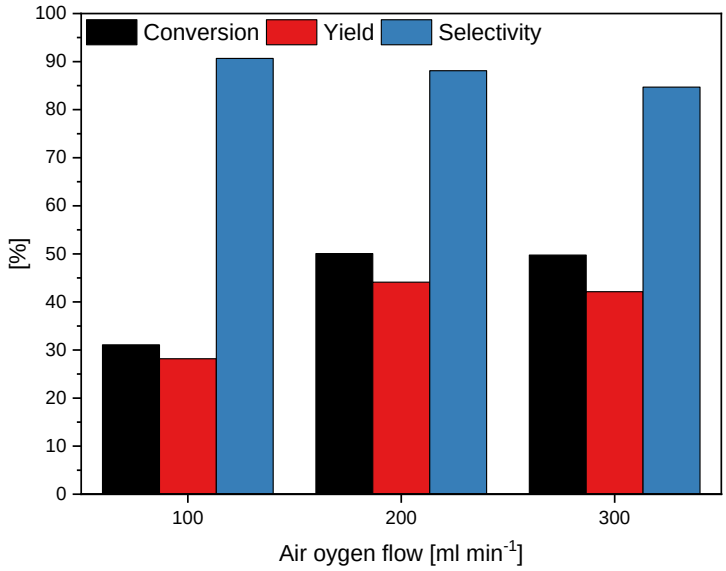

Figure 41. Influence of the air flow rate on the epoxidation of trans-stilbene catalyzed by DUT-5-BPyDC(10)-Co. Reaction conditions: 6 h, 150 °C, catalyst amount (0.02 mol% of cobalt), trans-stilbene (1 mmol), DMF (60 ml).

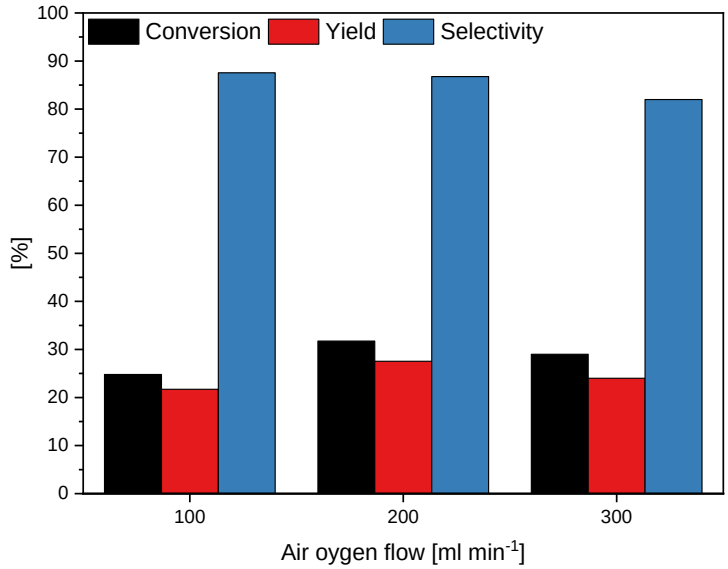

Figure 42. Influence of the air flow rate on the epoxidation of trans-stilbene catalyzed by DUT-5-BPyDC(10)-Mn^{2+}. Reaction conditions: 24 h, 150 °C, catalyst amount (0.02 mol% of manganese), trans-stilbene (1 mmol), DMF (60 ml).

The catalyst concentration was varied from 0.05 to 0.01 mol% based on the determined metal content (*cf.* ICP-OES measurements in Table 2). For DUT-5-BPyDC(10)-Co, the results were compared after 6 h (Table 11). The decrease of the cobalt amount from 0.05 to 0.02 mol% resulted in a drop of the *trans*-stilbene conversion from 73% to 58%. A further decrease to 0.01 mol% catalyst led to a decrease of the conversion to 34%. The highest selectivity was achieved using 0.02 mol% cobalt (91%). Despite the small catalyst amount, high yields were obtained with high turnover numbers. An increase of the turnover number from 1300 for 0.05 mol% to 3000 for 0.01 mol% was observed. By reducing the amount of manganese, the conversion of *trans*-stilbene decreased from 54 to 19% and the selectivity increased from 83 to 90%, which caused an increase of the turnover numbers was found from 500 to 1700.

Table 11. Influence of the catalyst concentration on the epoxidation of trans-stilbene catalyzed by DUT-5-BPyDC(10)-Co. Reaction conditions: 6 h, 150 °C, air flow (200 ml/min), trans-stilbene (1 mmol), DMF (60 ml).

Entry	Catalyst amount [mol%]	Conversion [%]	Yield [%]	Selectivity [%]	TON
1	0.05	73	64	87	1300
2	0.02	59	54	91	2700
3	0.01	34	29	85	3000

Table 12 Influence of the catalyst concentration on the epoxidation of trans-stilbene catalyzed by DUT-5-BPyDC(10)-Mn^{2+}. Reaction conditions: 24 h, 150 °C, air flow (200 ml/min), trans-stilbene (1 mmol), DMF (60 ml).

Entry	Catalyst amount [mol%]	Conversion [%]	Yield [%]	Selectivity [%]	TON
1	0.05	54	45	83	900
2	0.02	32	28	87	1400
3	0.01	19	17	90	1700

The next investigations focused on variations of the substrate concentration. The molar amount of *trans*-stilbene was increased from 1 to 5 mmol, whereas the amounts of the catalyst (6.4 mg) and solvent (60 ml) were not changed. Thus, the catalyst/substrate ratio decreased from 0.02 to 0.002 mol% of cobalt and manganese, respectively, with increasing amount of *trans*-stilbene. For DUT-5-BPyDC(10)-Co, nearly full conversion was achieved after 24 h regardless of the substrate concentration, hence, the results were compared after 6 h (Table 13). The conversion decreased from 55% for 1 mmol *trans*-stilbene to 45% for 5 mmol *trans*-stilbene amount. Surprisingly, only a slightly decrease of the conversion was observed (Figure 43a). An experiment with 10 mmol *trans*-stilbene showed a further decrease to 22% conversion. Despite the marginal decrease of the conversion, the absolute amount of formed product increased from 0.50 to 3.84 mmol (Figure 43b). Consequently, an increase of the turnover numbers was observed and also increased turnover frequencies (TOF) from 420 to 1770 h^{-1} after 6 h. By using DUT-5-BPyDC(10)-Mn^{2+}, the conversion dropped from 32 to 13%, whereas the determined turnover numbers and turnover frequencies (after 6 h) were nearly similar (Table 14).

Table 13. Influence of the substrate concentration on the epoxidation of trans-stilbene catalyzed by DUT-5-BPyDC(10)-Co. Reaction conditions: 6 h, 150 °C, catalyst (6.4 mg), air flow (200 ml/min), DMF (60 ml).

Entry	molar amount of *trans*-stilbene [mmol]	Catalyst amount [mol%]	Conversion [%]	Yield [%]	Selectivity [%]	TON	TOF [h^{-1}]
1	1	0.0200	55	50	90	2500	420
2	2	0.0100	57	52	91	5200	870
3	3	0.0067	58	49	85	7400	1230
4	4	0.0050	48	41	85	8100	1350
5	5	0.0040	45	42	94	11000	1770

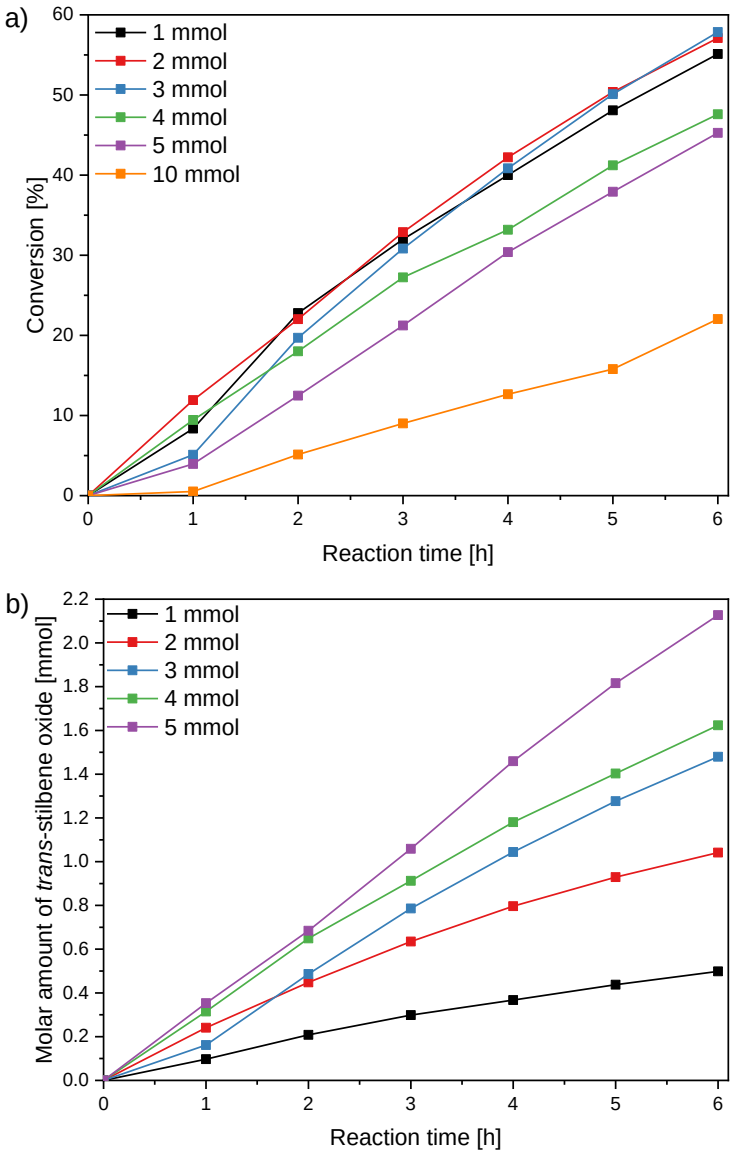

Figure 43. Conversion of trans-stilbene (a) and molar amount of the formed trans-stilbene oxide (b) with increasing molar amount of trans-stilbene by using DUT-5-BPyDC(10)-Co. Reaction conditions: 24 h, 150 °C, DUT-5-BPyDC(10)-Co (6.4 mg), air flow (200 ml/min), DMF (60 ml).

Table 14. Influence of the substrate concentration on the epoxidation of trans-stilbene catalyzed by DUT-5-BPyDC(10)-Mn^{2+}. Reaction conditions: 24 h, 150 °C, catalyst (6.4 mg), air flow (200 ml/min), DMF (60 ml).

Entry	molar amount of *trans*-stilbene [mmol]	Catalyst amount [mol%]	Conversion [%]	Yield [%]	Selectivity [%]	TON	TOF [h^{-1}][a]
1	1	0.02	32	28	87	1400	125
2	2	0.01	25	23	92	2300	120
3	3	0.0067	17	15	86	2200	130
4	4	0.005	20	17	86	3400	230
5	5	0.004	13	11	87	2800	200

[a)] Determined after 6 h.

Since a promoting effect of benzaldehyde was reported for a cobalt-based MOF catalyst in literature [206], the role of the formed benzaldehyde was investigated using DUT-5-BPyDC(10)-Co. Therefore, 0.1 equivalents of benzaldehyde were added as an additive to the reaction mixture. The observed reaction rate was much higher than the reaction rate without the benzaldehyde additive. The conversion of *trans*-stilbene was 93% after 6 h and, thus, 34% higher than the conversion reached without benzaldehyde. The remarkable decrease of the yield of *trans*-stilbene oxide might indicate that over-oxidation occurred. These results proved the promoting effect of benzaldehyde in the cobalt-catalyzed epoxidation of *trans*-stilbene. Since around 10% benzaldehyde was formed as side product by using DUT-5-BPyDC(10)-Co, the effects, which were observed in the experiments with variation of the substrate concentration (Table 13), might also be explained by this promoting effect.

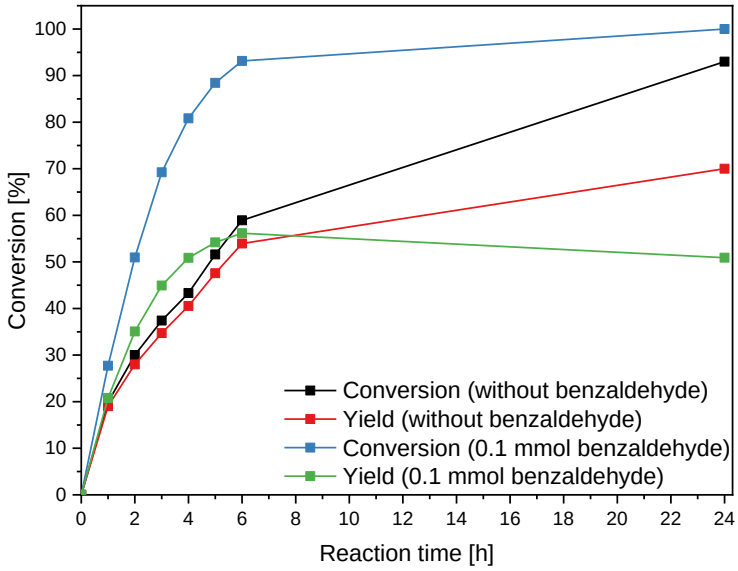

Figure 44. The effect of benzaldehyde on the conversion and yield of trans-stilbene epoxidation catalyzed by DUT-5-BPyDC(10)-Co. Reaction conditions: 24 h, 150 °C, catalyst amount (0.02 mol% of cobalt), air flow (200 ml/min), trans-stilbene (1 mmol), DMF (60 ml).

Combining these results, the reaction parameters of 24 h, 150 °C, 0.02 mol% catalyst amount, 200 ml/min air flow and 1 mmol *trans*-stilbene in 60 ml DMF were found to be the optimal conditions. Under these conditions, the catalytic performance of DUT-5-BPyDC(10)-Mn^{3+}, DUT-5-NH_2(10)-Sal-Co, DUT-5-NH_2(10)-Sal-Mn^{2+} and DUT-5-NH_2(10)-Sal-Mn^{3+} were tested and compared with each other. The cobalt-containing DUT-5 catalysts showed a significantly higher activity than their manganese counterparts (Figure 45). The results obtained with DUT-5-BPyDC(10)-Co and DUT-5-NH_2(10)-Sal-Co after 24 h were comparable. However, the comparison of the Mn^{2+} catalysts resulted in a higher conversion for DUT-5-

NH_2(10)-Sal-Mn^{2+} (44%) than for DUT-5-BPyDC(10)-Mn^{2+} (32%), whereas the same selectivity (86%) was achieved. DUT-5-BPyDC(10)-Mn^{3+} and DUT-5-NH_2(10)-Sal-Mn^{3+} did not differ significantly from the Mn^{2+} materials.

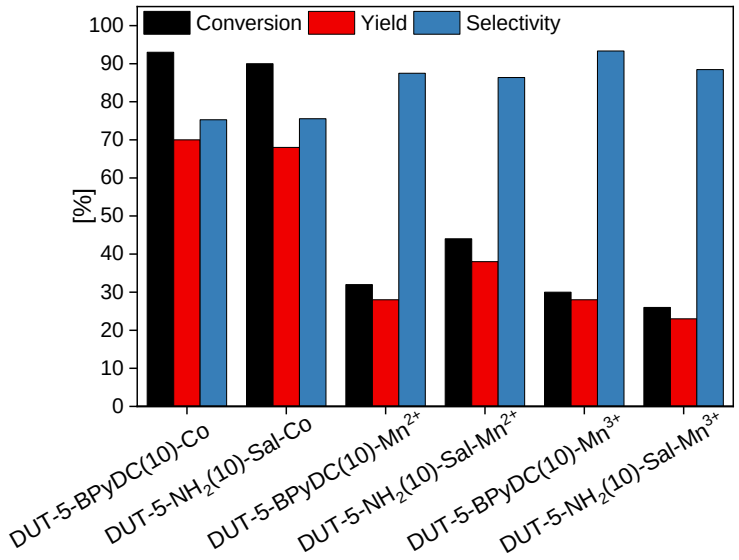

Figure 45. Comparison of the conversion, yield and selectivity for the different DUT-5 catalysts. Reaction conditions: 24 h, 150 °C, catalyst amount (0.02 mol% of metals), air flow (200 ml/min), trans-stilbene (1 mmol), DMF (60 ml).

Heterogeneity tests were performed using a hot filtration experiments with DUT-5-BPyDC(10)-Co. The catalyst was removed after 2.5 h reaction time and the reaction was continued without the solid catalyst. The results showed that the conversion and yield of *trans*-stilbene oxide increased only slightly after catalyst removal (Figure 46a). In comparison to the control experiment, which was run at the same time with catalyst, the reaction rate of the hot filtration test was much lower and, thus, indicated that the reaction was mainly catalyzed heterogeneously. A conversion of 49% and a yield of 45% were achieved after hot filtration, whereas the control experiment gave a conversion of 90% and a yield of 69%. Due to the fact that the particle size of the DUT-5 catalysts after the synthesis was very small (<1.6 µm), the particles had to be granulated before use to obtain particle sizes of 200 – 500 µm to facilitate an effective catalyst removal. Even though the hot filtration test and control experiment were conducted without stirring, a grinding of the DUT-5 particles during the catalytic tests could not be excluded. Thus, the observed activity after filtration might also originate from DUT-5-BPyDC(10)-Co particles, although a certain degree of contributions from dissolved species could not be excluded.

Finally, the reusability of DUT-5-BPyDC(10)-Co could be proven by using the catalyst in two consecutive runs without loss of activity (Figure 46b). For this purpose, the catalyst was filtered

after the first catalytic reaction, washed, dried at room temperature and reused in a second reaction under the same conditions. Although granulated powder material was used, a grinding of the particles was observed and, thus, the amount of recovered catalyst was not sufficient for a third run.

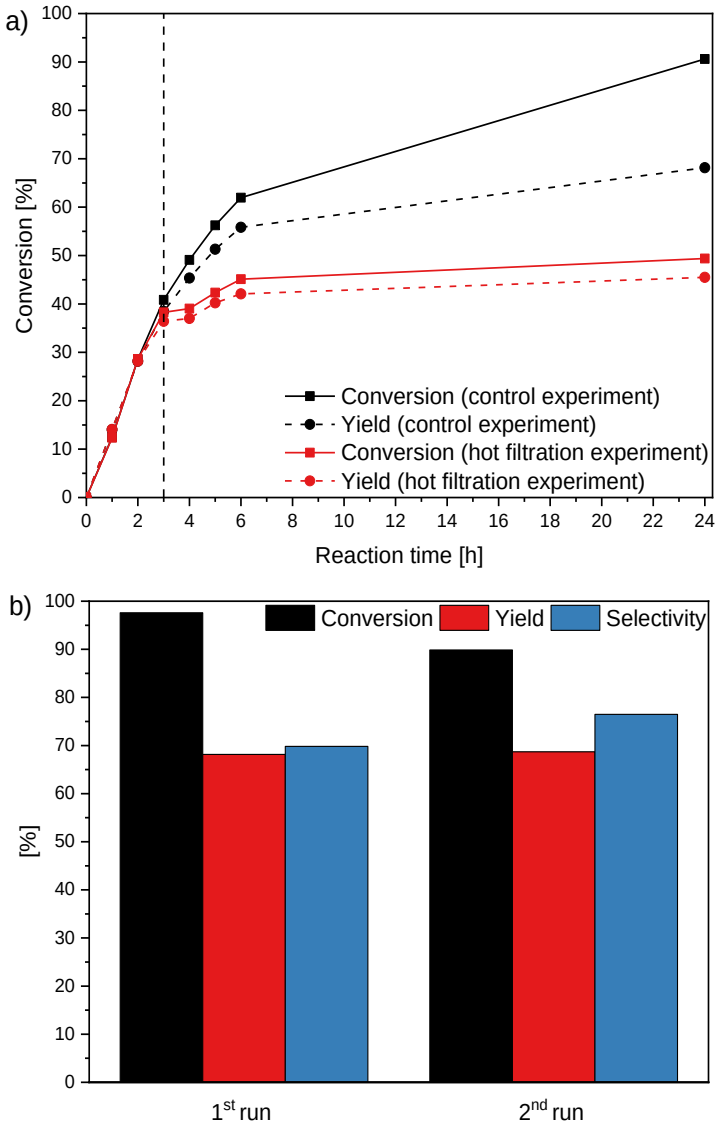

Figure 46. a) Comparison of conversion and yield of trans-stilbene epoxidation with and without catalyst removal after 2.5 h (as indicated by vertical line). b) Conversion and yield in two cycles of trans-stilbene epoxidation. . Reaction conditions: 24 h, 150 °C, granulated DUT-5-BPyDC(10)-Co (0.02 mol% of cobalt), air flow (200 ml/min), trans-stilbene (1 mmol), DMF (60 ml).

4.3 Aerobic oxidation of benzyl alcohol

The oxidation of benzyl alcohol was chosen as a catalytic test reaction for the synthesized cobalt-based DUT-5 catalysts (syntheses described in chapter 3.1.2 and 3.2.2.2). Since the

different positioning of the cobalt-centers within the pores of DUT-5-BPyDC(10) and DUT-5-NH_2(10)-Sal did not significantly affect the oxidation of *trans*-stilbene, the pore accessibility should be examined using benzyl alcohol as substrate, which is smaller than *trans*-stilbene. For this, the effect of DUT-5-BPyDC(10)-Co, DUT-5-NH_2(10)-Sal-Co, DUT-5-NH_2(10)-Pyal-Co, DUT-5-NH_2(10)-Imal-Co, DUT-5-$(NH_2)_2$(5)-Sal-Co, DUT-5-$(NH_2)_2$(5)-Pyal-Co and DUT-5-$(NH_2)_2$(5)-Imal-Co on conversion, yield and selectivity of the oxidation of benzyl alcohol should be tested and compared.

In a typical reaction, the oxidation of benzyl alcohol was performed using air as oxidizing agent resulting in benzaldehyde as the main product. Apart from that, also benzyl benzoate was found in minor quantity as a byproduct using GC-MS analysis. First, different reaction parameters, such as temperature, oxidant flow rate, catalyst concentration and substrate concentration, were investigated using DUT-5-BPyDC(10)-Co as the catalyst (Scheme 24). A reaction time of 6 hours, 140 °C reaction temperature, 200 ml/min air flow, 0.01 mol% catalyst concentration and 1 mmol benzyl alcohol in 30 ml DMF were chosen as standard reaction parameters. Conversion, yield and selectivity were evaluated by variation of one reaction parameter at a time, whereas the others remained unchanged, and quantified by GC analysis using biphenyl as internal standard.

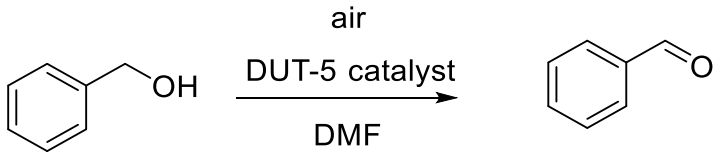

Scheme 24. Oxidation of benzyl alcohol resulting in benzaldehyde as main product catalyzed by cobalt-based DUT-5 materials.

A first test reaction was performed using DUT-5-BPyDC(10)-Co under the chosen standard conditions. The catalyst showed remarkable activity with a conversion of 87% and 48% yield of benzaldehyde. In order to ensure that cobalt was truly the active site for the oxidation reaction, blank tests were conducted without solid catalyst and with DUT-5-BPyDC(10) without further immobilization of cobalt. Both reactions resulted in a conversion of 4%, which indicated that the formation of benzaldehyde was truly induced by the cobalt-based MOF catalyst (Figure 47).

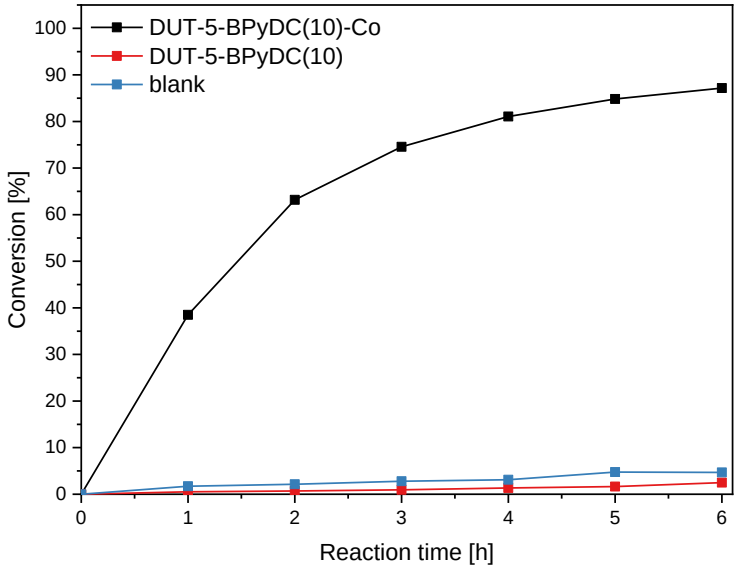

Figure 47. Comparison of the conversion with DUT-5-BPyDC(10)-Co, DUT-5-BPyDC(10) and without solid catalyst in the oxidation of benzyl alcohol. Reaction conditions: benzyl alcohol (1 mmol), biphenyl (0.33 mmol) as internal standard, air flow (200 ml/min), DMF (30 ml), 140 °C, 6 h. Red line: DUT-5-BPyDC(10) (3 mg). Blue line: DUT-5-BPyDC(10)-Co (0.01 mol% of cobalt).

For the catalytic screening, the influence of the reaction temperature was tested. Therefore, the reaction temperature was varied from 80 to 140 °C. As expected, the conversion of benzyl alcohol increased with higher temperatures, which can be explained by the increasing reaction rate. The increase of the temperature from 80 to 140 °C led to an increase of the conversion from 48% to 86% after 6 h. (Figure 48). At higher reaction temperatures more byproducts were formed resulting in decreased selectivity from 70% at 80 °C to 54% at 140 °C.

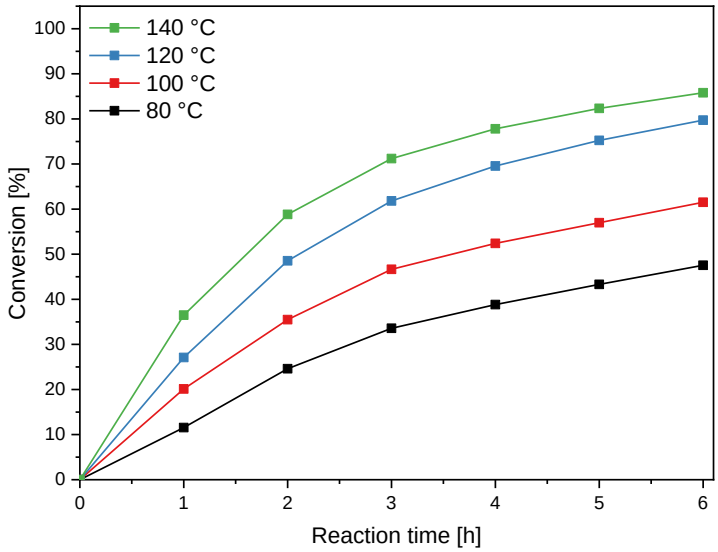

Figure 48. Influence of the reaction temperature on the conversion of benzyl alcohol. Reaction conditions: benzyl alcohol (1 mmol), biphenyl (0.33 mmol) as internal standard, air flow (200 ml/min), DUT-5-BPyDC(10)-Co (0.01 mol% of cobalt), DMF (30 ml), 6 h.

Next, the dependency of conversion, yield and selectivity on the air flow rate of the oxidant was investigated. The applied flow rates ranged from 100 to 300 ml/min (Figure 49). A higher flow rate had only a slight influence on the oxidation of benzyl alcohol. The conversion increased from 80 to 89% after 6 hours, whereas the yield and selectivity decreased from 47% and 59% to 42% and 47%, respectively.

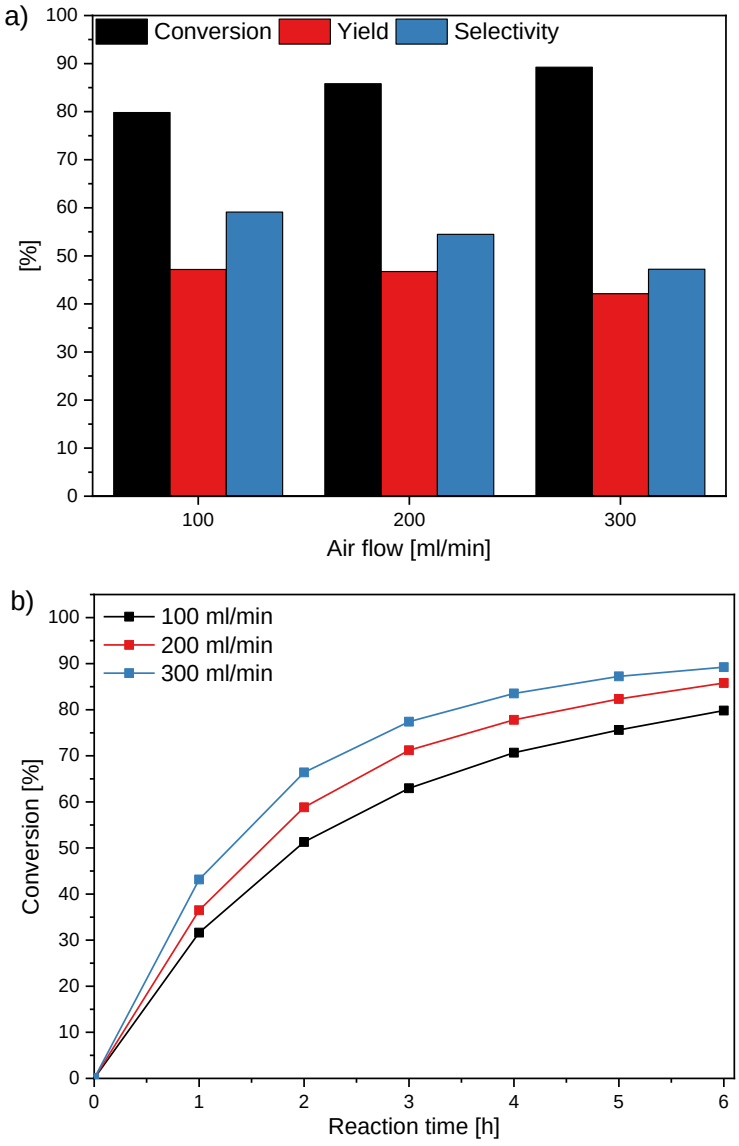

Figure 49. Influence of the air flow on conversion, yield and selectivity (a) and time-dependent conversion of benzyl alcohol (b). Reaction conditions: benzyl alcohol (1 mmol), biphenyl (0.33 mmol) as internal standard, DUT-5-BPyDC(10)-Co (0.01 mol% of cobalt), DMF (30 ml), 140 °C, 6 h.

In the following experiment, different catalyst concentrations were examined by varying the catalyst loading from 0.05 to 0.0005 mol% based on the determined cobalt content (*cf.* ICP-OES measurements in Table 2). A decrease of the catalyst concentration from 0.05 to 0.01 mol% did not have much influence on the conversion of benzyl alcohol. Thus, the results

observed for the reaction containing 0.05 mol% catalyst were almost equal to those performed with 0.01 mol% catalyst (Figure 50b). The conversion only decreased from 89 to 87%, whereas the selectivity increased from 51 to 55%. A further reduction of the catalyst amount, led to a decreased conversion of 80% with 0.005 mol%, 70% with 0.001 mol% and 45% with 0.0005 mol% catalyst (Figure 50a). Moreover, lower amounts of the catalyst led to an increased selectivity towards benzaldehyde up to 69%. The catalyst amount of 0.05 mol% cobalt gave a turnover number (TON) of 900 after 6 h, which increased up to 62000 with decreasing the catalyst concentration to 0.0005 mol% (Table 15). A cobalt concentration of 0.01 mol% was chosen as standard for the following tests.

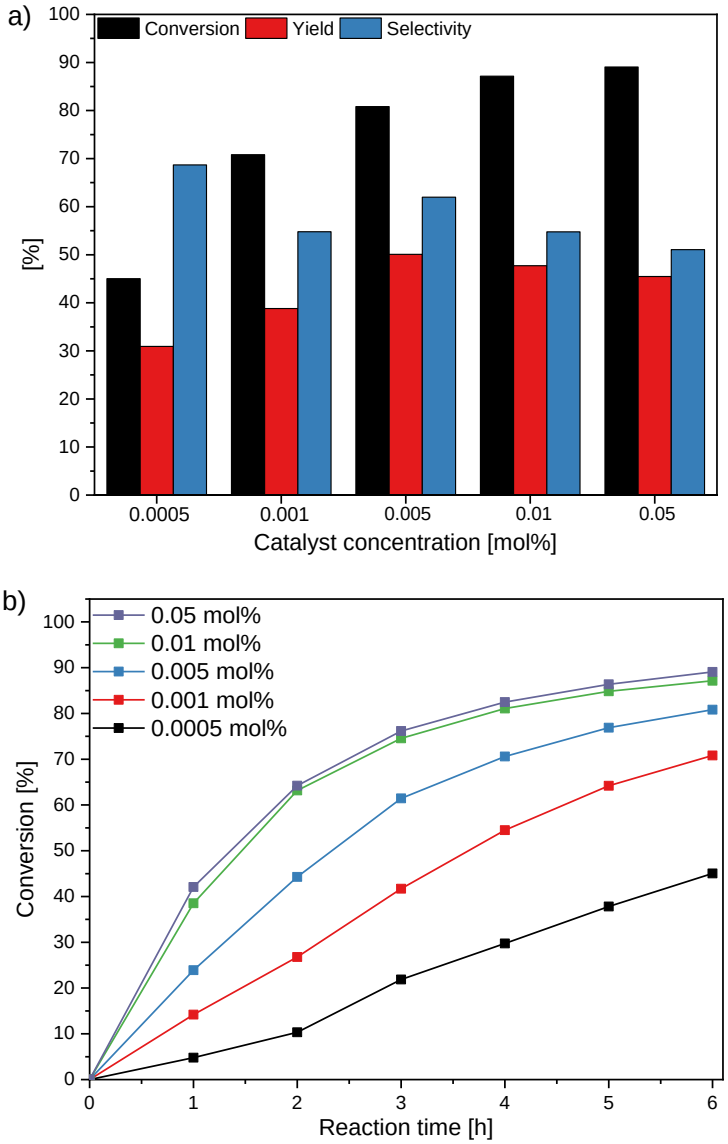

Figure 50. Influence of the catalyst concentration on conversion, yield and selectivity (a) and time-dependent conversion of benzyl alcohol (b). Reaction conditions: benzyl alcohol (1 mmol), biphenyl (0.33 mmol) as internal standard, air flow (200 ml/min), DMF (30 ml), 140 °C, 6 h.

Table 15. Turnover numbers (TONs) and turnover frequencies (TOFs) after 6 h with decreasing catalyst concentration of DUT-5-BPyDC(10)-Co. Reaction conditions: benzyl alcohol (1 mmol), biphenyl (0.33 mmol) as internal standard, air flow (200 ml/min), DMF (30 ml), 140 °C, 6 h.

Entry	Catalyst concentration [mol%]	TON	TOF [h^{-1}]
1	0.05	900	150
2	0.01	4800	800
3	0.005	10000	1700
4	0.001	39000	6500
5	0.0005	62000	10300

The influence of the substrate concentration was evaluated by varying the amount of benzyl alcohol from 1 to 5 mmol while keeping the amount of catalyst and solvent constant. The results of the performed reactions at 140 °C did not show significant changes in conversion, yield or selectivity. In order to make the influence more visible, the reactions were performed at 80 °C, since the catalyst was less active at lower temperatures (Figure 51a).By increasing the substrate amount from 1 to 4 mmol, the conversion decreased from 43 to 29% and the selectivity increased from 70 to 86%. Furthermore, an increase of the molar amount of formed benzaldehyde from 0.16 to 0.80 mmol was observed with higher amount of benzyl alcohol (Figure 51b). The high efficiency of the catalyst was shown by the determined turnover numbers, which increased from 2900 to 10000 with increasing benzyl alcohol amount from 1 to 4 mmol at 80 °C (Table 16). These observations indicated the correlation of reaction rate and substrate concentration.

Table 16. Turnover numbers (TONs) and turnover frequencies (TOFs) after 6 h with increasing substrate concentration. Reaction conditions: biphenyl (0.33 mmol) as internal standard, air flow (200 ml/min), DUT-5-BPyDC(10)-Co (0.01 mol% of cobalt), DMF (30 ml), 6 h.

Entry	molar amount of benzyl alcohol [mmol]	Catalyst amount [mol%]	140 °C		80 °C	
			TON	TOF [h^{-1}]	TON	TOF [h^{-1}]
1	1	0.0100	4600	770	2900	480
2	2	0.0050	10400	1700	5800	970
3	3	0.0033	14200	2400	8500	1400
4	4	0.0026	20000	3300	10000	1700

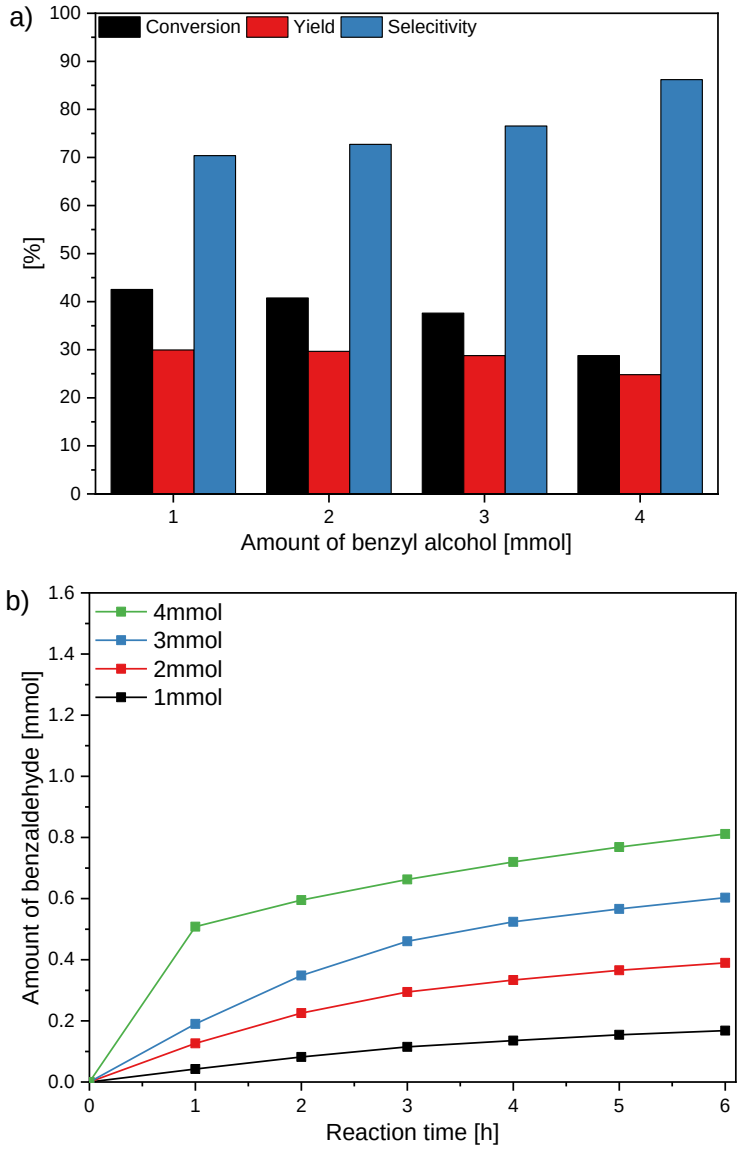

Figure 51. Influence of the substrate concentration on conversion, yield and selectivity (a). Molar amount of formed benzaldehyde with increasing molar amount of benzyl alcohol (b). Reaction conditions: biphenyl (0.33 mmol) as internal standard, air flow (200 ml/min), DUT-5-BPyDC(10)-Co (0.01 mol% of cobalt), DMF (30 ml), 80 °C, 6 h.

Summarizing the obtained results, the chosen reaction parameters were found to be ideal (1 mmol benzyl alcohol, 0.33 mmol biphenyl as internal standard, 200 ml/min air flow, 0.01 mol% cobalt concentration, 30 ml DMF, 140 °C reaction temperature and 6 h reaction time). Using these parameters, a conversion of 85%, a yield of 47% and a selectivity of 54% were obtained with DUT-5-BPyDC(10)-Co. The catalytic performance of the differently modified amine-based catalysts was evaluated and compared to those results obtained by DUT-5-BPyDC(10)-Co. After 6 h reaction time, the obtained conversions (88 –90%) did not vary significantly (Figure 52a), though higher yields (52 – 56%) and selectivities (58 – 64%) were observed for the amine-based catalysts. Moreover, higher selectivities were already observed starting from one hour onwards (Figure 52b). Thus, a significantly higher activity was

observed for the amine-based catalyst materials, in which the cobalt centers were located farther inside of the pore centers, compared to DUT-5-BPyDC(10)-Co, which featured cobalt centers close to the walls of the framework. Obviously, the cobalt centers in the pores of the amine-based catalysts might be better accessible for benzyl alcohol as substrate. Since the catalysts DUT-5-BPyDC(10)-Co and DUT-5-NH_2(10)-Sal-Co did not show any differences in the epoxidation of *trans*-stilbene (*cf.* chapter 4.2), the substrate might reach only the outer surface of the catalytically active sites, which can be explained by the larger size of *trans*-stilbene compared to benzyl alcohol.

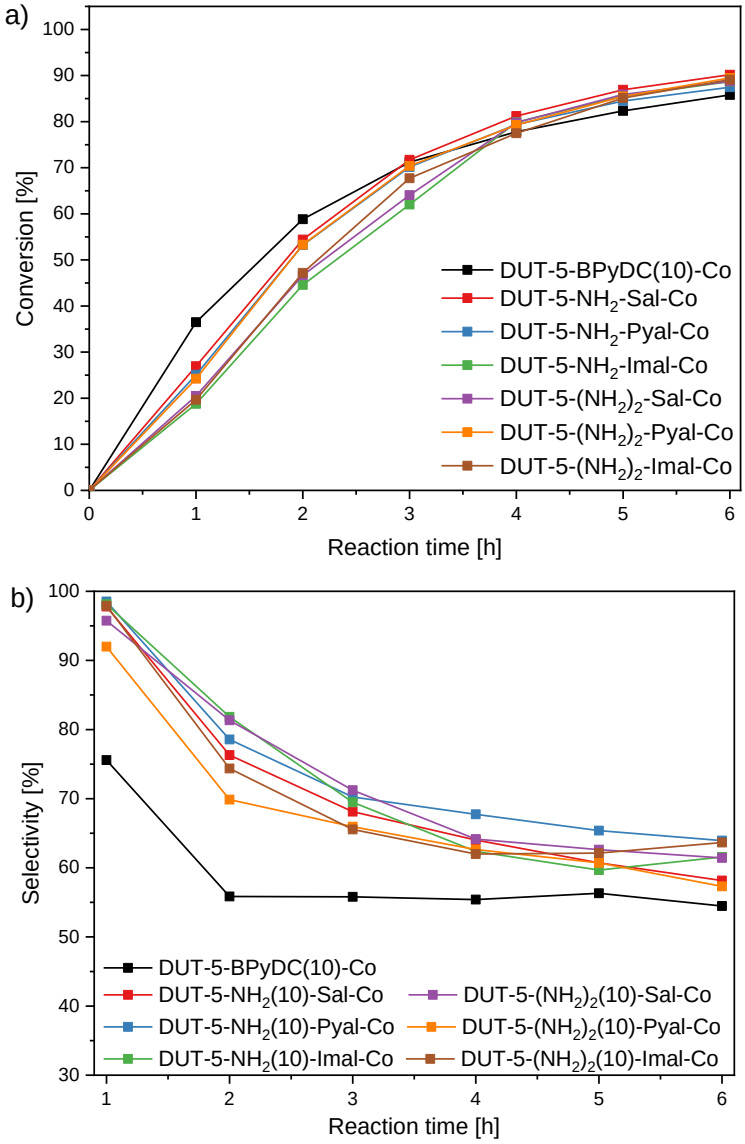

Figure 52. Comparison of conversion (a) and selectivity (b) of the catalysts in the oxidation of benzyl alcohol. Reaction conditions: benzyl alcohol (1 mmol), biphenyl (0.33 mmol) as internal standard, air flow (200 ml/min), catalyst (0.01 mol%), DMF (30 ml), 140 °C, 6 h.

Hot filtration tests were performed to prove that the reaction is catalyzed *via* a heterogeneous pathway. The tests were carried out using DUT-5-BPyDC(10)-Co and DUT-5-NH_2(10)-Sal-

Co. Granulated catalyst materials (200 – 500 µm sieve fraction) were used to facilitate an easier filtration of the solid powder. The solid catalyst was filtered off from the reaction mixture after 2 h reaction and the reaction were continued for another 4 hours. At the same time, a control experiment was performed without removing the catalyst.

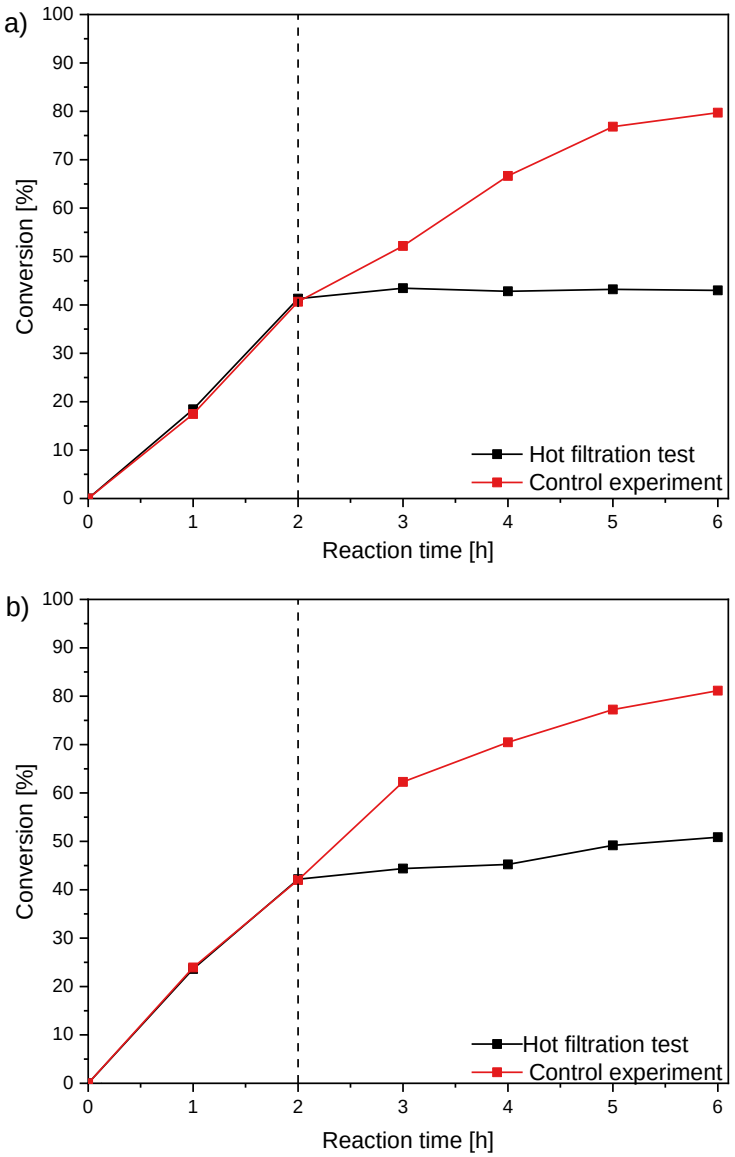

Figure 53. Comparison of the conversion of benzyl alcohol with and without catalyst removal after 2 h (as indicated by vertical line) using DUT-5-BPyDC(10)-Co (a) and DUT-5-NH_2(10)-Sal-Co (b). Reaction conditions: benzyl alcohol (1 mmol), biphenyl (0.33 mmol) as internal standard, air flow (200 ml/min), catalyst (0.01 mol%), DMF (30 ml), 140 °C, 6 h.

As shown in Figure 53, conversion and yield increased after removal of both catalysts, but at a much lower rate compared to the control experiment. This indicated that the oxidation of benzyl alcohol was mainly catalyzed heterogeneously, although minor contributions of dissolved cobalt species could not be ruled out completely. Apart from that, the observed activity after

catalyst removal also originate from very small particles that could not be removed from the reaction mixture after filtration.

5 Summary and Conclusions

In the present thesis, new single-site catalysts with MIL-53(Al) and DUT-5 structure, which contained defined metal complexes, were established. First, mixed-linker DUT-5 materials with additional 2,2'-bipyridine-5,5'-dicarboxylate (BPyDC) linkers were synthesized under solvothermal conditions. The formation of the DUT-5 structure as well as the absence of residual acid molecules in the pores could be proved *via* PXRD and ATR-IR spectroscopy. High porosities were obtained for materials with high specific surface areas up to S_{BET} = 2000 m^2/g. Furthermore, a qualitative analysis of the incorporated bipyridine-functionalities was performed using ATR-IR and ^{13}C solid-state NMR spectroscopy, whereas the amount of the BPyDC linkers could be quantitatively determined *via* ^{1}H liquid-phase NMR spectroscopy. DUT-5-BPyDC(10) was subsequently used for the immobilization of palladium, nickel, copper, cobalt and manganese ions. The use of a low bipyridine content was intended to obtain well-distributed metal complexes within the framework and, hence, minimize or completely exclude pore blocking. The metal-containing DUT-5-BPyDC(10) materials showed high crystallinity after the post-synthetic metalation process and were featured high surface areas. The quantitative incorporation of the metals was confirmed *via* ICP-OES analysis, which indicated a partial metal incorporation of the bipyridine moieties. XAS analysis proved the successful immobilization of the metal ions as well-defined complexes for all materials and the absence of other undesired metal-containing species like clusters or nanoparticles.

An amine-functionalized MIL-53(Al) material containing equal amounts of benzyl-1,4-dicarboxylate (BDC) and 2-aminobenzyl-1,4-dicarboxylate (ABDC) linkers was synthesized, whose amine groups were covalently modified with maleic anhydride *via* post-synthetic modification. The resulting bidentate side groups were subsequently used for the immobilizion of manganese(III) ions. The modification of the amine groups could be verified by ATR-IR and ^{1}H NMR spectroscopy, which confirmed the presence of the linker in the desired ratio (1:1) and revealed that 7% of the amine groups were successfully modified with maleic anhydride.

In a further step, amine-functionalized DUT-5 materials were synthesized, which represented the elongated form of MIL-53-NH_2. The larger pore dimensions of DUT-5 (22.7 Å × 19.2 Å) might facilitate the introduction of more complex substrates and, thus, provide an improved accessibility for substrate molecules during catalytic reactions. For this purpose, two different mixed-linker DUT-5 materials containing 10% of 2-amino-4,4'-biphenyldicarboxylate (ABPDC) or 5% of 2,2'-diamino-4,4'-biphenyldicarboxylate (dABPDC) linkers were

synthesized. The resulting amine-functionalized materials were post-synthetically modified with salicylaldehyde (Sal), 2-pyridinecarboxaldehyde (Pyal) and 2-imidazolecarboxaldehyde (Imal) resulting in Schiff base ligands as side groups. DUT-5-NH_2(10)-Sal was subsequently used for the immobilization of cobalt, manganese(II) and manganese(III) ions, while the remaining materials were only used for the complexation of cobalt ions. According to PXRD, ATR-IR spectroscopy and N_2 physisorption techniques, all materials exhibited high crystallinities and porosities without any changes in the structure after post-synthetic modification processes. ^{1}H NMR spectroscopy showed that 8% of 2-amino-4,4'-dicarboxylate linkers were incorporated into the DUT-5 structure. A quantitative determination of the diamine-functionalized materials could not be achieved due to the low amine content. Furthermore, a partial modification of the amine groups could be qualitatively proven *via* ^{1}H NMR spectroscopy. The incorporated metals were quantified by ICP-OES analysis.

In addition, an alkyne-functionalized DUT-5 material was synthesized and subsequently modified with a gold azide *via* inorganic click reactions (iClick). Therefore, 10% of 4,4'-biphenyldicarboxylate (BPDC) linkers were replaced by 2-ethynyl-4,4'-biphenyldicarboxylate (EBPDC). The obtained DUT-5-C_2H(10) material was post-synthetically modified with N_3AuPPh_3 resulting in a goldtriazolate compound as a side group. The covalently modified gold complex within the framework material could be qualitatively proven *via* ^{1}H NMR spectroscopy and quantitatively *via* ICP-OES analysis, which featured 3.64 wt% gold and a modification degree of 57% of the alkyne groups. The successful incorporation of the gold complex could be confirmed using XAS analysis. Furthermore, the gold-containing DUT-5 material proved to be fluorescent.

Cobalt- and manganese-containing immobilized mixed-linker MOF materials were chosen for applications in aerobic oxidation reactions including epoxidation or alcohol oxidation reactions. Thereby, different reaction parameters were screened to test the influence of the resulting catalysts using oxygen from air and catalytic activities and selectivities of the different catalysts were compared. Furthermore, for all catalytic reactions, the heterogeneity and hot filtrations tests and recycling tests proved that the reactions mainly proceeded heterogeneously

First, MIL-53(Al)-NH_2(50)-Mal-Mn was applied in the aerobic epoxidation of α-pinene. The catalytic tests were performed in a cooperation with the group of Prof. Meier (Karlsruhe Institute of Technology). Manganese(III)acetate as homogeneous catalyst was used for parameter screening. The optimized reaction conditions were then applied to the manganese(III)-containing MIL-53(Al) catalyst, which showed a remarkable catalytic

performance. The α-pinene oxidation resulted in 31% conversion and 17% pinene oxide formation using 0.5 mol% catalyst concentration and, thus, the MOF-based system had a higher activity as its homogeneous counterpart. The accumulated turnover number of the MOF catalyst (166) was considerably higher than the TON of the homogeneous catalyst (23).

Moreover, DUT-5 materials containing cobalt, manganese(II) and manganese(III) ions were tested in the epoxidation reaction of *trans*-stilbene using low catalyst concentrations of 0.02 mol%, which were sufficient to activate the oxidant. Under optimized conditions, high *trans*-stilbene conversions up to 93% and a yield up to 73% of *trans*-stilbene oxide was achieved using DUT-5-BPyDC(10)-Co. Thus, the cobalt-containing catalysts featured a significantly higher activity than their manganese counterparts. DUT-5-BPyDC(10)-Mn^{2+} provided a conversion of 32% and yield of 28%, which were comparable to the results obtained by DUT-5-BPyDC(10)-Mn^{3+}. Despite the different metal positions within the framework pores, the comparison between the metal-containing DUT-5-BPyDC(10) and DUT-5-NH_2(10)-Sal catalysts showed no differences in activity except for the manganese(II)-containing DUT-5 materials. DUT-5-NH_2(10)-Sal-Mn^{2+} (44%) gave a significantly higher conversion compared to its counterpart DUT-5-BPyDC(10)-Mn^{2+} (32%).

Finally, all cobalt-containing DUT-5 materials synthesized in this work, were used as single-site catalyst in the benzyl alcohol oxidation. Using the optimized reaction parameters, the reaction catalyzed with DUT-5-BPyDC(10)-Co (0.01 mol%) resulted in a conversion of 86% and a yield of 47% benzaldehyde. Interestingly, with regard to the positions of the metal centers, the amine-functionalized materials showed higher conversions (88 – 90%) and selectivities compared to the bipyridine-functionalized catalyst. Since benzyl alcohol is smaller than *trans*-stilbene, the higher activity of the amine-functionalized DUT-5 catalysts might be explained by an increased accessibility of the cobalt centers for benzyl alcohol, in which cobalt centers were located farther inside the pore systems, whereas *trans*-stilbene might only have reached the outer surface of the framework. In order to gain more insights into these catalytic reactions, mechanistic studies *via in situ* XAS analysis could be interesting.

In conclusion, metal-organic frameworks represent a promising class of materials for the design of heterogeneous single-site catalysts. The approach of post-synthetic modification in combination with the concept of mixed-linker MOFs leads to tailor-made catalysts with remarkable catalytic performances, which are highly attractive for future applications.

6 Experimental part

6.1 Materials

All chemicals were purchased from Sigma-Aldrich, Merck, Alfa Aesar, VWR Chemicals or ABCR. The functionalized linkers (2-amino-4,4'-biphenyldicarboxylic acid, 2,2'-diamino-4,4'-biphenyldicarboxylic acid and 2-ethinyl-4,4'-dicarboxylic acid) were synthesized by the group of Professor Bräse (Institute of Organic Chemistry, Karlsruhe Institute of Technology). N_3AuPPh_3 was synthesized by the group of Professor Roesky (Institute of Inorganic Chemistry, Karlsruhe Institute of Technology). All chemicals were used without further purification. If not stated otherwise, the starting point of a reaction was defined by placing the reaction vessel in the respective preheated heating medium and the end was defined as removing it. Reaction times and drying durations refer to this starting and end points. Only glass filter funnel of porosity 5 were used.

6.2 Methods

6.2.1 Powder X-ray diffraction (PXRD)

Powder X-ray diffraction measurements were performed using a Bruker D8 Advance. The samples were analyzed in the range $2\,\Theta = 4 - 50°$ using Cu Kα radiation (1.54 Å). The step size was $2\,\Theta = 0.0164°$ with a dwell time of 2 s.

6.2.2 Attenuated total reflection infrared spectroscopy (ATR-IR)

ATR-IR data were acquired using a FT-IR spectrometer Vertex 70 from Bruker Optics equipped with a Golden Gate Single Reflection ATR sample cell from Specac and a liquid nitrogen cooled MCT detector. The data were collected from 4500 cm^{-1} to 600 cm^{-1} and the arithmetic average of 400 measurements was taken for each spectrum.

6.2.3 Nitrogen physisorption measurements

Prior to the nitrogen physisorption, the samples were activated for 20 h at 130 °C in vacuum. Measurements were carried out using a Belsorp mini II from BEL Japan. The specific surface area (S_{BET}) and the total pore volume (tpv) was determined by the BET method (Brunauer, Emmett, Teller) and the BEL Master software. The micropore volume (mpv) was determined using the t-plot method.

6.2.4 Thermogravimetric analysis (TG)

Differential thermal analysis/thermogravimetry (DTA/TG) was performed with a NETZSCH STA 409C applying α-Al_2O_3 as crucible material and reference sample. The samples were heated under air flow from room temperature to 1000 °C with a heating rate of 5 K/min.

6.2.5 Nuclear magnetic resonance spectroscopy (NMR)

10 mg of the samples were digested in 0.5 mL 1 molar NaOD/D_2O and 0.2 ml DMF-d_7. Spectra were recorded on a Bruker Ascend 400 MHz NMR spectrometer. Chemical shifts were referenced to DMF-d_7 and are reported relative to tetramethylsilane.

6.2.6 Atomic absorption spectroscopy (AAS)

For AAS measurements, a Z-6100 Polarized Zeeman atomic absorption spectrometer from Hitachi was used. MIL-53(Al)-NH_2(50)-Mal-Mn was digested in 7 ml aqua regia and diluted with 93 ml distilled water.

6.2.7 Inductively coupled plasma optical emission spectrometry (ICP-OES)

For ICP-OES measurements, an iCAP 6500 Duo from Thermo Scientific and a six-point calibration were used. The metal-containing DUT-5 frameworks (5 mg) were first pyrolyzed at 850 °C for 2 h and were afterwards digested in boiling HCl, which was evaporated and the residues were dissolved in diluted HNO_3.

6.2.8 Fluorescence microscopy

For fluorescence microscopy images, an Olympus IX81 microscope, which was equipped with a XM10 monochrome CCD camera and regulated with the CellTM software, was used with a filtercube U-MF2FITC.

6.2.9 Gas chromatography (GC)

For GC measurements, a GC-2030 Plus from Shimadzu with a non-polar column (SH-Rtx-624, length: 30 m, diameter: 0.25 mm, film thickness: 1.4 μm) and a FID detector was used. 1 μl of the sample was injected and vaporized at 250 °C. The column was heated from 50 °C to 230 °C at a rate of 7 K/min.

6.2.10 X-ray absorption spectroscopy

X-ray absorption spectroscopy (XAS) experiments were performed at PETRA III Extension beamline P65 (energy range: 4 - 44 keV) at DESY (Deutsches Elektronensynchrotron) in Hamburg (Germany). For the measurements at the Ni K-, Cu K-, Co K-, Mn K- and Au L_3-edges, a Si(111) C-type double crystal monochromator was used. The beam current was 100 mA with a ring energy of 6.08 GeV. All samples were prepared as pellets using cellulose as binder. The amount of sample used for the preparation of the pellets was calculated using the software package XAFS mass (with a pellet area of 1 cm^3). All spectra were recorded in continuous scan modes in transmission and fluorescence at ambient temperature and pressure in the range of -150 eV to 1000 eV around the edge in 180 s. For the data analysis, transmission data were used. For calibration, the corresponding metal foils were measured as a reference simultaneously with the samples.

The data treatment was performed using the Demeter software package.[224] In order to compensate for the oversampling of the continuous scan mode, the data points of the obtained spectra were reduced with the help of the 'rebin'-function of the Athena software (edge region: -50 to +50 eV; pre-edge grid: 5 eV; XANES grid: 0.5 eV; EXAFS grid: 0.05 $Å^{-1}$). For data evaluation, a Victoreen-type polynomial was subtracted from the spectrum to remove the background using the Athena software. The first inflection point was taken as energy E_0. The EXAFS analysis was performed using the Artemis software. The fits were performed by using structure data of similar metal complexes.[213-217,225-235]

6.3 Synthetic procedures

6.3.1 Synthesis of DUT-5

A suspension of $AlCl_3 \cdot 6\ H_2O$ (0.152 g, 0.625 mmol, 1.00 eq.) and 4,4'-biphenyldicarboxylic acid (H_2BPDC, 0.151 g, 0.625 mmol, 1.00 eq.) in 10 ml of DMF were added in a closed reaction vessel, which was immersed in an oil bath and stirred for 24 h at 120 °C. After hot filtration, the material was washed with 3 × 25 ml hot DMF (100 °C). The solid was dried overnight at room temperature and then for 3 days at 130 °C.

6.3.2 Synthesis of mixed-linker DUT-5-BPyDC

Mixed-linker metal-organic frameworks based on DUT-5 containing 10% and 25% 2,2'-bipyridine-5,5'-dicarboxylate (BPyDC) were synthesized. A suspension of $AlCl_3 \cdot 6\ H_2O$

(0.755 g, 3.13 mmol, 1.00 eq.), 4,4'-biphenyldicarboxylic acid (H_2BPDC) and 2,2'-bipyridine-5,5'-biphenyldicarboxylic acid (H_2BPyDC) (ratios are listed in Table 17) in 50 ml of DMF were added in a closed reaction vessel, which was immersed in an oil bath and stirred for 24 h at 120 °C. After hot filtration, the material was washed with 6 × 25 ml hot DMF (100 °C). The solid was dried overnight at room temperature and then for 3 days at 130 °C.

Table 17. Used molar amounts and masses for the synthesis of mixed-linker DUT-5-BPyDC.

	n(H_2BPDC) [mmol]	m(H_2BPDC) [g]	n(H_2ByPDC) [mmol]	m(H_2BPyDC) [g]
DUT-5-BPyDC(10)	2.813	0.681	0.313	0.076
DUT-5-BPyDC(25)	2.344	0.568	0.781	0.191

6.3.3 Synthesis of DUT-5-BPyDC(100)

A suspension of $AlCl_3 \cdot 6\,H_2O$ (0.152 g, 0.625 mmol, 1.00 eq.) and 2,2'-bipyridine-5,5'-biphenyldicarboxylic acid (H_2BPyDC, 0.153 g, 0.625 mmol, 1.00 eq.) in 10 ml of DMF were added in a closed reaction vessel, which was immersed in an oil bath and stirred for 24 h at 120 °C. After hot filtration, the material was washed with 3 × 25 ml hot DMF (100 °C). The solid was dried overnight at room temperature and then for 3 days at 130 °C.

6.3.4 Post-synthetic metalation of DUT-5-BPyDC(10)

The metal salt (0.90 eq with regard to the BPyDC amount, see Table 18) dissolved in 5 ml DMF was added to a suspension of DUT-5-BPyDC(10) (0.220 g, 0.774 mmol, 1.00 eq.) in 15 ml of DMF and was shaken for 6 h at room temperature. After filtration, the material was washed with 3 × 25 ml DMF, dried overnight at room temperature and then for 3 h at 130 °C.

Table 18. Used molar amounts and masses of the metal precursors for the post-synthetic metalation of DUT-5-BPyDC(10).

	n(metal salt) [mmol]	m(metal salt) [g]	Resulting materials
$Pd(CH_3COO)_2$	0.070	0.016	DUT-5-BPyDC(10)-Pd
$Ni(CH_3COO)_2 \cdot 4\ H_2O$	0.070	0.017	DUT-5-BPyDC(10)-Ni
$Cu(CH_3COO)_2 \cdot H_2O$	0.070	0.016	DUT-5-BPyDC(10)-Cu
$Co(NO_3)_2 \cdot 6\ H_2O$	0.070	0.020	DUT-5-BPyDC(10)-Co
$Mn(CH_3COO)_2$	0.070	0.012	DUT-5-BPyDC(10)-Mn^{2+}
$Mn(CH_3COO)_3 \cdot 2\ H_2O$	0.070	0.019	DUT-5-BPyDC(10)-Mn^{3+}

6.3.5 Synthesis of MIL-53(Al)-NH_2(50)

MIL-53-NH_2(50) was synthesized according to a modified procedure of MIL-53(Al)-NH_2.[135] 2-Aminobenzyl-1,4-dicarboxylic acid (H_2ABDC, 0.483 g, 2.67 mmol, 1 eq) and benzyl-1,4-dicarboxylic acid (H_2BDC, 0.444 g, 2.67 mmol, 1.00 eq) were dissolved in H_2O (20 ml) and DMF (50 ml) at 90 °C. A solution of $Al(NO_3)_3 \cdot 9\ H_2O$ (2.00 g, 5.33 mmol, 2.00 eq) in H_2O (5 ml) was added and the reaction mixture was stirred at 90 °C for 24 h. After filtration, the material was washed with DMF (3 × 25 ml) and H_2O (1 × 25 ml) and dried overnight at room temperature and then for 3 days at 130 °C in air.

6.3.6 Post-synthetic modification of MIL-53-NH_2(50)

MIL-53-NH_2(50) was modified in a two-step PSM reaction.

First step: maleic anhydride (0.471 g, 4.80 mmol, 4.00 eq based on the number of amine groups) was dissolved in acetonitrile (60 ml). MIL-53-NH_2(50) (0.517 g, 2.40 mmol, 1.00 eq) was suspended in the solution and the reaction mixture was heated to 80 °C for 24 h. After filtration, the resulting material was washed with acetonitrile (4 × 20 ml), DMF (1 × 20 ml) and H_2O (1 × 20 ml). The solid was dried overnight at room temperature and then for 3 days at 130 °C in air.

Second step: $Mn(OAc)_2 \cdot 2\ H_2O$ (0.0242 g, 0.09 mmol, 1.00 eq) was dissolved in ethanol (40 ml). MIL-53-NH_2(50)-Mal (0.441 g, 2.5 mmol, 1.00 eq) was suspended in this solution and the reaction mixture was heated to 60 °C for 24 h. After filtration, the resulting material was washed with ethanol (4 × 20 ml). The solid was dried overnight at room temperature and then for 3 days at 130 °C in air.

6.3.7 Synthesis of DUT-5-NH_2(10)

A suspension of $AlCl_3 \cdot 6\ H_2O$ (0.755 g, 3.13 mmol, 1.00 eq.), 4,4'-biphenyldicarboxylic acid (H_2BPDC, 0.681 g, 2.81 mmol, 0.90 eq.) and 2-amino-4,4'-biphenyldicarboxylic acid (H_2ABPDC, 0.313 mmol, 0.076 g, 0.10 eq.) in 50 ml of DMF were added in a closed reaction vessel, which was immersed in an oil bath and stirred for 24 h at 120 °C. After hot filtration, the material was washed with 6 × 25 ml hot DMF (100 °C). The solid was dried overnight at room temperature and then for 3 days at 130 °C.

6.3.8 Synthesis of DUT-5-$(NH_2)_2$(5)

A suspension of $AlCl_3 \cdot 6\ H_2O$ (0.755 g, 3.13 mmol, 1.00 eq.), 4,4'-biphenyldicarboxylic acid (H_2BPDC, 0.681 g, 2.81 mmol, 0.95 eq.) and 2,2'-diamino-4,4'-biphenyldicarboxylic acid (H_2dABPDC, 0.313 mmol, 0.085 g, 0.05 eq.) in 50 ml of DMF were added in a closed reaction vessel, which was immersed in an oil bath and stirred for 24 h at 120 °C. After hot filtration, the material was washed with 6 × 25 ml hot DMF (100 °C). The solid was dried overnight at room temperature and then for 3 days at 130 °C.

6.3.9 Post-synthetic modification of amine-functionalized DUT-5

DUT-5-NH_2(10) and DUT-5-$(NH_2)_2$(5) were modified in a two-step PSM reaction.

First step: DUT-5-NH_2(10) (0.200 g, 0.700 mmol, 1.00 eq) or DUT-5-$(NH_2)_2$(5) (0.200 g, 0.700 mmol, 1.00 eq.) was activated for 4 h under vacuum and was suspended in 10 ml toluene afterwards. The respective aldehyde (8.00 eq. with regard to the amino groups, see Table 19) was dissolved in 10 ml toluene and was acidified with acetic acid (pH = 4-5). The aldehyde solution was added to the MOF suspension and was shaken for 3 days at 60 °C. After filtration, the material was washed with 3 × 25 ml toluene, dried overnight at room temperature and then for 3 days at 130 °C.

Second step: $Co(NO_3)_2 \cdot 6\ H_2O$ (0.019 g, 0.067 mmol, 0.90 eq with regard to the modification degree) dissolved in 5 ml DMF was added to a suspension of modified amine-functionalized DUT-5 (0.220 g, 0.740 mmol, 1.00 eq.) in 15 ml of DMF and was shaken for 6 h at 80 °C. After filtration, the material was washed with 3 × 25 ml DMF, dried overnight at room temperature and then for 3 h at 130 °C.

Table 19. Used amounts and masses of aldehydes for the post-synthetic modification of DUT-5-NH_2.

Aldehyde	DUT-5-NH_2(10)		DUT-5-$(NH_2)_2$(5)	
	n(aldehyde) [mmol]	m(aldehyde) [g]	n(aldehyde) [mmol]	m(aldehyde) [g]
Salicylaldehyde	0.560	0.068	1.11	0.136
2-Pyridinecarboxaldehyde	0.560	0.060	1.11	0.119
2-Imidazolcarboxaldehyde	0.560	0.538	1.11	0.107

6.3.10 Synthesis of DUT-5-C_2H(10)

A suspension of $AlCl_3 \cdot 6\ H_2O$ (0.755 g, 3.13 mmol, 1.00 eq.), 4,4'-biphenyldicarboxylic acid (H_2BPDC, 0.137 g, 0.563 mmol, 0.90 eq.) and 2-ethinyl-4,4'-biphenyldicarboxylic acid (H_2EBPDC, 0.313 mmol, 0.062 g, 0.10 eq.) in 10 ml of DMF were added in a closed reaction vessel, which was immersed in an oil bath and stirred for 24 h at 120 °C. After hot filtration, the material was washed with 3 × 25 ml hot DMF (100 °C). The solid was dried overnight at room temperature and then for 3 days at 130 °C.

6.3.11 Post-synthetic modification of DUT-5-C_2H(10)-[(triazole)$AuPPh_3$]

DUT-5-C_2H(10) (0.200 g, 0.689 mmol, 1.00 eq.) was activated for 4 h under vacuum and was suspended in 10 ml toluene afterwards. N_3AuPPh_3 (0.276 mmol, 4.00 eq. with regard to the alkyne groups) was dissolved in 10 ml of dichloromethane (DCM) and the solution was added to the MOF suspension and was shaken for 2 days at room temperature. The reaction mixture was filtered off and the solid was dried overnight at room temperature and then for 3 days at 130 °C.

6.4 Catalytic tests

Catalytic test reactions were performed in a 100 mL three-necked flask equipped with a reflux condenser, magnetic stir bar, and gas inlet. Biphenyl was used as internal GC standard. Reaction temperature, flow rate, catalyst concentration and substrate concentration were varied to establish the optimized reaction conditions. Reaction products were quantified by GC techniques. For this, aliquots were taken at regular intervals and diluted with dichloromethane (1 mL).

6.4.1 Epoxidation of α-pinene

In a typical reaction, the flask was charged with a solvent mixture (30 ml, DMF/diethyl carbonate, 10:90), α-pinene (0.136 g, 1.00 mmol, 1.00 eq), catalyst (0.250 mol% Mn) and biphenyl (0.0386 g, 0.250 mmol, 0.250 eq) as internal GC standard. Then, the flask was immersed in an oil bath and kept at 130 °C under vigorous stirring (1000 rpm) for 6 h. Compressed air was continuously fed to the reaction mixture through the gas inlet at 50 mL/min.

Recycling experiment: The catalyst was recovered from the reaction mixture by filtration (glass filter, por. 5) after 6 h for recycling experiments. Then, the catalyst was washed thoroughly with diethyl carbonate and dried at room temperature. The recycled catalyst was subsequently reused for another aerobic oxidation of α-pinene maintaining the same reaction conditions.

Hot filtration test: For a hot filtration test, the catalyst was removed from the hot reaction mixture after 3 h by filtration (glass filter, por. 5). The reaction was continued without the solid catalyst for another 5 h. To follow the reaction progress, GC samples were taken hourly.

6.4.2 Epoxidation of *trans*-stilbene

In a typical reaction, the flask was charged with DMF (60 ml), *trans*-stilbene (0.1803 g, 1.00 mmol, 1.00 eq.), catalyst (0.02 mol% Co or Mn) and biphenyl (0.154 g, 1.00 mmol, 1.00 eq.) as internal GC standard. Then, the flask was immersed in an oil bath and kept at 150 °C under vigorous stirring (450 rpm) for 24 h. Compressed air was continuously fed to the reaction mixture through the gas inlet at 200 ml/min.

Recycling experiment: The catalyst was recovered from the reaction mixture by filtration (glass filter, por. 5) after 24 h for recycling experiments. Then, the catalyst was washed thoroughly with DMF and dried at room temperature. The recycled catalyst was subsequently reused for another aerobic oxidation of *trans*-stilbene maintaining the same reaction conditions.

Hot filtration test: For a hot filtration test, the catalyst was removed from the hot reaction mixture after 2 h by filtration (glass filter, por. 5). The reaction was continued without the solid catalyst for another 22 h. To follow the reaction progress, GC samples were taken hourly.

6.4.3 Oxidation of benzyl alcohol

In a typical reaction, the flask was charged with DMF (30 mL), benzyl alcohol (0.1801 g, 1.00 mmol, 1.00 eq), catalyst (0.01 mol% Co) and biphenyl (0.0509 g, 0.33 mmol, 0.33 eq) as

internal GC standard. Then, the flask was immersed in an oil bath and kept at 140 °C under vigorous stirring (450 rpm) for 6 h. Compressed air was continuously fed to the reaction mixture through the gas inlet at 200 mL/min.

Hot filtration test: For a hot filtration test, the catalyst was removed from the hot reaction mixture after 2.5 h by filtration (glass filter, por. 5). The reaction was continued without the solid catalyst for another 4.5 h. To follow the reaction progress, GC samples were taken hourly.

6.4.4 Determination of conversion, yield and selectivity

The gas chromatograph was calibrated to determine conversion, selectivity and yield. For this, five standard solutions containing authentic samples of starting material, product and an internal standard (biphenyl) were prepared and measured. Calibration curves were obtained by plotting the ratio of internal standard peak area to the mass of internal standard in the solution against the ratio of analyte peak area to the mass of analyte. The slope of the calibration lines is the response factor R_x, which takes into account the differences in the detector response between the analyte and the standard:

$$R_x = \frac{A_{is}/m_{is}}{A_x/m_x}$$

with A_{is}: peak area of the internal standard, A_x: peak area of the analyte, m_{is}: mass of the internal standard, and m_x: mass of the analyte.

Masses were calculated using the following equation:

$$m_x = \frac{m_{is}}{A_{is}} * A_x * R_x$$

Conversion, yield and selectivity were calculated as follows:

$$conversion = \left(\frac{n_0(starting\ material) - n(starting\ material)}{n_0(starting\ material)}\right) * 100$$

$$yield = \left(\frac{n(product)}{n_0(starting\ material)}\right) * 100$$

$$selectivity = \left(\frac{yield}{conversion}\right) * 100$$

7 Abbreviations and symbols

AAS	atomic absorption spectroscopy
ABDC	2-aminobenzene-1,4-dicarboxylate
ABPDC	2-amino-4,4’-biphenyldicarboxylate
ATR	attenuated total reflection
BDC	benzene-1,4-carboxylate
BET	Brunauer-Emmett-Teller methos
BINOL	1,1‘-bi-2-naphtol
BPDC	4,4‘-biphenyldicarboxylate
BPyDC	2,2’-bipyridine-5,5’-dicarboxylate
CAU	Christian-Albrechts-Universität (Kiel)
cf.	compare (lt. c*onfer*)
COMOC	Centre for Ordered Materials, Organometallics and Catalysis
CSD	Cambridge Structural Database
CuAAC	cupper(I)-catalyzed alkyne-azide aycloaddition
CVD	chemical vapor deposition
dABPDC	2,2’-diamino-4,4’-biphenyldicarboxylate
DCM	dichloromethane
DEC	diethyl carbonate
DESY	Deutsches Elektronensynchroton
DMF	*N*,*N*-dimethylformamide
DTA	differential thermal analysis
DUT	Dresden University of Technology
e.g.	for example (lt. *exempli gratia*)
EBPDC	2-ethinyl-4,4’-biphenyldicarboxylate
EPR	electron paramagnetic resonance

eq.	equivalent
EXAFS	extended X-ray absorption fine structure
FID	flame ionization detector
GC	gas chromatography
GC-MS	gas chromatography-mass spectroscopy
H_2ABDC	2-aminobenzene-1,4-dicarboxylic acid
H_2ABPDC	2-amino-4,4'-biphenyldicarboxylic acid
H_2BDC	benzene-1,4-dicarboxylic acid
H_2BPDC	4,4'-biphenyldicarboxylic acid
H_2BPyDC	2,2'-bipyridine-5,5'-dicarboxylic acid
H_3BTC	benzene-1,3,5-tricarboxylic acid
H_4btec	1,2,4,5-benzenetetracarboxylic acid
H_2dABPDC	2,2'-diamino-4,4'-biphenyldicarboxylic acid
H_2EBPDC	2-ethinyl-4,4'-biphenyldicarboxylic acid
HKUST	Hong Kong University of Science and Technology
iClick	inorganic click
ICP-OES	inductively coupled plasma optical emission spectroscopy
Imal	2-imidazolecarboxaldehyde
IR	infrared
IRMOF	isoreticular metal-organic framework
KIT	Karlsruhe Institute fot Technology
Mal	maleic anhydride
MC-MOF	mixed-component metal-organic framework
MIL	Matériaux de l'Institut Lavoisier
MIXMOF	mixed-linker metal-organic framework
MNP	metal nanoparticle

MOF	metal-organic framework
mpv	micropore volume
MTV-MOF	multi-variate metal-organic framework
NMR	nuclear magnetic resonance
PCP	porous coordination polymer
PSD	post-synthetic deprotection
PSE	post-synthetic exchange
PSM	post-synthetic modification
PXRD	powder X-ray diffraction
Pyal	2-pyridinecarboxaldehyde
RUB	Ruhr University Bochum
Sal	salicylaldehyde
S_{BET}	specific surface area determined by the BET method
SBU	secondary building unit
STA	University of St. Andrews
TBHP	*tert*-butyl hydroperoxide
TEMPO	(2,2,6,6-tetramethylpiperidin-1-yl)oxyl
TFA	trifluoroacetic acid
TG	thermogravimetric analysis
TMS	tetramethylsilane
TOF	turnover frequency
TON	turnover number
Tpv	total pore volume
UiO	University of Oslo
UMCM	University of Michigan Crystalline Material
XANES	X-ray absorption near edge structure

XAS	X-ray absorption spectroscopy
XPS	X-ray photoelectron spectroscopy
XRD	X-ray diffraction

8 References

[1] M. Eddaoudi, D. B. Moler, H. Li, B. Chen, T. M. Reineke, M. O'Keeffe, O. M. Yaghi, *Acc. Chem. Res.* **2001**, *34*, 319–330.

[2] S. L. James, *Chem. Soc. Rev.* **2003**, *32*, 276.

[3] O. M. Yaghi, M. O'Keeffe, N. W. Ockwig, H. K. Chae, M. Eddaoudi, J. Kim, *Nature* **2003**, *423*, 705–714.

[4] S. T. Meek, J. A. Greathouse, M. D. Allendorf, *Adv. Mater.* **2011**, *23*, 249–267.

[5] M. Kondo, T. Yoshiromi, K. Seki, H. Matsuzaka, S. Kitagawa, *Angew. Chem. Int. Ed.* **1997**, *36*, 1725–1727.

[6] S. Kitagawa, M. Kondo, *Bull. Chem. Soc. Jpn.* **1998**, *71*, 1739–1753.

[7] S. Kitagawa, R. Kitaura, S.-i. Noro, *Angew. Chem. Int. Ed.* **2004**, *43*, 2334–2375.

[8] H.-C. J. Zhou, S. Kitagawa, *Chem. Soc. Rev.* **2014**, *43*, 5415–5418.

[9] O. M. Yaghi, G. Li, H. Li, *Nature* **1995**, *378*, 703–706.

[10] O. M. Yaghi, H. Li, *J. Am. Chem. Soc.* **1995**, *117*, 10401–10402.

[11] H. Li, M. Eddaoudi, T. L. Groy, O. M. Yaghi, *J. Am. Chem. Soc.* **1998**, *120*, 8571–8572.

[12] H. Li, M. Eddaoudi, M. O'Keeffe, O. M. Yaghi, *Nature* **1999**, *402*, 276–279.

[13] G. Férey, *Chem. Mater.* **2001**, *13*, 3084–3098.

[14] C. Serre, F. Millange, C. Thouvenot, M. Noguès, G. Marsolier, D. Louër, G. Férey, *J. Am. Chem. Soc.* **2002**, *124*, 13519–13526.

[15] G. Férey, C. Mellot-Draznieks, C. Serre, F. Millange, J. Dutour, S. Surblé, I. Margiolaki, *Science* **2005**, *309*, 2040–2042.

[16] G. Férey, *Chem. Soc. Rev.* **2008**, *37*, 191–214.

[17] A. Y. Robin, K. M. Fromm, *Coord. Chem. Rev.* **2006**, *250*, 2127–2157.

[18] P. Z. Moghadam, A. Li, S. B. Wiggin, A. Tao, A. G. P. Maloney, P. A. Wood, S. C. Ward, D. Fairen-Jimenez, *Chem. Mater.* **2017**, *29*, 2618–2625.

[19] O. K. Farha, I. Eryazici, N. C. Jeong, B. G. Hauser, C. E. Wilmer, A. A. Sarjeant, R. Q. Snurr, S. T. Nguyen, A. Ö. Yazaydın, J. T. Hupp, *J. Am. Chem. Soc.* **2012**, *134*, 15016–15021.

[20] G. Férey, C. Serre, *Chem. Soc. Rev.* **2009**, *38*, 1380–1399.

[21] A. Schneemann, V. Bon, I. Schwedler, I. Senkovska, S. Kaskel, R. A. Fischer, *Chem. Soc. Rev.* **2014**, *43*, 6062–6096.

[22] M. Eddaoudi, J. Kim, N. Rosi, D. Vodak, J. Wachter, M. O'Keeffe, O. M. Yaghi, *Science* **2002**, *295*, 469–472.

[23] J. L.C. Rowsell, O. M. Yaghi, *Microporous Mesoporous Mater.* **2004**, *73*, 3–14.

[24] B. Rungtaweevoranit, C. S. Diercks, M. J. Kalmutzki, O. M. Yaghi, *Faraday Discuss. R. Soc. Chem.* **2017**, *201*, 9–45.

[25] F. Millange, C. Serre, G. Férey, *Chem. Commun.* **2002**, 822–823.

[26] K. Barthelet, J. Marrot, D. Riou, G. Férey, *Angew. Chem. Int. Ed.* **2002**, *41*, 281.

[27] F. Millange, R. I. Walton, *Isr. J. Chem.* **2018**, *58*, 1019–1035.

[28] T. Loiseau, C. Serre, C. Huguenard, G. Fink, F. Taulelle, M. Henry, T. Bataille, G. Férey, *Chem. Eur. J.* **2004**, *10*, 1373–1382.

[29] P. Horcajada, S. Surblé, C. Serre, D.-Y. Hong, Y.-K. Seo, J.-S. Chang, J.-M. Grenèche, I. Margiolaki, G. Férey, *Chem. Commun.* **2007**, 2820–2822.

[30] J. P. S. Mowat, V. R. Seymour, J. M. Griffin, S. P. Thompson, A. M. Z. Slawin, D. Fairen-Jimenez, T. Düren, S. E. Ashbrook, P. A. Wright, *Dalton Trans.* **2012**, *41*, 3937–3941.

[31] C. Volkringer, T. Loiseau, N. Guillou, G. Férey, E. Elkaïm, A. Vimont, *Dalton Trans.* **2009**, 2241–2249.

[32] E. V. Anokhina, M. Vougo-Zanda, X. Wang, A. J. Jacobson, *J. Am. Chem. Soc.* **2005**, *127*, 15000–15001.

[33] A. S. Munn, G. J. Clarkson, F. Millange, Y. Dumont, R. I. Walton, *CrystEngComm* **2013**, *15*, 9679.

[34] T. Ahnfeldt, D. Gunzelmann, T. Loiseau, D. Hirsemann, J. Senker, G. Ferey, N. Stock, *Inorg. Chem.* **2009**, *48*, 3057–3064.

[35] S. Biswas, T. Ahnfeldt, N. Stock, *Inorg. Chem.* **2011**, *50*, 9518–9526.

[36] F. Niekiel, M. Ackermann, P. Guerrier, A. Rothkirch, N. Stock, *Inorg. Chem.* **2013**, *52*, 8699–8705.

[37] H. Reinsch, D. de Vos, *Microporous Mesoporous Mater.* **2014**, *200*, 311–316.

[38] H. Reinsch, R. S. Pillai, R. Siegel, J. Senker, A. Lieb, G. Maurin, N. Stock, *Dalton Trans.* **2016**, *45*, 4179–4186.

[39] T. Loiseau, C. Mellot-Draznieks, H. Muguerra, G. Férey, M. Haouas, F. Taulelle, *C. R. Chim.* **2005**, *8*, 765–772.

[40] I. Senkovska, F. Hoffmann, M. Fröba, J. Getzschmann, W. Böhlmann, S. Kaskel, *Microporous Mesoporous Mater.* **2009**, *122*, 93–98.

[41] E. D. Bloch, D. Britt, C. Lee, C. J. Doonan, F. J. Uribe-Romo, H. Furukawa, J. R. Long, O. M. Yaghi, *J. Am. Chem. Soc.* **2010**, *132*, 14382–14384.

[42] P. V. Dau, M. Kim, S. J. Garibay, F. H. L. Münch, C. E. Moore, S. M. Cohen, *Inorg. Chem.* **2012**, *51*, 5671–5676.

[43] S. Couck, Y.-Y. Liu, K. Leus, G. V. Baron, P. van der Voort, J. F. M. Denayer, *Microporous Mesoporous Mater.* **2015**, *206*, 217–225.

[44] S. Halis, N. Reimer, A. Klinkebiel, U. Lüning, N. Stock, *Microporous Mesoporous Mater.* **2015**, *216*, 13–19.

[45] A. Krajnc, T. Kos, N. Zabukovec Logar, G. Mali, *Angew. Chem. Int. Ed.* **2015**, *54*, 10535–10538.

[46] M. A. Gotthardt, S. Grosjean, T. S. Brunner, J. Kotzel, A. M. Gänzler, S. Wolf, S. Bräse, W. Kleist, *Dalton Trans.* **2015**, *44*, 16802–16809.

[47] Y.-Y. Liu, S. Couck, M. Vandichel, M. Grzywa, K. Leus, S. Biswas, D. Volkmer, J. Gascon, F. Kapteijn, J. F. M. Denayer et al., *Inorg. Chem.* **2013**, *52*, 113–120.

[48] H. Depauw, I. Nevjestić, G. Wang, K. Leus, F. Callens, E. de Canck, K. de Buysser, H. Vrielinck, P. van der Voort, *J. Mater. Chem. A* **2017**, *5*, 24580–24584.

[49] X. Liu, W. Qi, Y. Wang, R. Su, Z. He, *Nanoscale* **2017**, *9*, 17561–17570.

[50] P. J. Larson, J. L. Cheney, A. D. French, D. M. Klein, B. J. Wylie, A. F. Cozzolino, *Inorg. Chem.* **2018**.

[51] F. Carson, S. Agrawal, M. Gustafsson, A. Bartoszewicz, F. Moraga, X. Zou, B. Martín-Matute, *Chem. Eur. J.* **2012**, *18*, 15337–15344.

[52] L. Chen, Z. Gao, Y. Li, *Catal. Today* **2015**, *245*, 122–128.

[53] P. Valvekens, E. D. Bloch, J. R. Long, R. Ameloot, D. E. de Vos, *Catal. Today* **2015**, *246*, 55–59.

[54] R. van Zeeland, X. Li, W. Huang, L. M. Stanley, *RSC Adv.* **2016**, *6*, 56330–56334.

[55] J. H. Cavka, S. Jakobsen, U. Olsbye, N. Guillou, C. Lamberti, S. Bordiga, K. P. Lillerud, *J. Am. Chem. Soc.* **2008**, *130*, 13850–13851.

[56] S. J. Garibay, S. M. Cohen, *Chem. Commun.* **2010**, *46*, 7700–7702.

[57] M. Kandiah, M. H. Nilsen, S. Usseglio, S. Jakobsen, U. Olsbye, M. Tilset, C. Larabi, E. A. Quadrelli, F. Bonino, K. P. Lillerud, *Chem. Mater.* **2010**, *22*, 6632–6640.

[58] M. Kandiah, S. Usseglio, S. Svelle, U. Olsbye, K. P. Lillerud, M. Tilset, *J. Mater. Chem.* **2010**, *20*, 9848.

[59] A. Schaate, P. Roy, A. Godt, J. Lippke, F. Waltz, M. Wiebcke, P. Behrens, *Chem. Eur. J.* **2011**, *17*, 6643–6651.

[60] M. J. Katz, Z. J. Brown, Y. J. Colon, P. W. Siu, K. A. Scheidt, R. Q. Snurr, J. T. Hupp, O. K. Farha, *Chem. Commun.* **2013**, *49*, 9449–9451.

[61] M. Kim, S. J. Garibay, S. M. Cohen, *Inorg. Chem.* **2011**, *50*, 729–731.

[62] M. Kim, J. F. Cahill, Y. Su, K. A. Prather, S. M. Cohen, *Chem. Sci.* **2012**, *3*, 126–130.

[63] A. M. Rasero-Almansa, A. Corma, M. Iglesias, F. Sánchez, *ChemCatChem* **2014**, *6*, 3426–3433.

[64] L. Chen, S. Rangan, J. Li, H. Jiang, Y. Li, *Green Chem.* **2014**, *16*, 3978–3985.

[65] H. Fei, S. M. Cohen, *Chem. Commun.* **2014**, *50*, 4810–4812.

[66] H. Fei, M. D. Sampson, Y. Lee, C. P. Kubiak, S. M. Cohen, *Inorg. Chem.* **2015**, *54*, 6821–6828.

[67] A. E. Platero-Prats, A. Bermejo Gómez, L. Samain, X. Zou, B. Martín-Matute, *Chem. Eur. J.* **2015**, *21*, 861–866.

[68] C. H. Hendon, J. Bonnefoy, E. A. Quadrelli, J. Canivet, M. B. Chambers, G. Rousse, A. Walsh, M. Fontecave, C. Mellot-Draznieks, *Chem. Eur. J.* **2016**, *22*, 3713–3718.

[69] H. Ali-Moussa, R. Navarro Amador, J. Martinez, F. Lamaty, M. Carboni, X. Bantreil, *Mater. Lett.* **2017**, *197*, 171–174.

[70] L. Braglia, E. Borfecchia, L. Maddalena, S. Øien, K. A. Lomachenko, A. L. Bugaev, S. Bordiga, A. V. Soldatov, K. P. Lillerud, C. Lamberti, *Catal. Today* **2017**, *283*, 89–103.

[71] J. Li, X. Yu, M. Xu, W. Liu, E. Sandraz, H. Lan, J. Wang, S. M. Cohen, *J. Am. Chem. Soc.* **2017**, *139*, 611–614.

[72] A. D. Burrows, *CrystEngComm* **2011**, *13*, 3623.

[73] W. Kleist, F. Jutz, M. Maciejewski, A. Baiker, *Eur. J. Inorg. Chem.* **2009**, *2009*, 3552–3561.

[74] H. Deng, C. J. Doonan, H. Furukawa, R. B. Ferreira, J. Towne, C. B. Knobler, B. Wang, O. M. Yaghi, *Science* **2010**, *327*, 846–850.

[75] K. Koh, A. G. Wong-Foy, A. J. Matzger, *Chem. Commun.* **2009**, 6162–6164.

[76] J. Bitzer, W. Kleist, *Chem. Eur. J.* **2018**.

[77] W. Kleist, M. Maciejewski, A. Baiker, *Thermochim. Acta* **2010**, *499*, 71–78.

[78] S. Marx, W. Kleist, J. Huang, M. Maciejewski, A. Baiker, *Dalton Trans.* **2010**, *39*, 3795–3798.

[79] Z. Wang, S. M. Cohen, *J. Am. Chem. Soc.* **2007**, *129*, 12368–12369.

[80] M. Ranocchiari, C. Lothschutz, D. Grolimund, J. A. van Bokhoven, *Proc. R. Soc. A* **2012**, *468*, 1985–1999.

[81] Y. Jiang, J. Huang, S. Marx, W. Kleist, M. Hunger, A. Baiker, *J. Phys. Chem. Lett.* **2010**, *1*, 2886–2890.

[82] T. Lescouet, E. Kockrick, G. Bergeret, M. Pera-Titus, D. Farrusseng, *Dalton Trans.* **2011**, *40*, 11359–11361.

[83] T. Lescouet, E. Kockrick, G. Bergeret, M. Pera-Titus, S. Aguado, D. Farrusseng, *J. Mater. Chem.* **2012**, *22*, 10287.

[84] M. Pera-Titus, T. Lescouet, S. Aguado, D. Farrusseng, *J. Phys. Chem. C* **2012**, *116*, 9507–9516.

[85] M. A. Gotthardt, R. Schoch, T. S. Brunner, M. Bauer, W. Kleist, *ChemPlusChem* **2015**, *80*, 188–195.

[86] M. Kubo, H. Hagi, A. Shimojima, T. Okubo, *Chem. Asian. J.* **2013**, *8*, 2801–2806.

[87] M. Lammert, S. Bernt, F. Vermoortele, D. E. de Vos, N. Stock, *Inorg. Chem.* **2013**, *52*, 8521–8528.

[88] T. Fukushima, S. Horike, Y. Inubushi, K. Nakagawa, Y. Kubota, M. Takata, S. Kitagawa, *Angew. Chem. Int. Ed.* **2010**, *49*, 4820–4824.

[89] L. Z. Vegard, *Physik* **1921**, *5*, 17–26.

[90] H. Reinsch, S. Waitschat, N. Stock, *Dalton Trans.* **2013**, *42*, 4840–4847.

[91] J. Yang, X. Yan, T. Xue, Y. Liu, *RSC Adv.* **2016**, *6*, 55266–55271.

[92] H. Liu, F.-G. Xi, W. Sun, N.-N. Yang, E.-Q. Gao, *Inorg. Chem.* **2016**, *55*, 5753–5755.

[93] X. Zhu, J. Gu, J. Zhu, Y. Li, L. Zhao, J. Shi, *Adv. Funct. Mater.* **2015**, *25*, 3847–3854.

[94] F. L. Morel, S. Pin, T. Huthwelker, M. Ranocchiari, J. A. van Bokhoven, *Phys. Chem. Chem. Phys.* **2015**, *17*, 3326–3331.

[95] A. J. Rossini, A. Zagdoun, M. Lelli, J. Canivet, S. Aguado, O. Ouari, P. Tordo, M. Rosay, W. E. Maas, C. Copéret et al., *Angew. Chem. Int. Ed.* **2012**, *51*, 123–127.

[96] K. K. Tanabe, S. M. Cohen, *Chem. Rev.* **2011**, *40*, 498–519.

[97] S. M. Cohen, *Chem. Rev.* **2012**, *112*, 970–1000.

[98] Z. Wang, S. M. Cohen, *Chem. Soc. Rev.* **2009**, *38*, 1315–1329.

[99] A. D. Burrows, S. M. Cohen, *CrystEngComm* **2012**, *14*, 4095.

[100] A. D. Burrows, C. G. Frost, M. F. Mahon, C. Richardson, *Angew. Chem. Int. Ed.* **2008**, *47*, 8482–8486.

[101] Z. Yin, S. Wan, J. Yang, M. Kurmoo, M.-H. Zeng, *Coord. Chem. Rev.* **2019**, *378*, 500–512.

[102] K. K. Tanabe, Z. Wang, S. M. Cohen, *J. Am. Chem. Soc.* **2008**, *130*, 8508–8517.

[103] S. J. Garibay, Z. Wang, K. K. Tanabe, S. M. Cohen, *Inorg. Chem.* **2009**, *48*, 7341–7349.

[104] K. K. Tanabe, S. M. Cohen, *Angew. Chem. Int. Ed.* **2009**, *48*, 7424–7427.

[105] Z. Wang, K. K. Tanabe, S. M. Cohen, *Inorg. Chem.* **2009**, *48*, 296–306.

[106] Z. Wang, S. M. Cohen, *Angew. Chem. Int. Ed.* **2008**, *47*, 4699–4702.

[107] J. S. Costa, P. Gamez, C. A. Black, O. Roubeau, S. J. Teat, J. Reedijk, *Eur. J. Inorg. Chem.* **2008**, *2008*, 1551–1554.

[108] C. Volkringer, S. M. Cohen, *Angew. Chem. Int. Ed.* **2010**, *49*, 4644–4648.

[109] T. Haneda, M. Kawano, T. Kawamichi, M. Fujita, *J. Am. Chem. Soc.* **2008**, *130*, 1578–1579.

[110] A. D. Burrows, L. L. Keenan, *CrystEngComm* **2012**, *14*, 4112.

[111] M. J. Ingleson, J. P. Barrio, J. B. Guilbaud, Y. Z. Khimyak, M. J. Rosseinsky, *Chem. Commun.* **2008**, 2680–2682.

[112] H. C. Kolb, M. G. Finn, K. B. Sharpless, *Angew. Chem. Int. Ed.* **2001**, *40*, 2004–2021.

[113] Y. Goto, H. Sato, S. Shinkai, K. Sada, *J. Am. Chem. Soc.* **2008**, *130*, 14354–14355.

[114] T. Gadzikwa, G. Lu, C. L. Stern, S. R. Wilson, J. T. Hupp, S. T. Nguyen, *Chem. Commun.* **2008**, 5493–5495.

[115] M. Savonnet, D. Bazer-Bachi, N. Bats, J. Perez-Pellitero, E. Jeanneau, V. Lecocq, C. Pinel, D. Farrusseng, *J. Am. Chem. Soc.* **2010**, *132*, 4518–4519.

[116] X.-C. Yi, F.-G. Xi, Y. Qi, E.-Q. Gao, *RSC Adv.* **2015**, *5*, 893–900.

[117] J. D. Evans, C. J. Sumby, C. J. Doonan, *Chem. Soc. Rev.* **2014**, *43*, 5933–5951.

[118] C.-D. Wu, A. Hu, L. Zhang, W. Lin, *J. Am. Chem. Soc.* **2005**, *127*, 8940–8941.

[119] X.-P. Zhou, Z. Xu, M. Zeller, A. D. Hunter, *Chem. Commun.* **2009**, 5439–5441.

[120] K. Oisaki, Q. Li, H. Furukawa, A. U. Czaja, O. M. Yaghi, *J. Am. Chem. Soc.* **2010**, *132*, 9262–9264.

[121] T. Jacobs, R. Clowes, A. I. Cooper, M. J. Hardie, *Angew. Chem. Int. Ed.* **2012**, *51*, 5192–5195.

[122] D. Feng, W.-C. Chung, Z. Wei, Z.-Y. Gu, H.-L. Jiang, Y.-P. Chen, D. J. Darensbourg, H.-C. Zhou, *J. Am. Chem. Soc.* **2013**, *135*, 17105–17110.

[123] W. Morris, B. Volosskiy, S. Demir, F. Gándara, P. L. McGrier, H. Furukawa, D. Cascio, J. F. Stoddart, O. M. Yaghi, *Inorg. Chem.* **2012**, *51*, 6443–6445.

[124] Y. Wu, L. Wei, H. Wang, L. Chen, Q. Zhang, *Comput. Mater. Sci.* **2016**, *111*, 79–85.

[125] C. Wang, Z. Xie, K. E. deKrafft, W. Lin, *J. Am. Chem. Soc.* **2011**, *133*, 13445–13454.

[126] K. Leus, Y.-Y. Liu, M. Meledina, S. Turner, G. van Tendeloo, P. van der Voort, *J. Catal.* **2014**, *316*, 201–209.

[127] S. Abednatanzi, P. G. Derakhshandeh, A. Abbasi, P. van der Voort, K. Leus, *ChemCatChem* **2016**, *8*, 3672–3679.

[128] C. J. Doonan, W. Morris, H. Furukawa, O. M. Yaghi, *J. Am. Chem. Soc.* **2009**, *131*, 9492–9493.

[129] B. Liu, S. Jie, Z. Bu, B.-G. Li, *RSC Adv.* **2014**, *4*, 62343–62346.

[130] J. Hou, Y. Luan, J. Tang, A. M. Wensley, M. Yang, Y. Lu, *J. Mol. Catal. A: Chem* **2015**, *407*, 53–59.

[131] R. Sun, B. Liu, B.-G. Li, S. Jie, *ChemCatChem* **2016**, *8*, 3261–3271.

[132] G. Yuan, Y. Tian, J. Liu, H. Tu, J. Liao, J. Yang, Y. Yang, D. Wang, N. Liu, *Chem. Eng. J.* **2017**, *326*, 691–699.

[133] M. Pintado-Sierra, A. M. Rasero-Almansa, A. Corma, M. Iglesias, F. Sánchez, *J. Catal.* **2013**, *299*, 137–145.

[134] A. M. Rasero-Almansa, A. Corma, M. Iglesias, F. Sánchez, *Green Chem.* **2014**, *16*, 3522–3527.

[135] M. A. Gotthardt, A. Beilmann, R. Schoch, J. Engelke, W. Kleist, *RSC Adv.* **2013**, *3*, 10676–10679.

[136] J.-R. Li, R. J. Kuppler, H.-C. Zhou, *Chem. Soc. Rev.* **2009**, *38*, 1477–1504.

[137] J.-R. Li, J. Sculley, H.-C. Zhou, *Chem. Rev.* **2012**, *112*, 869–932.

[138] P. Horcajada, R. Gref, T. Baati, P. K. Allan, G. Maurin, P. Couvreur, G. Férey, R. E. Morris, C. Serre, *Chem. Rev.* **2012**, *112*, 1232–1268.

[139] R. J. Kuppler, D. J. Timmons, Q.-R. Fang, J.-R. Li, T. A. Makal, M. D. Young, D. Yuan, D. Zhao, W. Zhuang, H.-C. Zhou, *Coord. Chem. Rev.* **2009**, *253*, 3042–3066.

[140] Y. Cui, Y. Yue, G. Qian, B. Chen, *Chem. Rev.* **2012**, *112*, 1126–1162.

[141] B. F. Hoskins, R. Robson, *J. Am. Chem. Soc.* **1990**, 1546–1554.

[142] M. Fujita, Y. J. Kwon, S. Washizu, K. Ogura, *J. Am. Chem. Soc.* **1994**, *116*, 1151–1152.

[143] A. Corma, H. García, F. X. Llabrés i Xamena, *Chem. Rev.* **2010**, *110*, 4606–4655.

[144] D. Farrusseng, S. Aguado, C. Pinel, *Angew. Chem. Int. Ed.* **2009**, *48*, 7502–7513.

[145] J. Lee, O. K. Farha, J. Roberts, K. A. Scheidt, S. T. Nguyen, J. T. Hupp, *Chem. Soc. Rev.* **2009**, *38*, 1450–1459.

[146] L. Ma, C. Abney, W. Lin, *Chem. Soc. Rev.* **2009**, *38*, 1248–1256.

[147] M. Ranocchiari, J. A. van Bokhoven, *Phys. Chem. Chem. Phys.* **2011**, *13*, 6388–6396.

[148] A. Dhakshinamoorthy, M. Alvaro, H. García, *Chem. Commun.* **2012**, *48*, 11275–11288.

[149] J. Gascon, A. Corma, F. Kapteijn, F. X. Llabrés i Xamena, *ACS Catalysis* **2014**, *4*, 361–378.

[150] J. Liu, L. Chen, H. Cui, J. Zhang, L. Zhang, C.-Y. Su, *Chem. Soc. Rev.* **2014**, *43*, 6011–6061.

[151] S. Bhattacharjee, Y.-R. Lee, P. Puthiaraj, S.-M. Cho, W.-S. Ahn, *Catal. Surv. Asia* **2015**, *19*, 203–222.

[152] A. H. Chughtai, N. Ahmad, H. A. Younus, A. Laypkov, F. Verpoort, *Chem. Soc. Rev.* **2015**, *44*, 6804–6849.

[153] A. Dhakshinamoorthy, A. M. Asiri, H. García, *Catal. Sci. Technol.* **2016**, *6*, 5238–5261.

[154] S. M. J. Rogge, A. Bavykina, J. Hajek, H. García, A. I. Olivos-Suarez, A. Sepúlveda-Escribano, A. Vimont, G. Clet, P. Bazin, F. Kapteijn et al., *Chem. Soc. Rev.* **2017**, *46*, 3134–3184.

[155] L. Zhu, X.-Q. Liu, H.-L. Jiang, L.-B. Sun, *Chem. Rev.* **2017**, *117*, 8129–8176.

[156] A. Dhakshinamoorthy, Z. Li, H. García, *Chem. Soc. Rev.* **2018**, *47*, 8134–8172.

[157] L. Jiao, Y. Wang, H.-L. Jiang, Q. Xu, *Adv. Mater.* **2018**, *30*, e1703663.

[158] A. Dhakshinamoorthy, M. Alvaro, A. Corma, H. Garcia, *Dalton Trans.* **2011**, *40*, 6344–6360.

[159] A. Dhakshinamoorthy, H. Garcia, *Chem. Soc. Rev.* **2012**, *41*, 5262–5284.

[160] J. Juan-Alcañiz, J. Gascon, F. Kapteijn, *J. Mater. Chem.* **2012**, *22*, 10102.

[161] Q. Yang, Q. Xu, H.-L. Jiang, *Chem. Soc. Rev.* **2017**, *46*, 4774–4808.

[162] S. Hermes, M.-K. Schröter, R. Schmid, L. Khodeir, M. Muhler, A. Tissler, R. W. Fischer, R. A. Fischer, *Angew. Chem. Int. Ed.* **2005**, *44*, 6237–6241.

[163] M. Meilikhov, K. Yusenko, R. A. Fischer, *J. Am. Chem. Soc.* **2009**, *131*, 9644–9645.

[164] M. Meilikhov, K. Yusenko, A. Torrisi, B. Jee, C. Mellot-Draznieks, A. Pöppl, R. A. Fischer, *Angew. Chem. Int. Ed.* **2010**, *49*, 6212–6215.

[165] A. Aijaz, A. Karkamkar, Y. J. Choi, N. Tsumori, E. Rönnebro, T. Autrey, H. Shioyama, Q. Xu, *J. Am. Chem. Soc.* **2012**, *134*, 13926–13929.

[166] A. Aijaz, Q.-L. Zhu, N. Tsumori, T. Akita, Q. Xu, *Chem. Commun.* **2015**, *51*, 2577–2580.

[167] Y.-Z. Chen, Y.-X. Zhou, H. Wang, J. Lu, T. Uchida, Q. Xu, S.-H. Yu, H.-L. Jiang, *ACS Catal.* **2015**, *5*, 2062–2069.

[168] Q. Yang, Y.-Z. Chen, Z. U. Wang, Q. Xu, H.-L. Jiang, *Chem. Commun.* **2015**, *51*, 10419–10422.

[169] T. Ishida, M. Nagaoka, T. Akita, M. Haruta, *Chem. Eur. J.* **2008**, *14*, 8456–8460.

[170] H.-L. Jiang, B. Liu, T. Akita, M. Haruta, H. Sakurai, Q. Xu, *J. Am. Chem. Soc.* **2009**, *131*, 11302–11303.

[171] K. Schlichte, T. Kratzke, S. Kaskel, *Microporous Mesoporous Mater.* **2004**, *73*, 81–88.

[172] L. Alaerts, E. Séguin, H. Poelman, F. Thibault-Starzyk, P. A. Jacobs, D. E. de Vos, *Chem. Eur. J.* **2006**, *12*, 7353–7363.

[173] A. Henschel, K. Gedrich, R. Kraehnert, S. Kaskel, *Chem. Commun.* **2008**, 4192–4194.

[174] Z. Fang, B. Bueken, D. E. de Vos, R. A. Fischer, *Angew. Chem. Int. Ed.* **2015**, *54*, 7234–7254.

[175] F. Vermoortele, B. Bueken, G. Le Bars, B. van de Voorde, M. Vandichel, K. Houthoofd, A. Vimont, M. Daturi, M. Waroquier, V. van Speybroeck et al., *J. Am. Chem. Soc.* **2013**, *135*, 11465–11468.

[176] Y. K. Hwang, D.-Y. Hong, J.-S. Chang, S. H. Jhung, Y.-K. Seo, J. Kim, A. Vimont, M. Daturi, C. Serre, G. Férey, *Angew. Chem. Int. Ed.* **2008**, *47*, 4144–4148.

[177] M. Banerjee, S. Das, M. Yoon, H. J. Choi, M. H. Hyun, S. M. Park, G. Seo, K. Kim, *J. Am. Chem. Soc.* **2009**, *131*, 7524–7525.

[178] D. Yang, S. O. Odoh, T. C. Wang, O. K. Farha, J. T. Hupp, C. J. Cramer, L. Gagliardi, B. C. Gates, *J. Am. Chem. Soc.* **2015**, *137*, 7391–7396.

[179] H. Noh, Y. Cui, A. W. Peters, D. R. Pahls, M. A. Ortuño, N. A. Vermeulen, C. J. Cramer, L. Gagliardi, J. T. Hupp, O. K. Farha, *J. Am. Chem. Soc.* **2016**, *138*, 14720–14726.

[180] Z. Li, N. M. Schweitzer, A. B. League, V. Bernales, A. W. Peters, A. B. Getsoian, T. C. Wang, J. T. Miller, A. Vjunov, J. L. Fulton et al., *J. Am. Chem. Soc.* **2016**, *138*, 1977–1982.

[181] K. Manna, P. Ji, Z. Lin, F. X. Greene, A. Urban, N. C. Thacker, W. Lin, *Nature Comm.* **2016**, *7*, 12610 - 12621.

[182] J. Gascon, U. AKTAY, M. HERNANDEZALONSO, G. VANKLINK, F. Kapteijn, *J. Catal.* **2009**, *261*, 75–87.

[183] S. Hasegawa, S. Horike, R. Matsuda, S. Furukawa, K. Mochizuki, Y. Kinoshita, S. Kitagawa, *J. Am. Chem. Soc.* **2007**, *129*, 2607–2614.

[184] Seo, Whang, Lee, Jun, Oh, Jeon, Kim, *Nature* **2000**, *404*, 982–986.

[185] G. Akiyama, R. Matsuda, H. Sato, M. Takata, S. Kitagawa, *Adv. Mater.* **2011**, *23*, 3294–3297.

[186] Y.-X. Zhou, Y.-Z. Chen, Y. Hu, G. Huang, S.-H. Yu, H.-L. Jiang, *Chem. Eur. J.* **2014**, *20*, 14976–14980.

[187] M. J. Ingleson, J. P. Barrio, J. Bacsa, C. Dickinson, H. Park, M. J. Rosseinsky, *Chem. Commun.* **2008**, 1287–1289.

[188] K. Mo, Y. Yang, Y. Cui, *J. Am. Chem. Soc.* **2014**, *136*, 1746–1749.

[189] K. Leus, Y.-Y. Liu, P. van der Voort, *Catal. Rev. Sci. Eng.* **2014**, *56*, 1–56.

[190] Z. Guo, B. Liu, Q. Zhang, W. Deng, Y. Wang, Y. Yang, *Chem. Rev.* **2014**, *43*, 3480–3524.

[191] R. A. Sheldon, I. W. C. E. Arends, G.-J. ten Brink, A. Dijksman, *Acc. Chem. Res.* **2002**, *35*, 774–781.

[192] C. Parmeggiani, F. Cardona, *Green Chem.* **2012**, *14*, 547.

[193] T. Mallat, A. Baiker, *Chem. Rev.* **2004**, *104*, 3037–3058.

[194] A. Dhakshinamoorthy, M. Alvaro, H. García, *Catal. Sci. Technol.* **2011**, *1*, 856–867.

[195] K. Brown, S. Zolezzi, P. Aguirre, D. Venegas-Yazigi, V. Paredes-García, R. Baggio, M. A. Novak, E. Spodine, *Dalton Trans.* **2009**, *24*, 1422–1427.

[196] A. Corma, M. T. Navarro, F. Rey, *Chem. Commun.* **1998**, 1899–1900.

[197] K. Leus, I. Muylaert, M. Vandichel, G. B. Marin, M. Waroquier, V. van Speybroeck, P. van der Voort, *Chem. Commun.* **2010**, *46*, 5085–5087.

[198] N. V. Maksimchuk, K. A. Kovalenko, S. S. Arzumanov, Y. A. Chesalov, M. S. Melgunov, A. G. Stepanov, V. P. Fedin, O. A. Kholdeeva, *Inorg. Chem.* **2010**, *49*, 2920–2930.

[199] W. Zhang, J. L. Loebach, S. R. Wilson, E. N. Jacobsen, *J. Am. Chem. Soc.* **1990**, *112*, 2801–2803.

[200] T. Katsuki, *Coord. Chem. Rev.* **1995**, *140*, 189–214.

[201] S.-H. Cho, B. Ma, S. T. Nguyen, J. T. Hupp, T. E. Albrecht-Schmitt, *Chem. Commun.* **2006**, 2563–2565.

[202] A. Bhunia, M. A. Gotthardt, M. Yadav, M. T. Gamer, A. Eichhofer, W. Kleist, P. W. Roesky, *Chemistry* **2013**, *19*, 1986–1995.

[203] S. Bhattacharjee, D.-A. Yang, W.-S. Ahn, *Chem. Commun.* **2011**, *47*, 3637–3639.

[204] Y. Lu, M. Tonigold, B. Bredenkötter, D. Volkmer, J. Hitzbleck, G. Langstein, *Z. Anorg. Allg. Chem.* **2008**, *634*, 2411–2417.

[205] M. Tonigold, Y. Lu, B. Bredenkötter, B. Rieger, S. Bahnmüller, J. Hitzbleck, G. Langstein, D. Volkmer, *Angew. Chem.* **2009**, *121*, 7682–7687.

[206] M. J. Beier, W. Kleist, M. T. Wharmby, R. Kissner, B. Kimmerle, P. A. Wright, J.-D. Grunwaldt, A. Baiker, *Chem. Eur. J.* **2012**, *18*, 887–898.

[207] F. X. Llabrés i Xamena, A. ABAD, A. Corma, H. Garcia, *J. Catal.* **2007**, *250*, 294–298.

[208] S. Proch, J. Herrmannsdörfer, R. Kempe, C. Kern, A. Jess, L. Seyfarth, J. Senker, *Chem. Eur. J.* **2008**, *14*, 8204–8212.

[209] A. Dhakshinamoorthy, M. Alvaro, H. García, *ACS Catal.* **2010**, *1*, 48–53.

[210] H. Fei, J. Shin, Y. S. Meng, M. Adelhardt, J. Sutter, K. Meyer, S. M. Cohen, *J. Am. Chem. Soc.* **2014**, *136*, 4965–4973.

[211] C. Kaes, A. Katz, M. W. Hosseini, *Chem. Rev.* **2000**, *100*, 3553–3590.

[212] A. Titze-Alonso, *Master Thesis*, Bochum, Ruhr University Bochum, **2019**.

[213] S. N. Cherni, A. Driss, T. Jouini, *Acta Crystallogr., Sect. C: Cryst. Struct. Commun.* **1999**, *55*, 1248–1250.

[214] S. Asbrink, A. Waskowska, *J. Phys.: Condens. Matter.* **1991**, *3*, 8173–8180.

[215] Z. G. Li, G. H. Wang, J. J. Niu, J. W. Xu, N. H. Hu, *Acta Crystallogr., Sect. C: Cryst. Struct. Commun.* **2007**, *63*, 94-96.

[216] R. E. Pacalo, E. K. Graham, *Phys. Chem. Miner.* **1991**, *18*, 69–80.

[217] S. Geller, *Acta Crystallogr., Sect. B: Struct. Sci.* **1971**, *27*, 821–828.

[218] K. C. Gupta, A. K. Sutar, *Coord. Chem. Rev.* **2008**, *252*, 1420–1450.

[219] D. V. Partyka, J. B. Updegraff, M. Zeller, A. D. Hunter, T. G. Gray, *Organometallics* **2007**, *26*, 183–186.

[220] T. J. Del Castillo, S. Sarkar, K. A. Abboud, A. S. Veige, *Dalton Trans.* **2011**, *40*, 8140–8144.

[221] P. Guo, *Catal. Comm.* **2015**, *68*, 58–60.

[222] A. R. Powers, X. Yang, T. J. Del Castillo, I. Ghiviriga, K. A. Abboud, A. S. Veige, *Dalton Trans.* **2013**, *42*, 14963–14966.

[223] A. R. Powers, I. Ghiviriga, K. A. Abboud, A. S. Veige, *Dalton Trans.* **2015**, *44*, 14747–14752.

[224] B. Ravel, M. Newville, *J. Synchroton Rad.* **2005**, *12*, 537–541.

[225] J. E. Sarneski, L. J. Brzezinski, B. Anderson, M. Didiuk, R. Manchanda, R. H. Crabtree, G. W. Brudvig, G. K. Schulte, *Inorg. Chem.* **1993**, *32*, 3265–3269.

[226] H. Torayama, T. Nishide, H. Asada, M. Fujiwara, T. Matsushita, *Polyhedron* **1997**, *16*, 3787–3794.

[227] A. Czylkowska, R. Kruszynski †, D. Czakis-Sulikowska, T. J. Bartczak, *J. Coord. Chem.* **2006**, *57*, 239–247.

[228] V. R. Pedireddi, M. R. Shimpi, J. V. Yakhmi, *Macromol. Symp.* **2006**, *241*, 83–87.

[229] Y. Cao, J.-F. Zhang, F.-L. Bei, C. Zhang, J.-Y. Yang, Y.-L. Song, *Inorg. Chem. Commun.* **2007**, *10*, 1214–1217.

[230] S. Benmansour, F. Setifi, S. Triki, F. Thétiot, J. Sala-Pala, C. J. Gómez-García, E. Colacio, *Polyhedron* **2009**, *28*, 1308–1314.

[231] L. Thomassen, *J. Am. Chem. Soc.* **1940**, *62*, 1134–1136.

[232] H. Duan, S. Sengupta, J. L. Petersen, N. G. Akhmedov, X. Shi, *J. Am. Chem. Soc.* **2009**, *131*, 12100–12102.

[233] S. Das, S. Biswas, S. Mukherjee, J. Bandyopadhyay, S. Samanta, I. Bhowmick, D. K. Hazra, A. Ray, P. P. Parui, *RSC Adv.* **2014**, *4*, 9656–9659.

[234] N. Saravanan, P. Selvam, *Acta Crystallogr., Sect. E: Struct. Rep. Online* **2014**, *70*, 326-327.

[235] T. Feng, D. Bu, H. Lei, *Polyhedron* **2018**, *148*, 109–117.

Appendix A

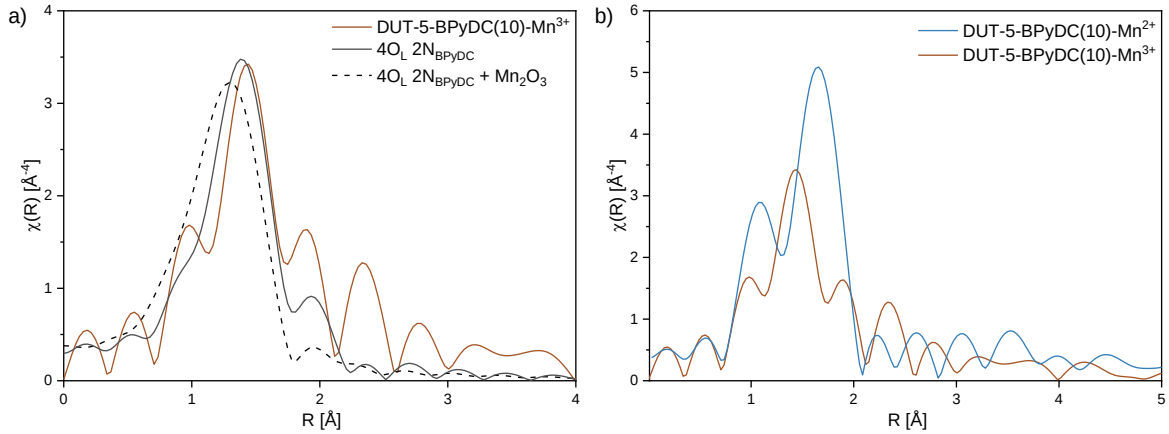

Figure A1. Fourier-transformed experimental EXAFS spectra, the fit of the first complex shell and the fit of the first complex shell with the corresponding metal oxide of DUT-5-BPyDC(10)-Mn^{3+} (a) and comparison of the Fourier-transformed EXAFS spectra of DUT-5-BPyDC(10)-Mn^{2+} and -Mn^{3+} (b).

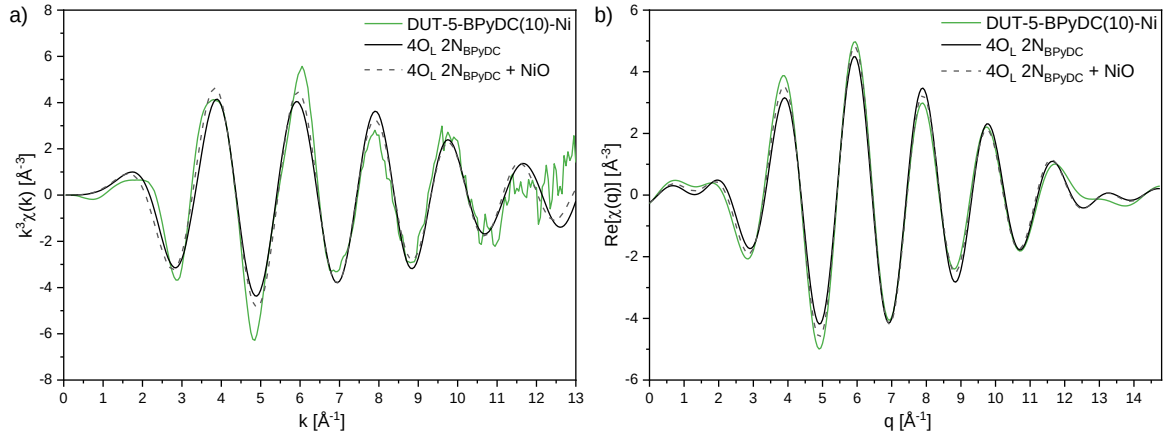

Figure A2. Ni K-edge EXAFS spectra of DUT-5-BPyDC(10)-Ni, plotted in k-space (a) and q-space (b).

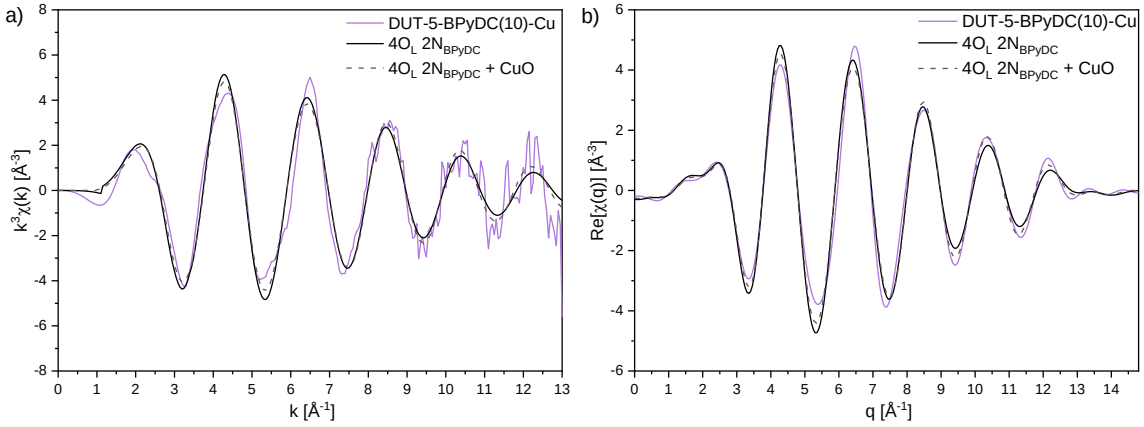

Figure A3. Cu K-edge EXAFS spectra of DUT-5-BPyDC(10)-Cu, plotted in k-space (a) and q-space (b).

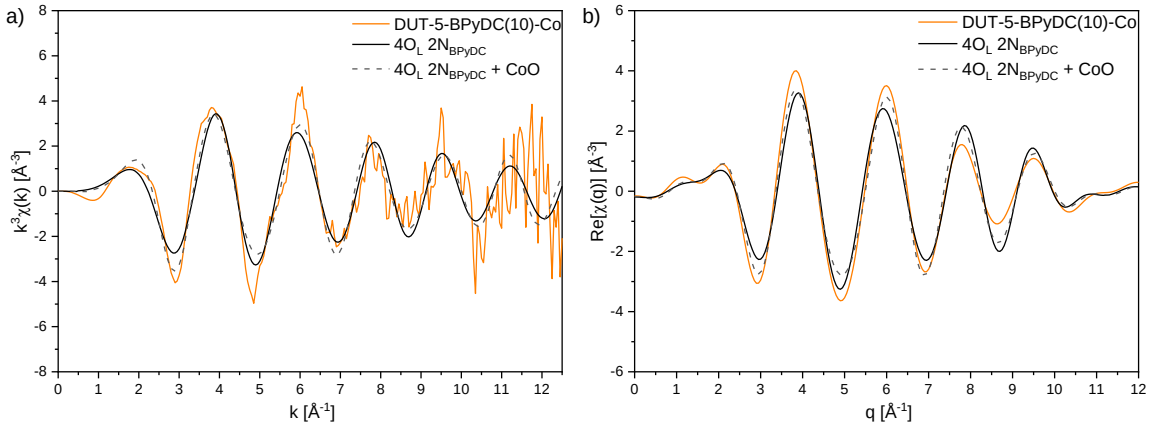

Figure A4. Co K-edge EXAFS spectra of DUT-5-BPyDC(10)-Co, plotted in k-space (a) and q-space (b).

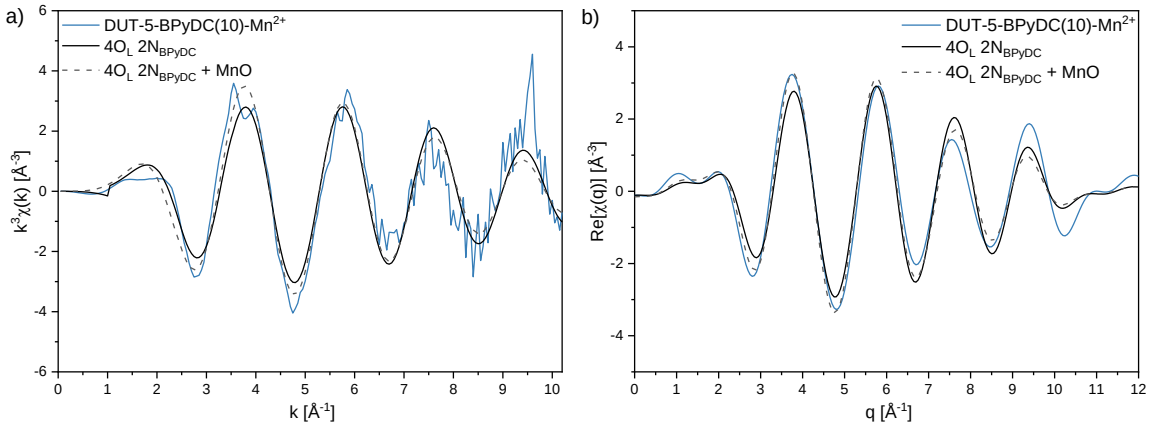

Figure A5. Mn K-edge EXAFS spectra of DUT-5-BPyDC(10)-Mn^{2+}, plotted in k-space (a) and q-space (b).

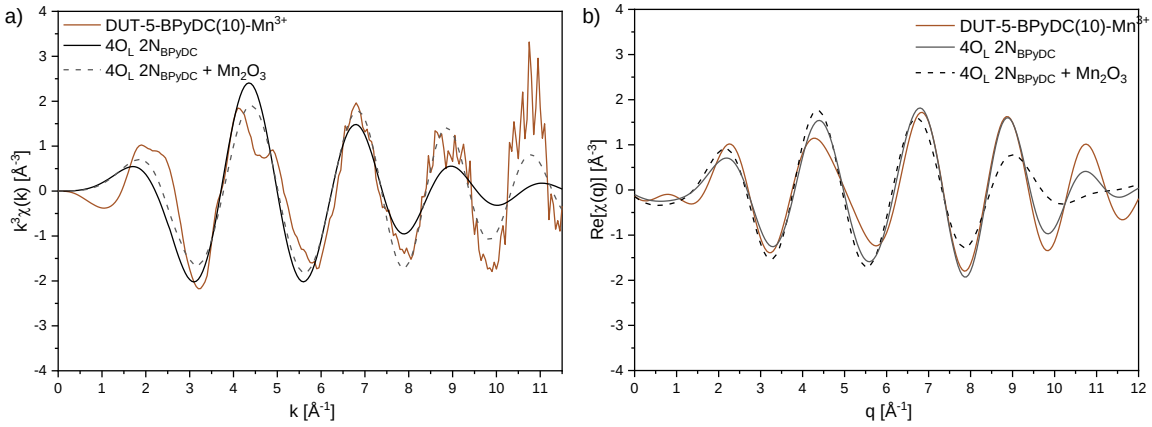

Figure A6. Mn K-edge EXAFS spectra of DUT-5-BPyDC(10)-Mn^{3+}, plotted in k-space (a) and q-space (b).

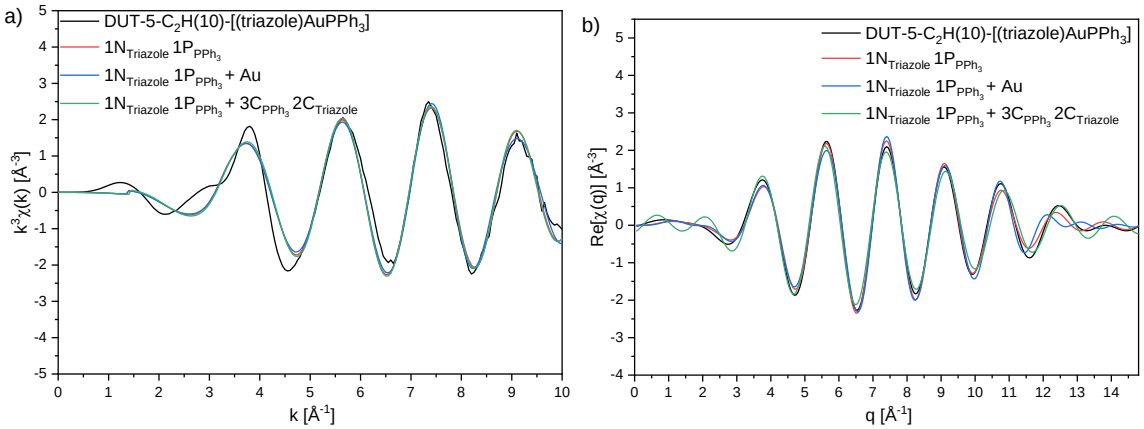

Figure A7. Au L3-edge EXAFS spectra of DUT-5-C2H(10)-[(triaziole)AuPPh3]+, plotted in k-space (a) and q-space (b).

Table A1.Fitting parameters of the EXAFS analysis and the results for the spectra of DUT-5-BPyDC(10)-Ni.

Entry	Fitting model	Abs-Bs	N(Bs)	R(Abs-Bs) [Å]
1	4 O_L 2N_{BPyDC}	Ni-O	4_{fix}	2.02 ± 0.02
		Ni-N	2_{fix}	2.17 ± 0.09
		$S_0^2{}_{fix}$ = 0.80; ΔE_0 = 0.1 ± 5.5 eV; χ^2_{red} = 450; R = 0.03;		
		σ^2 [Å] = 0.003 ± 0.003 Å^2		
2	4 O_L 2N_{BPyDC} + NiO	Ni-O	6_{fix}	2.03 ± 0.01
		Ni-Ni	0.1 ± 0.2	3.03 ± 0.12
		$S_0^2{}_{fix}$ = 0.80; ΔE_0 = -5.3 ± 1.8 eV; χ^2_{red} = 114; R = 0.01;		
		σ^2 [Å] = 0.006 ± 0.001 Å^2		

Table A2. Fitting parameters of the EXAFS analysis and the results for the spectra of DUT-5-BPyDC(10)-Cu.

Entry	Fitting model	Abs-Bs	N(Bs)	R(Abs-Bs) [Å]
1	4 O_L 2N_{BPyDC}	Cu-O	4_{fix}	1.96 ± 0.01
		Cu-N	2_{fix}	1.88 ± 0.05
		$S_0^2{}_{fix}$ = 0.87; ΔE_0 = 3.6 ± 2.3 eV; χ^2_{red} = 20; R = 0.03;		
		σ^2 [Å] = 0.004 ± 0.002 Å^2		
2	4 O_L 2N_{BPyDC} + CuO	Cu-O	6_{fix}	1.93 ± 0.02
		Cu-Cu	0.5 ± 0.6	2.90 ± 0.07
		$S_0^2{}_{fix}$ = 0.87; ΔE_0 = 4.9 ± 2.8 eV; χ^2_{red} = 241; R = 0.06;		
		σ^2 [Å] = 0.009 ± 0.001 Å^2		

Table A3. Fitting parameters of the EXAFS analysis and the results for the spectra of DUT-5-BPyDC(10)-Co.

Entry	Fitting model	Abs-Bs	N(Bs)	R(Abs-Bs) [Å]
1	4 O_L 2N_{BPyDC}	Co-O	4_{fix}	2.08 ± 0.02
		Co-N	2_{fix}	1.95 ± 0.02
		$S_0^2{}_{fix}$ = 0.77; ΔE_0 = 0.8 ± 3.0 eV; χ^2_{red} = 53; R = 0.07; σ^2 [Å] = 0.002 ± 0.001 Å^2		
2	4 O_L 2N_{BPyDC} + CoO	Co-O	6_{fix}	2.07 ± 0.02
		Co-Co	0.5 ± 0.5	2.98 ± 0.08
		$S_0^2{}_{fix}$ = 0.77; ΔE_0 = -0.5 ± 3.9 eV; χ^2_{red} = 29; R = 0.03; σ^2 [Å] = 0.010 ± 0.001 Å^2		

Table A4. Fitting parameters of the EXAFS analysis and the results for the spectra of DUT-5-BPyDC(10)-Mn^{2+}.

Entry	Fitting model	Abs-Bs	N(Bs)	R(Abs-Bs) [Å]
1	4 O_L 2N_{BPyDC}	Mn-O	4_{fix}	2.13 ± 0.02
		Mn-N	2_{fix}	2.29 ± 0.02
		$S_0^2{}_{fix}$ = 0.70; ΔE_0 = 3.8 ± 3.0 eV; χ^2_{red} = 31; R = 0.09; σ^2 [Å] = 0.004 ± 0.002 Å^2		
2	4 O_L 2N_{BPyDC} + MnO	Mn-O	6_{fix}	2.13 ± 0.02
		Mn-Mn	0.3 ± 0.7	3.12 ± 0.15
		$S_0^2{}_{fix}$ = 0.70; ΔE_0 = -3.3 ± 2.9 eV; χ^2_{red} = 31; R = 0.07; σ^2 [Å] = 0.010 ± 0.002 Å^2		

Table A5. Fitting parameters of the EXAFS analysis and the results for the spectra of DUT-5-BPyDC(10)-Mn^{3+}.

Entry	Fitting model	Abs-Bs	N(Bs)	R(Abs-Bs) [Å]
1	4 O_L 2N_{BPyDC}	Mn-O	4_{fix}	1.89 ± 0.03
		Mn-N	2_{fix}	2.19 ± 0.02
		$S_0^2{}_{fix}$ = 0.70; ΔE_0 = -6.5 ± 7.4 eV; χ^2_{red} = 130; R = 0.07; σ^2 [Å] = 0.008 ± 0.002 Å^2		
2	4 O_L 2N_{BPyDC} + Mn_2O_3	Mn-O	6_{fix}	1.84 ± 0.06
		Mn-Mn	-1.4 ± 2.1	3.00 ± 0.13
		$S_0^2{}_{fix}$ = 0.70; ΔE_0 = -16.5 ± 10.1 eV; χ^2_{red} = 157; R = 0.37; σ^2 [Å] = 0.016 ± 0.001 Å^2		

Table A6. Fitting parameters of the EXAFS analysis and the results for the spectra of DUT-5-C_2H(10)-[(triaziole)AuPPh_3].

Entry	Fitting model	Abs-Bs	N(Bs)	R(Abs-Bs) [Å]
1	1$N_{Triazole}$ 1P	Au-N	1_{fix}	2.01 ± 0.04
		Au-P	1_{fix}	2.28 ± 0.02
		$S_0^2{}_{fix}$ = 0.87; ΔE_0 = 7.5 ± 4.7 eV; χ^2_{red} = 416; R = 0.04; σ^2 [Å] = 0.003 ± 0.002 Å^2		
2	1$N_{Triazole}$ 1P + Au	Au-N	1_{fix}	2.02 ± 0.04
		Au-P	1_{fix}	2.28 ± 0.02
		Au-Au	0.4 ± 0.3	3.00 ± 0.04
		$S_0^2{}_{fix}$ = 0.87; ΔE_0 = 7.8 ± 4.1 eV; χ^2_{red} = 339; R = 0.06; σ^2 [Å] = 0.004 ± 0.001 Å^2		
3	1$N_{Triazole}$ 1P + $C_{Triazole}$	Au-N	1_{fix}	2.03 ± 0.03
		Au-P	1_{fix}	2.24 ± 0.01
		Au-C	1.2 ± 1.9	3.27 ± 0.07
		Au-C	2.2 ± 1.1	3.40 ± 0.07
		$S_0^2{}_{fix}$ = 0.87; ΔE_0 = 3.7 ± 2.9 eV; χ^2_{red} = 260; R = 0.06; σ^2 [Å] = 0.003 ± 0.001 Å^2		

Appendix B

Danksagung

An dieser Stelle möchte ich mich ganz herzlich bei all denen bedanken, die direkt oder indirekt zum Gelingen dieser Arbeit beigetragen haben.

Zuallererst möchte ich mich bei Prof. Dr. Wolfgang Kleist für die freundliche Aufnahme in seine Arbeitsgruppe, für das interessante Thema meiner Doktorarbeit, für die lehrreiche Zeit sowie insbesondere für das entgegengebrachte Vertrauen über die gesamte Promotion bedanken.

Ein ganz besonderer Dank geht an Johannes Bitzer, für die erfolgreiche Zusammenarbeit, für die umfangreichen wissenschaftlichen Diskussionen, für die stete Hilfsbereitschaft und Ratschläge, das Korrekturlesen dieser Arbeit und zuletzt für die angenehme und lustige Atmosphäre während der Arbeit.

Weiterhin möchte ich mich bei allen Mitgliedern der AG Nanocat RUB, insbesondere Milada Teubnerova, Leif Schwensow, Alba Titze-Alonso und Tim Herrendorf, für das besonders gute Arbeitsklima bedanken.

Bei Alba Titze-Alonso und Johannes Bitzer möchte ich mich für die Auswertung der XAS Daten bedanken. Bei Prof. Dr. Matthias Bauer und seinen Mitarbeitern möchte ich mich dafür bedanken, dass sie die XAS Messungen einiger Proben durchgeführt haben. Bei DESY Hamburg bedanke ich mich für die zur Verfügung gestellte Messzeit an der Messlinie P65 und Dr. Edmund Welter für seine Unterstützung während dieser Messzeit.

Zudem möchte ich mich bei unseren Kooperationspartnern bedanken. Prof. Dr. Stefan Bräse und Dr. Ksenia Kutonova danke ich für die Synthese und das unkomplizierte, schnelle Bereitstellen der funktionalisierten Linker. Prof. Dr. Michael Meier und Yasmin Raupp danke ich für die angenehme Zusammenarbeit. Prof. Dr. Peter Roesky und Dr. Christoph Kaub danke ich für die Synthese des Goldazids, für die Hilfe bezüglich der Click-Reaktionen und für die zur Verfügung gestellten NMR-Messungen am KIT.

Außerdem möchte ich mich bei meinen Bachelor- und Masterstudenten, Charlotte Fritsch, Simon Oßwald, Micha Weinert, Alina Ouissa, Tim Herrendorf und Abdelkarim Roshdy, sowie

bei meinen Auslandsstudentinnen Alexandra Komargokina und Milada Teubnerova für ihren wissenschaftlichen Beitrag zu dieser Arbeit bedanken.

Für die Zeit am Karlsruher Institut für Technologie, möchte ich mich bei Prof. Dr. Jan-Dirk Grunwaldt für die Durchführung meiner Promotion am Lehrstuhl Chemische Technik und Katalyse (ITCP, KIT) und für das Bereitstellen der Messgeräte bedanken. Auch danke ich ihm für die unkomplizierte Übernahme des Korreferats.

Ein großes Dankeschön geht auch an den gesamten Arbeitskreis Grunwaldt. Paul Sprenger und Gülperi Cavusoglu möchte ich besonders für die angenehme, sehr lustige und facettenreiche Zeit im Büro danken. Für unsere gemeinsamen und lustigen Kafferunden bedanke ich mich bei Paul Sprenger, Gülperi Cavusoglu und Elen Ogel.

Für die Zeit an der Ruhr Universität Bochum, möchte ich mich bei Prof. Dr. Martin Muhler für das Bereitstellen der Messgeräte bedanken. Kevin Ollegott danke ich für die TG Messungen. Sven Anke danke ich für die lustige Zeit während der Praktikumsbetreuung. Außerdem möchte ich mich bei der gesamten Arbeitsgruppe des Lehrstuhls für Technische Chemie (RUB) für die angenehme Zeit bedanken.

Für die XRD Messungen möchte ich Hartmut Mammen (Mineralogie, RUB) und für die ICP-OES Messungen möchte ich Petra Düchting (AG Prof. Ute Krämer, Molekulargenetik und Physiologie der Pflanzen, RUB) danken. Daniel Siegmund (AG Prof. Nils Metzler-Nolte, AC I, Bioanorganische Chemie, RUB) danke ich für die Bildaufnahmen am Fluoreszenzmikroskop.

Zuallerletzt, gebührt mein Dank meinen Freunden für ihre Unterstützung, die niemals endende Motivation und den Ausgleich während dieser Arbeit. Ein großer Dank gilt meiner Familie, die mir stets Rückhalt gibt und mich unterstützt.